BOREAS An international journal of Quaternary research

An integrated geological characterization of the Mid-Pleistocene to Holocene geology of the Sørlige Nordsjø II offshore wind site, southern North Sea

HANNAH E. PETRIE, CHRISTIAN H. EIDE, HAFLIDI HAFLIDASON, JO BRENDRYEN AND TIMOTHY WATTON

BOREAS

Petrie, H. E., Eide, C. H., Haflidason, H., Brendryen, J. & Watton, T.: An integrated geological characterization of the Mid-Pleistocene to Holocene geology of the Sørlige Nordsjø II offshore wind site, southern North Sea. *Boreas*. https://doi.org/10.1111/bor.12647. ISSN 0300-9483.

Subsurface deposits in recently glaciated marine areas are highly heterogeneous, representing a range of glacial and postglacial environments and processes including glacitectonism, overconsolidation, fluvial and lacustrine deposition, and transgression. These heterogeneities are often linked to variations in engineering properties, with important implications for the design and installation of offshore wind infrastructure. In this study we present an integrated geological characterization of the Sørlige Nordsjø II offshore wind site, located in waters of 50–70 m depth along the southern border of the Norwegian North Sea, focusing on the evolution of the area's depositional setting during the late Quaternary period and its implications for offshore wind development. We integrate interpretations from a marine geological data set acquired in 2022 with legacy 3D seismic data and a review of the current understanding of the southern North Sea's complex glacial history. A preliminary ground model and accompanying risk map for the site is presented with five main geological units: (i) homogeneous and layered marine sands covering most of the site, with patchy distribution and coarser-grained deposits in the east; (ii) buried, layered channel deposits containing organic material and possible associated shallow gas; (iii) buried, stiff glacilacustrine clay deposits; (iv) a buried, layered, glacitectonized unit incised by tunnel valleys, with a sandy marine infill; and (v) mounded tills and glacitectonized deposits containing boulders, exposed to shallowly buried in the east. Salt diapirism and gas migration were also found to be important potential geohazards at the site. Three-dimensional seismic attribute maps were found to be a powerful aid to understanding the distribution and genesis of seismic facies identified on 2D high-resolution sub-bottom profiles. This type of data integration is an under-utilized methodology for generating detailed preliminary ground models, which can inform more cost-effective site survey and early foundation concept planning at geologically complex offshore wind sites.

Hannah E. Petrie (hannah.petrie@uib.no), Christian H. Eide, Haflidi Haflidason and Jo Brendryen, University of Bergen, Department of Earth Science, Allégaten 41, 5007 Bergen, Norway; Timothy Watton, Equinor Energy ASA, PB 8500, 4035 Stavanger, Norway; *received 30th June 2023, accepted 23rd December 2023.*

The ongoing expansion of offshore wind is playing an important role in decarbonizing the global energy sector (IEA 2019) and has the potential to improve energy security at lower costs than other technologies in the mid to long term (Rohrig *et al.* 2013). One way to reduce manufacturing and installation costs at new and ever larger offshore wind sites is to develop a better understanding of how the geological character of the seabed and shallow subsurface impact turbine foundation and cable design and installation, which can account for up to ~35% of the overall cost of an offshore wind development (Bhattacharya 2014). This is particularly true in areas with highly variable geology, where higher uncertainty in the distribution of soil units or their geotechnical properties can result in over-conservative foundation design (Muir Wood & Knight 2013).

In the North Sea, the geotechnical properties of the seabed and shallow subsurface sediments (and rock) have been heavily influenced by the glaciations and related eustatic sea-level changes which occurred in the Northern Hemisphere during the late Quaternary period (e.g. Le *et al.* 2014; Cotterill *et al.* 2017a; Emery *et al.* 2019a, b; Prins & Andresen 2019; Fleischer *et al.* 2023). Ice sheets repeatedly advanced onto the continental shelf from the highlands of the UK and Scandinavia, compressing and deforming the underlying sediments, changing the pore pressure conditions within them (Piotrowski *et al.* 2004) and depositing subglacial sediments (tills) containing a heterogeneous mix of clays, sands, gravels and boulders. In the tundra environments ahead of the ice-sheet margins, subaerial exposure and permafrost desiccated the soil, creating palaeosols with altered geotechnical properties such as overconsolidation (Cotterill *et al.* 2017a; Martin *et al.* 2017; Emery *et al.* 2019b) and subjecting exposed bedrock to freeze–thaw weathering (e.g. Thumann *et al.* 2017). The presence of overconsolidated soil layers can have a significant impact on the design requirements of offshore wind turbine foundations, such as length and wall thickness, and therefore the amount of material and capital expenditure required to develop the site. At the Dogger Bank offshore wind development zone in the British sector of the southern North Sea, for example, geological complexities including major glacitectonic folding and thrusting and the presence of overconsolidated glacilacustrine deposits have reportedly had important implications for foundation design and placement (Cotterill *et al.* 2017a, b).

DOI 10.1111/bor.12647

In this study, we focus on understanding how late Quaternary glacial and postglacial processes and environmental changes have influenced the shallow subsurface stratigraphy of the southern Norwegian North Sea, a region that was strongly impacted by the break-up of the last North Sea ice sheet and the opening of the Dogger Bank–Jutland Bank Gap (Sejrup *et al.* 2016; Hjelstuen *et al.* 2018). We combine observations from legacy 2D and 3D seismic data with shallow, high-resolution sub-bottom profiles, shallow core data and geotechnical borehole reporting to provide a preliminary site characterization for the Sørlige Nordsjø II offshore wind site (from here on referred to as SNII) within the broader geological context of the late Quaternary evolution of the North Sea. We also show how legacy 3D seismic data can aid correlation of seismic facies between higher resolution 2D sub-bottom profiles while also allowing shallow subsurface geohazards to be understood in the context of the deeper subsurface stratigraphy (e.g. salt diapirism, hydrocarbon migration).

The aims of this paper are threefold, to (i) build on the existing lithostratigraphic and geotechnical frameworks of the southern North Sea by integrating the results of a recent marine geological study of the SNII site with a review of existing geological and geotechnical investigations from SNII and the wider southern North Sea, (ii) present a preliminary ground model for SNII which divides the site into two geotechnical provinces and five seismic-based geological units and associated subunits, with contrasting geotechnical properties, and (iii) present a 'risk map' for SNII, highlighting the key potential geohazards and geotechnical challenges for offshore wind foundation design and installation. Furthermore, this contribution is intended to provide a relatively broad overview of the late Quaternary geology of the North Sea and its associated geotechnical properties and potential geohazards. This is intended to open the field of offshore wind site characterization up to geoscientists with backgrounds focused on the deeper subsurface geology of the North Sea and those without a background in geotechnics.

Study area

SNII is one of two open offshore renewable energy licence areas in the Norwegian North Sea, announced by the Norwegian Government in 2020 (the other is Utsira Nord, Fig. 1A) which are part of Norway's first licensing round for offshore wind (Norwegian Government 2022). SNII covers an area of ~2600 km^2, close to the southern boundary of the Norwegian North Sea (Fig. 1A). Water depths at SNII range between ~50 and 70 m, extending beyond the depth of the world's deepest bottom-fixed offshore windfarm at the time of writing (58.6 m, Seagreen Wind Energy). Like the well-studied Dogger Bank offshore wind zone (Cotterill *et al.* 2017a, b; Phillips *et al.* 2018, 2022; Roberts *et al.* 2018; Emery *et al.* 2019b, 2020), SNII is located close to the estimated line of the maximum extent of the last coalesced North Sea ice sheet (Sejrup *et al.* 2005; Bradwell *et al.* 2008; Ballantyne 2010; Hughes *et al.* 2016; Emery *et al.* 2019b) (Fig. 1A). Geological studies indicate that these ice-marginal areas experienced rapid variations in ice-sheet and meltwater dynamics towards the end of the last glaciation, as the climate began to warm, and the ice sheet began to break apart and destabilize ~20 000 years ago (Hjelstuen *et al.* 2018; Phillips *et al.* 2018; Ottesen *et al.* 2020). Developing a detailed understanding of how the dynamics of the last North Sea ice sheet(s) influenced depositional environmental changes in the SNII area is therefore key to informing depositional and preliminary ground models for this and future offshore wind sites in the area.

Geological history of the southern North Sea

Rifting, subsidence and salt diapirism

The North Sea basin owes its present-day configuration to multiple phases of stretching spanning from the Late Carboniferous through to the Late Jurassic period (see reviews by Faleide *et al.* (2015), Patruno *et al.* (2021) and Underhill & Richardson (2022)). SNII (Fig. 1A) lies above the Northern Permian Basin (e.g. Ziegler 1990; Anell *et al.* 2012), in which the thick evaporitic deposits of the Zechstein Group accumulated during the Permian period. Subsequent rifting and sediment loading caused the evaporitic deposits to mobilize, forming salt structures such as diapirs within the overlying sedimentary rock layers, with localized movements continuing into the Cenozoic (Figs 1B, S1).

During the early Cenozoic, post-rift thermal subsidence was centred along the axes of the Central Graben and Danish basins, with Quaternary subsidence generally following the same outlines (Westaway 2017). As a result, the central parts of the North Sea including SNII contain more than 2 km of Palaeogene and Neogene sediments and ~1 km of Quaternary sediments (Figs 1B, S1; Doré 1992; Huuse *et al.* 2001; Dowdeswell & Ottesen 2013; Lamb *et al.* 2018), which buried the underlying organic-rich Jurassic marine rocks sufficiently to generate hydrocarbons. In the southern North Sea, these migrated into anticlinal structures and intra-basinal highs formed through regional Late Cretaceous compression, combined with the movements of the Zechstein salt (Figs 1B, S1). Migration structures associated with these hydrocarbon accumulations (e.g. faults, pockmarks (e.g. Andresen *et al.* 2008) and gas chimneys) therefore represent potential geohazards to be screened for in the SNII area and other future offshore wind developments in the southern North Sea region.

The Quaternary glaciations

During the Pleistocene (~2.58 million to 11 700 years ago), the North Sea experienced multiple glaciations during which ice sheets advanced into the basin from the UK and Scandinavia (Ehlers 1990; Sejrup *et al*. 2005; Bradwell *et al*. 2008; Stoker *et al*. 2011; Lee *et al*. 2012; Ottesen *et al*. 2014; Rea *et al*. 2018). Broadly speaking, three major glaciations are defined: the Elsterian (or Anglian) spanning Marine Isotope Stage (MIS) 12 (*c*. 480–410 ka); the Saalian (or Wolstonian) (MIS 10 to MIS 6, *c*. 370–135 ka); and the Weichselian (or Devensian) (MIS 5d to MIS 2, *c*. 115–12 ka) (Figs 1, 2; Shackleton 1969). However, there remain challenges regarding the correlation of ice extent and timing between the different land areas bordering the North Sea, particularly for the older Elsterian and Saalian glaciations (e.g. Lauer & Weiss 2018). The respective interglacial periods, during which temperate terrestrial and marine conditions temporarily returned, are termed the Holsteinian (~MIS 11; Hughes *et al*. 2020) and the Eemian (MIS 5e) (Shackleton 1969; Mangerud *et al*. 1979; Mangerud 1991). In recent decades, 3D seismic mapping of subglacial meltwater valleys (tunnel valleys) in the North Sea has indicated a more complicated glacial history, with at least five to seven different generations of tunnel valleys identified (Kristensen *et al*. 2007; Lutz *et al*. 2009; Graham *et al*. 2010; Böse *et al*. 2012; Müther *et al*. 2012; Stewart *et al*. 2013).

Each advancing ice sheet eroded and deformed the soil and rock over which it advanced, as evidenced by multigenerational glacitectonic structures (Cotterill *et al*. 2017b; Roberts *et al*. 2018; Phillips *et al*. 2022) and tunnel valleys observed throughout the NW European lowlands and shallow subsurface of the North Sea (Ehlers *et al*. 1984; Wingfield 1989; Zagwijn 1989; Cameron *et al*. 1993; Sejrup *et al*. 1995; Ó Cofaigh 1996; Huuse & Lykke-Andersen 2000; Benn & Evans 2010; Stewart & Lonergan 2011; Kehew *et al*. 2012; van der Vegt *et al*. 2012; Kirkham *et al*. 2021). Some tunnel valleys are only partially infilled and remain visible as bathymetric lows on the seabed, particularly off the east coast of Scotland (Fig. 1A). Geomorphic features from the last deglaciation such as glacial lineations and moraine complexes marking former ice front positions also remain visible bathymetric features (Bradwell *et al*. 2008; Sejrup *et al*. 2016; Morén *et al*. 2018).

Tunnel valleys

In the Danish sector (bordering SNII to the south), tunnel valleys can be up to ~400 m deep and incise the base Pleistocene unconformity (Salomonsen 1995; Huuse & Lykke-Andersen 2000; Prins *et al*. 2020). The absolute ages of the tunnel valleys are often uncertain, and inferred from the age of the stratigraphy into which they incise, with very few of the tunnel valley fills themselves having been dated.

Tunnel valleys often contain highly heterogeneous sedimentary infills, which can comprise multigenerational erosion and infilling cycles (Fig. 2; Huuse *et al*. 2001). This can include remnants of coarse subglacial sediment, deposited during the formation of the valley (Praeg 2003; Benvenuti *et al*. 2018), postglacial fluvial sediments (Moreau & Huuse 2014; Fleischer *et al*. 2023), stiff glacilacustrine and homogeneous outwash sediments (Kirkham *et al*. 2021) and sandy interglacial marine sediments (Huuse & Lykke-Andersen 2000). Because the infill of the tunnel valley usually has different acoustic properties to the surrounding substrate, and the seismic facies within the valleys can be highly variable, seismic imaging beneath tunnel valleys is often poor or disturbed. This is sometimes exacerbated by the presence of shallow hydrocarbon accumulations (Huuse & Lykke-Andersen 2000; Praeg 2003; Ottesen *et al*. 2020).

The Late Weichselian glaciation

SNII is located ~75 km north of the inferred maximum extent of the Late Weichselian North Sea ice sheet and within the zone along which the British-Irish (BIIS) and Fennoscandian ice sheets (FIS) are postulated to have separated towards the end of the Late Weichselian glaciation (Fig. 1A; Sejrup *et al*. 2016; Hjelstuen *et al*. 2018; Roberts *et al*. 2018). Most ice reconstruction models for the North Sea require that the BIIS–FIS merged in the centre of the North Sea between 30 and 24 ka, followed by their separation and a late-stage readvance of a lobe of the BIIS (the North Sea Lobe) down the east coast of the UK between 21 and 17 ka (Rose 1985; Svendsen *et al*. 2004; Carr *et al*. 2006; Sejrup *et al*. 2009; Evans & Thomson 2010; Graham *et al*. 2011; Clark *et al*. 2012; Hughes *et al*. 2016; Evans *et al*. 2021). Clark *et al*. (2012) and Sejrup *et al*. (2016) propose that the BIIS and FIS were still coupled in the central North Sea as late as 19 ka on the basis of a surge of glacial meltwater deposits in the Norwegian Channel dated to 18.7 ka. However, Roberts *et al*. (2018) have suggested that the separation of the BIIS and FIS and marine inundation within the ice-free zone may have occurred as early as 22–21 and 21–19 ka, respectively.

Detailed studies of western Dogger Bank have revealed that the dynamics of the southern margin of the Late Weichselian ice sheet(s) were more complex than previously thought and created the core of the Dogger Bank structure through repeated folding and thrusting ahead of multiple advancing ice lobes, with ice streaming also occurring along parts of the margin (Cotterill *et al*. 2017a, b; Emery *et al*. 2020; Phillips *et al*. 2022). In addition, work to integrate the Late Weichselian lithostratigraphy of the Danish sector into the wider palaeoenvironmental context of the southern North Sea

has also helped to constrain the evolution of the margin's proglacial drainage systems at eastern Dogger Bank at the end of the Late Weichselian glaciation (Prins & Andresen 2019; Prins *et al.* 2020; Andresen *et al.* 2022). Areas to the NE of Dogger Bank (including SNII), however, remain understudied such that the timing and dynamics of the BIIS–FIS separation and glacial lake/meltwater drainage through the Dogger Bank–Jutland Bank Gap (south of SNII) (Sejrup *et al.* 2016; Hjelstuen *et al.* 2018) remain poorly understood.

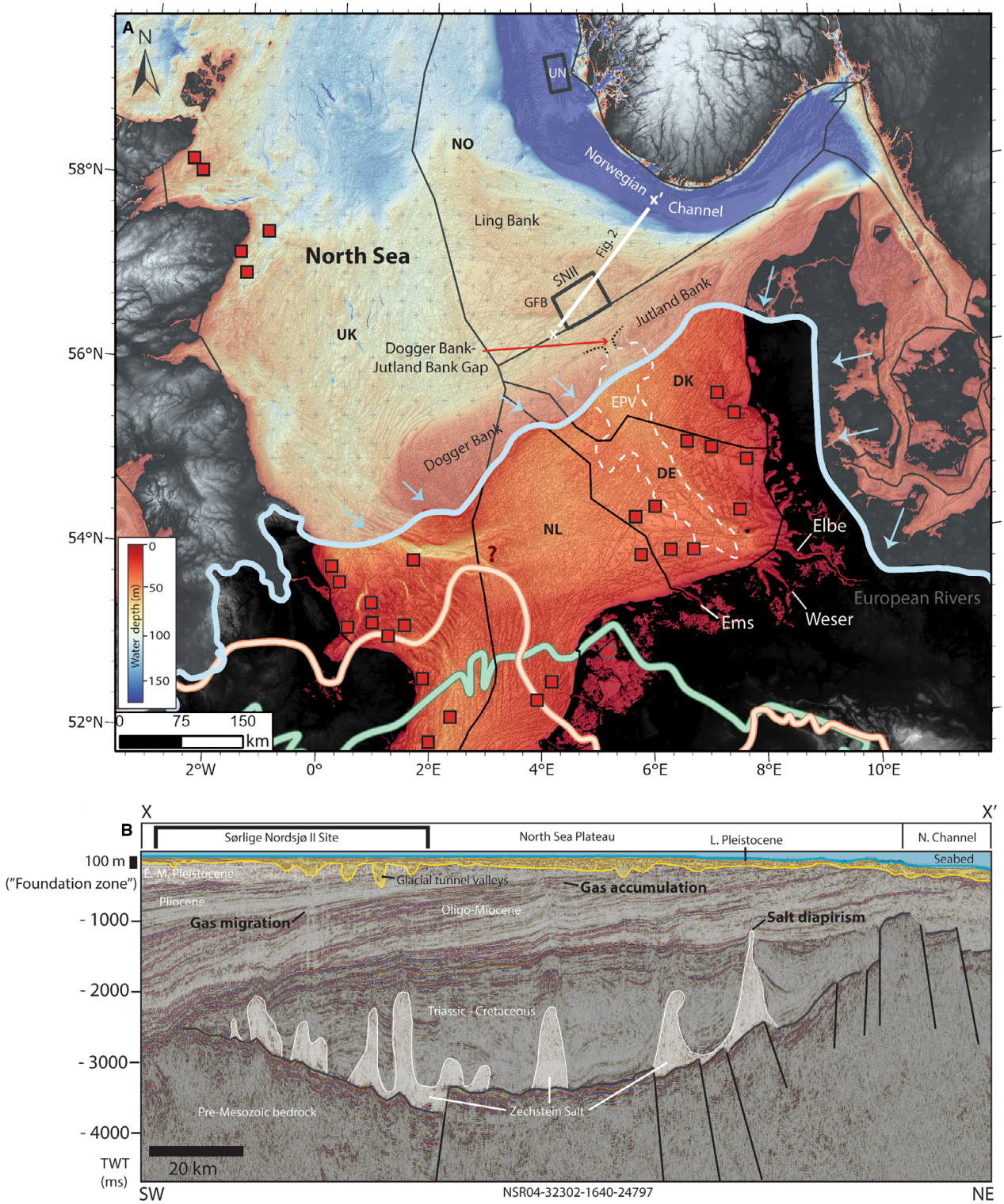

Fig. 1. A. Bathymetric hill-shaded map of the North Sea (GEBCO 2020) showing fully commissioned offshore wind farms (red squares) (TGS 2023) and inferred maximum ice-sheet extents for the Elsterian in light green (Huuse & Lykke-Andersen 2000 and references therein), Saalian in light orange (Huuse & Lykke-Andersen 2000 and references therein; Ehlers & Gibbard 2004; Gibbard & Clark 2011) and Late Weichselian in light blue (Emery *et al.* 2019b and references therein) glaciations. The outline of the Elbe Palaeovalley (EPV) from Özmaral (2018) is shown as a white dashed line. Norwegian offshore wind sites Utsira Nord (UN) and Sørlige Nordsjø II (SNII) are outlined in black. B. Southwest to NE 2D seismic profile running from SNII in the southern Norwegian North Sea to the southwestern edge of the Norwegian Channel, showing salt diapirs and associated gas migration structures in the Mesozoic and Cenozoic stratigraphy. The Mid-Pleistocene glacial erosion surface is shown in yellow. For version without annotations and interpretations, see Fig. S1. DK = Denmark; DE = Germany; E.-M. Pleistocene = Early–Middle Pleistocene; EPV = Elbe Palaeovalley; GFB = Greater Fish Bank; L. Pleistocene = Late Pleistocene; NL = Netherlands; N. Channel = Norwegian Channel; SNII = Sørlige Nordsjø II; TWT = two-way travel time; UN = Utsira Nord.

Deglaciation and marine inundation

Radiocarbon dates from glacimarine sediments on the North Sea Fan and in the Norwegian Channel (Fig. 1A) indicate that the northern margin of the North Sea ice sheet started to destabilize at ~19 ka (Sejrup *et al.* 2016; Morén *et al.* 2018). In contrast, the southern margin of the ice sheet may have started retreating much earlier, as indicated by glacilacustrine sediments deposited north of Dogger Bank after ~23 ka (Roberts *et al.* 2018).

During the early stages of deglaciation, the global eustatic sea level was ~120 m lower than today (Lambeck *et al.* 2014), meaning that much of the North Sea (excluding the Norwegian Channel) was above sea level. The landscape ahead of the retreating ice margins experienced rapid changes in the depositional environment as the climate warmed and sea levels rose, with ice-dammed glacial lakes developing then draining, glacial outwash channel systems flowing outwards from the ice margin (Cotterill *et al.* 2017b; Roberts *et al.* 2018; Emery *et al.* 2019b; Andresen *et al.* 2022) and the formerly ice-covered terrain and periglacial plains ahead of it eventually becoming occupied by rivers, marshlands, tidal inlets and finally the sea (Fitch *et al.* 2005; Cotterill *et al.* 2017b; Coughlan *et al.* 2018; Emery *et al.* 2020; Fleischer *et al.* 2023).

The partly ice-covered tundra that occupied the southern North Sea during the early stages of the deglaciation is sometimes referred to as Doggerland (e.g. Coles 1998; Gaffney *et al.* 2007; Bjerck 2021). Many investigations of the Doggerland palaeolandscape have been carried out by archaeologists (e.g. Fitch *et al.* 2005; Gaffney *et al.* 2020) while high-resolution subsurface data sets for offshore wind site investigations have allowed an even more detailed understanding to develop (Cotterill *et al.* 2017a, b; Roberts *et al.* 2018; Emery *et al.* 2019a, b, 2020; Phillips *et al.* 2022). Recent lithostratigraphic studies focusing on shallow cores and sub-bottom profiler data have also greatly contributed to the understanding of how the Doggerland landscape and drainage systems evolved during and after the retreat of the ice sheets (Coughlan *et al.* 2018; Andresen *et al.* 2022; Özmaral *et al.* 2022; Fleischer *et al.* 2023).

The largest Late Weichselian–Early Holocene palaeodrainage system in the southern North Sea was the Elbe Palaeovalley (EPV) (Fig. 1A; Konradi 2000; Özmaral 2018; Panin *et al.* 2020; Özmaral *et al.* 2022) that spans a width of ~40 km and length of 210 km, widening northwards where it approaches the Dogger Bank–Jutland Bank Gap (Fig. 1A). The River Elbe flowed northwards through the EPV and may have formed or exploited this gap (Andresen *et al.* 2022). Hjelstuen *et al.* (2018) propose that the gap is an incision created by a glacial lake outburst at ~18.5 ka, as the postulated Late Weichselian North Sea Lake located south of Dogger Bank overcame the topographic barrier that the Dogger–Jutland Bank then represented.

Seismic facies representing the different depositional phases within the EPV, ground-truthed by sediment core analysis, indicate a sedimentary infill that evolved from braided fluvial to estuarine deposition at around 10.8 cal. ka BP, to tidal and fully marine deposition after 8 cal. ka BP (Özmaral *et al.* 2022). In the northern parts of the valley, the base reflector is masked by blanking zones within the valley infill attributed to a high organic content within the basal incision fills, which have released biogenic methane gas (Özmaral *et al.* 2022).

The prograding units filling most of the EPV are generally covered by a transparent seismic facies which comprises sands and clayey silts, with a few well-preserved marine shells, and extend beyond the limits of the EPV. This unit began to be deposited after around 5.8 cal. ka BP, when sea level was about 10 m lower than today, and the rate of sea-level rise had slowed down (Vink *et al.* 2007). Holocene marine sands cover most of the North Sea plateau, with local subdivisions (Fig. 2) depending on the local inherited bathymetry and relative sea-level history.

A similar evolution is recorded within dendritic channels located to the NW of the EPV and SE of Dogger Bank (Prins & Andresen 2019; Papenmeier & Hass 2020; Andresen *et al.* 2022). These are postulated to have formed subglacially during either the Saalian or Late Weichselian glaciation, becoming altered by the Late Weichselian proglacial meltwater system which drained from the retreating ice-sheet margin towards the EPV. A Late Weichselian glacilacustrine facies is also identified in the area, supporting the existence of the postulated Late Weichselian North Sea Lake (Hjelstuen *et al.* 2018; Andresen *et al.* 2022).

It is postulated that seawater from the Atlantic gradually made its way southwards along an ice-free

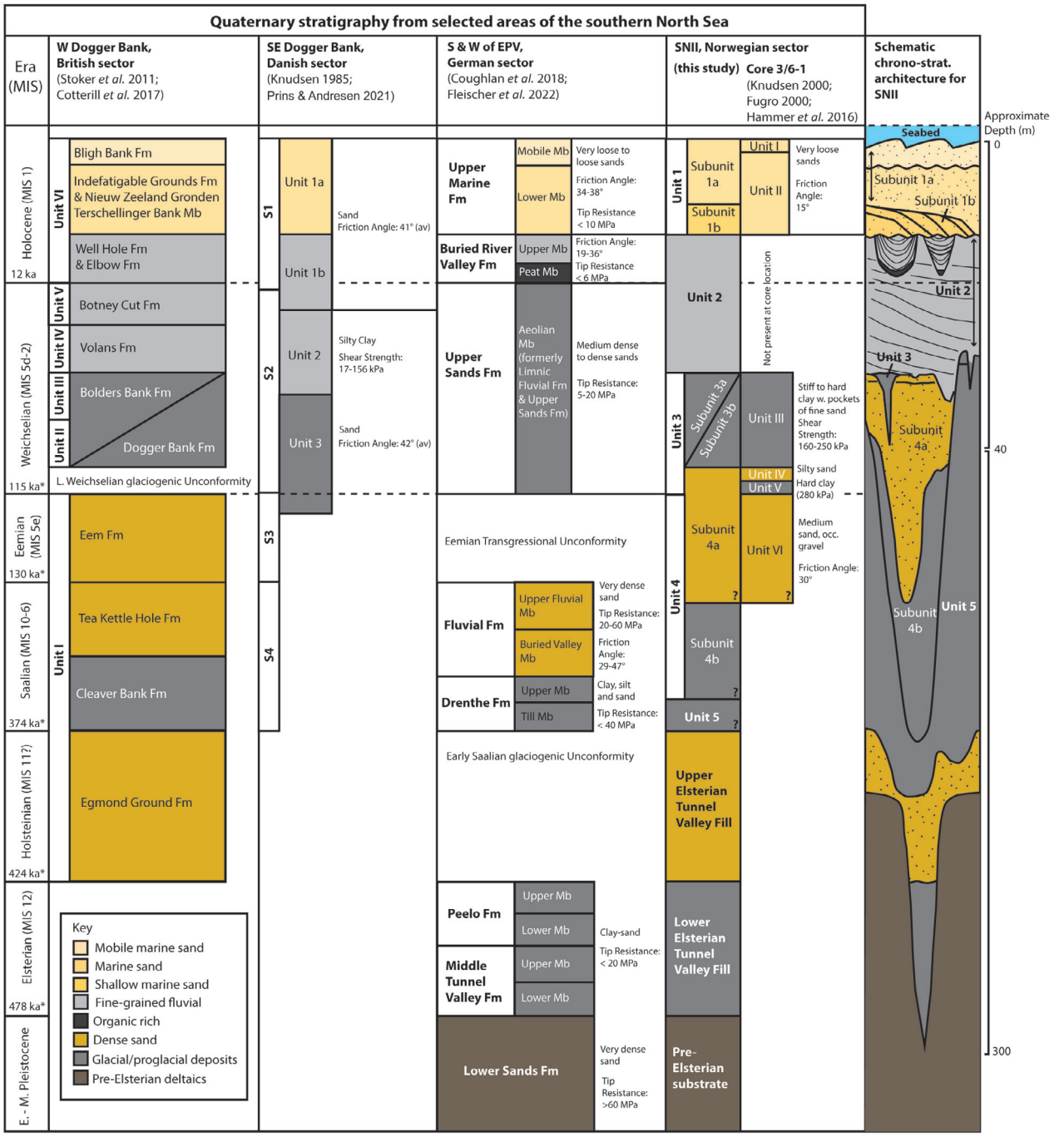

Fig. 2. A comparison of Quaternary lithostratigraphic units and their geotechnical properties (where available) defined in the western Dogger Bank area of the UK North Sea (Stoker *et al.* 2011; Cotterill *et al.* 2017b), the southeastern Dogger Bank area of the Danish North Sea (Knudsen 1985; Prins & Andresen 2021), the SNII area (this study, Fugro 2000; Knudsen 2000; Hammer *et al.* 2016) and the German sector of the North Sea (Coughlan *et al.* 2018; Fleischer *et al.* 2023). *Age correlations between geological era and Marine Isotope Stages from Shackleton (1969). Av = average; EPV = Elbe Palaeovalley; Fm = Formation; Mb = Member; MIS = Marine Isotope Stage; W = West.

zone between the retreating BIIS and FIS, eventually inundating Doggerland (Bradley *et al.* 2011; Clark *et al.* 2012; Sejrup *et al.* 2016; Becker *et al.* 2018; Roberts *et al.* 2018; Evans *et al.* 2021; Gandy *et al.* 2021). The sea would also have transgressed from the south, via the English Channel (Shennan *et al.* 2000; Cohen *et al.* 2017). Sea-level modelling indicates that Doggerland was fully submerged by 8–7.5 cal. ka BP (Shennan *et al.* 2000; Sturt *et al.* 2013; Cohen *et al.* 2017), although estimates of when the SNII area became inundated vary greatly, from

21 to 19 cal. ka BP (Roberts *et al*. 2018) to ~12 cal. ka BP (Hjelstuen *et al*. 2018), or later (~9 cal. ka BP) (Hammer *et al*. 2016; Gaffney *et al*. 2017).

Ground conditions in the southern North Sea

The rapid evolution of the depositional environment within previously glaciated marine areas such as the southern North Sea has important implications for the geotechnical properties of the shallow subsurface. These are known as the ground conditions, which must be evaluated to design suitable and cost-effective wind turbine foundations. This process is referred to as site characterization (e.g. Campbell 1984; Clayton & Power 2002; JeanJean *et al*. 2005; Evans *et al*. 2010; Power *et al*. 2011; Clare *et al*. 2012; Muir Wood & Knight 2013; DNV 2014; Velenturf *et al*. 2021). This generally involves dividing the shallow subsurface (~50–100 m) into units based to varying degrees on the geotechnical, geophysical and sedimentological properties of the soil layers encountered by geophysical and geotechnical surveying. In this context, the term soil refers to surficial unlithified sediments, not specifically only to palaeosols.

Although many geotechnical site surveys have been conducted in the North Sea, the understanding that these provide about individual infrastructure sites have rarely been integrated into the North Sea's late Quaternary lithostratigraphic framework. In recent years, however, a number of detailed geological studies with a focus on the geotechnical character of the late Quaternary stratigraphy of the southern North Sea have been published (Cotterill *et al*. 2017a, b; Coughlan *et al*. 2018; Prins & Andresen 2019; Cartelle *et al*. 2021; Fleischer *et al*. 2023). In the Norwegian sector, the late Quaternary lithostratigraphy and its geotechnical properties in the SNII area are presented briefly in Hammer *et al*. (2016) based on a core from the Fugro (2000) 3/6-1 geotechnical boring (Fig. 2).

Material and methods

Methods

This study combines an overview of the southern North Sea's late Quaternary lithostratigraphic units and their geotechnical characteristics in the vicinity of SNII, Dogger Bank and the northern EPV, with observations from bathymetric data, 2D and 3D seismic data, sub-bottom profiles, and vibrocores (Fig. 3). Interpretations from these data were integrated to define a preliminary ground model for SNII, which is divided into five units with contrasting geotechnical properties and implications for offshore wind turbine foundation design (Fig. 2). Ground model is a broad term used in engineering geology that encompasses conceptual, observational and analytical representations of the soil layers/bedrock present in the subsurface and their engineering properties (e.g. Parry *et al*. 2014) and can be presented as maps, 2D or 3D images or in text (OSIG 2014). In this study, the term preliminary ground model is used to describe our partly conceptual, partly observational 3D representation of the shallow subsurface at SNII which focuses on the distribution of sub-bottom profiler units identified within the upper ~40 m of the subsurface stratigraphy and their potential engineering properties as far as can be determined from the data and literature presently available.

Analysis of the deeper seismic stratigraphy is also used to place the model into the wider context of the southern North Sea's geological history and to evaluate potential geohazards linked to salt diapirism and the southern North Sea's active petroleum system.

Following a similar method to Prins & Andresen (2019), we demonstrate how geomorphological observations from legacy 3D seismic time and attribute slices can complement seismic facies analysis of high-resolution 2D sub-bottom profiles. This was a powerful tool for reconstructing the depositional environmental changes that occurred within SNII during the Late Weichselian to Holocene. In geotechnical hazard and risk assessment, the risk is defined as the likelihood of harm occurring from a specific hazard (e.g. Hamman 2009). We therefore summarized our preliminary geotechnical risk assessment for SNII by creating a colour-coded map showing areas associated with particular geohazards and their likelihood of causing harm (in this case, installation challenges for offshore wind turbine foundations).

Bathymetric data

At the time of writing, publicly available high-resolution bathymetric data are lacking in the southern Norwegian North Sea. In this study, the Olex bathymetric database (gridded to 5 × 5 m) was used to get an impression of the large-scale bathymetric features within and around SNII such as Greater Fish Bank, Dogger Bank, Jutland Bank and morainal ridges east and north of the site (Fig. 3A). The publicly available General Bathymetric Chart of the Oceans (GEBCO) (gridded to 30 arc seconds) has a lower resolution than Olex but gives continuous coverage where Olex contains gaps (Figs 1A, 3). The inferred maximum extents of the Saalian, Elsterian and Late Weichselian North Sea ice sheets, the outline of the EPV, inferred positions of the retreating Late Weichselian ice sheet and outlines of postulated Late Weichselian ice-dammed lakes from literature were displayed on the GEBCO (2020) map (Fig. 1A). Combined with observations from the SNII data set (Fig. 3B, C), this was used to create a series of depositional environment maps spanning the late glacial to early postglacial periods of the Late Weichselian and Holocene in the Dogger Bank–SNII–EPV region.

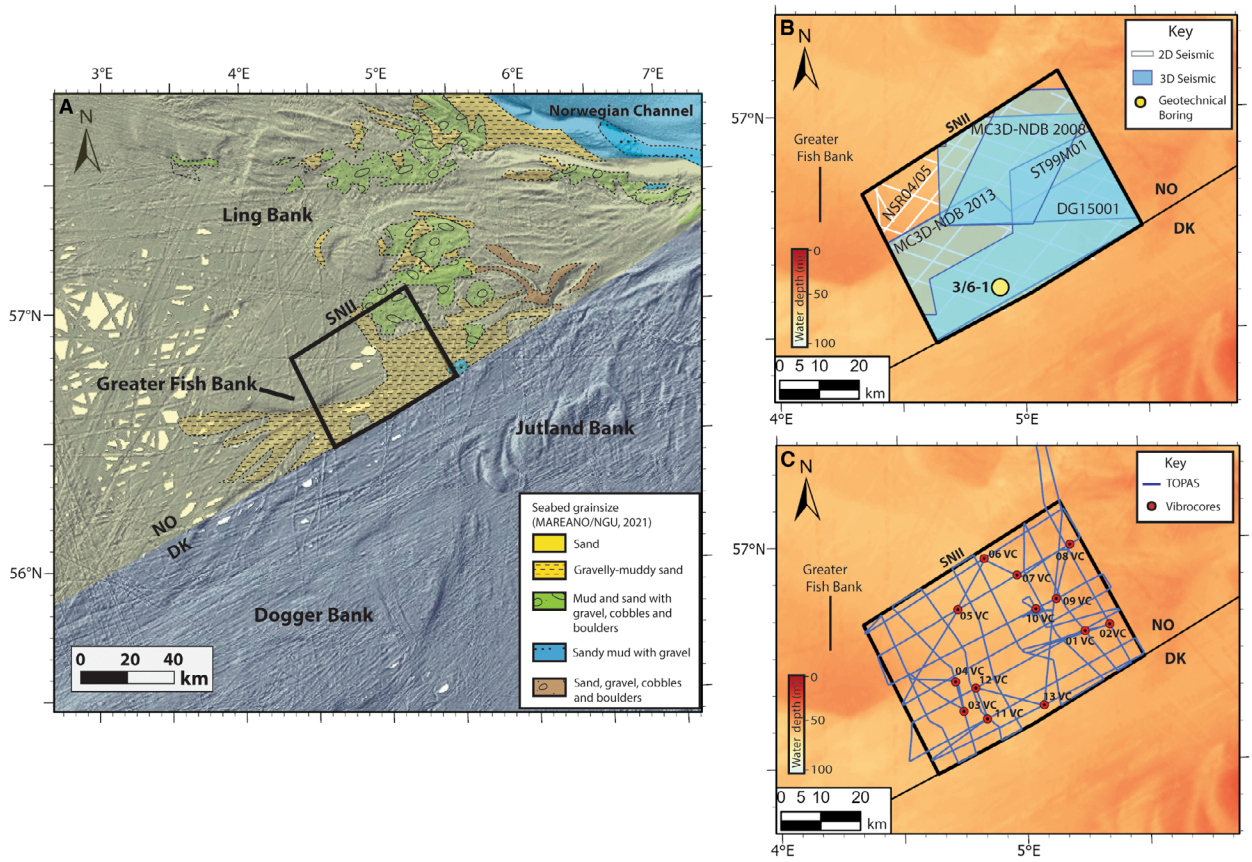

Fig. 3. A. Bathymetric map at SNII and surrounding area (www.olex.no) with seabed sediment grain size overlay (MAREANO/NGU 2021). B. Bathymetric map at SNII (GEBCO 2020) showing legacy 2D and 3D seismic data coverage from DISKOS (surveys NSR04/05, ST99M01 and DG15001) and PGS (surveys MC3D-NDB2008 and MC3D-NDB2013) and location of 3/6-1 geotechnical boring. C. Location of sub-bottom profiles and vibrocores acquired in 2022 (this study). DK = Denmark; NO = Norway.

2D and 3D seismic data

About 90% of SNII is covered by zero-phase, reverse polarity, 3D seismic data (surveys MC3D-NDB2008 and MC3D-NDB2013 (PGS), ST99M01 and DG15001 (DISKOS); Fig. 3B). The northwestern corner is only covered by 2D seismic surveys NSR04/05 (DISKOS) (also zero-phase, reverse polarity). As exploration surveys, these were originally processed with a focus on the deeper stratigraphy, so the near-seabed reflections have a lower signal-to-noise ratio than the deeper reflections, and strong acquisition-line imprints. ST99M01 suffers the most from these. MC3D-NDB2013 covers the southern half of SNII and has the best quality of all the surveys. DG15001 and MC3D-NDB2008 cover northeastern SNII and are also of good quality in the shallow section. The surveys have vertical resolutions of ~10 m in the shallow section, resolving ~10 m thick channel and lake features occurring a few metres below the seabed.

The main interval of interest for bottom-fixed offshore wind foundation design is the upper ~100 m of the subsurface stratigraphy. On conventional seismic data the only mappable reflection in this interval is the seabed reflection, which was auto-tracked on the 3D surveys. For depth conversion of the seabed reflection, the average velocity of seawater, 1500 m s^{-1}, was used. An approximate depth conversion scale (10 ms = 7.5 m) is given on all sub-bottom profiles shown in the paper, however, a wide range of sedimentary facies with significantly different estimated acoustic properties occur within the upper metres to tens of metres within SNII. The seismic velocities of the sediments were not explicitly measured in this study, but visual correlation of sedimentary units identified within the vibrocores to the seismic reflections observed in the sub-bottom profiles allowed estimated seismic velocities to be calculated in the cored seismic units. These ranged from 415 to 1800 m s^{-1} within the upper 6 m of the subsurface. Seismic amplitude, variance and frequency decomposition blend extractions and time slices were used to highlight geomorphological features resolved within and below the seabed reflection. These features were then investigated in greater detail using intersecting sub-bottom profiles and vibrocore acquisition on a marine geological cruise in June 2022 (Fig. 3C). For the deeper intervals (down to ~300 ms), time slices from the seismic, variance and frequency decomposition

blend cubes were used to investigate the more deeply buried geomorphic features. In the frequency decomposition cubes shown, low frequencies are represented by red and yellow colours, intermediate frequencies by green and light blue colours and high frequencies by dark blue colours. White areas represent parts of the data with relatively equal amounts of low, medium and high frequencies in the data.

Sub-bottom profiles

Nine-hundred kilometres of sub-bottom profiles were acquired at SNII (Fig. 3C) using the single, narrow beam TOPAS PS18 sub-bottom profiler system (which uses two high-frequency signals centred around 18 kHz; Kongsberg 2019). TOPAS profiles have a high vertical resolution of ~0.3 m, and a penetration capability of up to 130 m below the seabed. In practice, the imaging below 30–40 m on the SNII profiles was quite poor, despite using a chirp pulse to increase the signal-to-noise ratio and penetration. The gathered profiles indicate variations in acoustic impedance, but do not distinguish between 'hard' or 'soft' signatures. The profiles were acquired in a grid-like pattern, approximately parallel to the edges of the SNII site, with separations of 5–10 km (Fig. 3C). Priority was given to targeting features of interest identified on 3D seismic data. The raw data were converted to SEG-Y files for importation to the Petrel seismic interpretation software. Time and time-thickness maps were generated for the seismo-stratigraphic boundaries interpreted on the profiles, with the aid of core logs and observed sedimentary facies.

Vibrocores

Thirteen vibrocores were acquired at SNII (Fig. 3C) with a Geo-Corer 6000 high-frequency vibrocoring system which has a barrel length of 5.8 m. A GEOTEK non-destructive multisensor core logger was used to measure the gamma density (equivalent to bulk density) and magnetic susceptibility in all of the cores after the methodology of Gunn & Best (1998). Three of the cores were then split into halves for conducting core scan photography, sedimentary logging and shear strength measurements using the Swedish fall cone method (Hansbo 1957). The sedimentary facies were logged by visual inspection of composition, texture, gradation, sedimentary structure and fossil content.

Geotechnical boring

The report 'Soil investigation and spud can penetration analysis' for North Sea block 3/6 (Fugro 2000) was provided by ENI. It includes a summary of the soil conditions at the location of the 3/6-1 boring in southwestern SNII (Fig. 3B) based on geotechnical measurements on samples taken from the 37.2-m-long core retrieved there. In this study, the findings of the report have been used to ground-truth some of the seismic units observed in our sub-bottom profiler data set (i.e. determine their lithology and geotechnical properties). The geotechnical investigation of the core included laboratory measurements of peak friction angle, undrained shear strength, density, particle size distribution and other tests on a smaller number of samples, which give an indication of how coarse, fine, soft or hard some of the mapped sub-bottom profiler facies in SNII are.

The Fugro analysis divides the borehole into lithostratigraphic units with a soil description and geotechnical laboratory measurements given for each. Hammer *et al.* (2016) conducted radiocarbon dating and grain size analysis on the core and correlated the lithostratigraphic units with depositional environment information derived from foraminiferal analysis by Knudsen (2000) (an internal Norsk Agip AS report). We use this analysis as a basis to interpret the depositional environment of some of the seismic units identified on sub-bottom profiler in this study. The SNII area, however, is very laterally heterogeneous, and the lithostratigraphic units identified in the 3/6-1 core are not entirely representative of other parts of the ~2600 km^2 site.

Results

Seabed geomorphology

SNII is located on the southern part of a relatively shallow area of the southern Norwegian North Sea known as Ling Bank (Figs 1A, 3A), where water depths range between ~50 and 70 m. The site is also located about 60 km north of the northeastern tip of Dogger Bank and about the same distance NW of the smaller Jutland Bank (Figs 1A, 3A). Dogger Bank and Jutland Bank can be traced along a single SW to NE trending line (parallel to the inferred maximum extent of the Late Weichselian ice sheet, Fig. 1A) but are separated by a ~10-km-wide area of deeper water (Fig. 3A), which has previously been interpreted as a possible fluvial incision resulting from glacial lake outburst flooding (Hjelstuen *et al.* 2018) and/or erosion by the Elbe River (Andresen *et al.* 2022). The SNII area lies ~60 km NW of the gap and so was probably directly in the path of the drainage systems which passed through the gap from the south (perhaps from the EPV, Fig. 1A). This is further supported by the presence of northward prograding deposits a few metres below the seabed north of SNII, in the northern part of Ling Bank (Hjelstuen *et al.* 2018).

A shallow (~50 m deep) Holocene sandbank (Greater Fish Bank) occupies the northwestern corner of SNII (Fig. 3A). East and NE of the site, pronounced arc-shaped and linear ridges are common. The shallow (~50 m deep) eastern part of SNII is characterized by a series of smaller, more subtle ridges and mounds (Fig. 3A), which, based on the presence of mud and sand

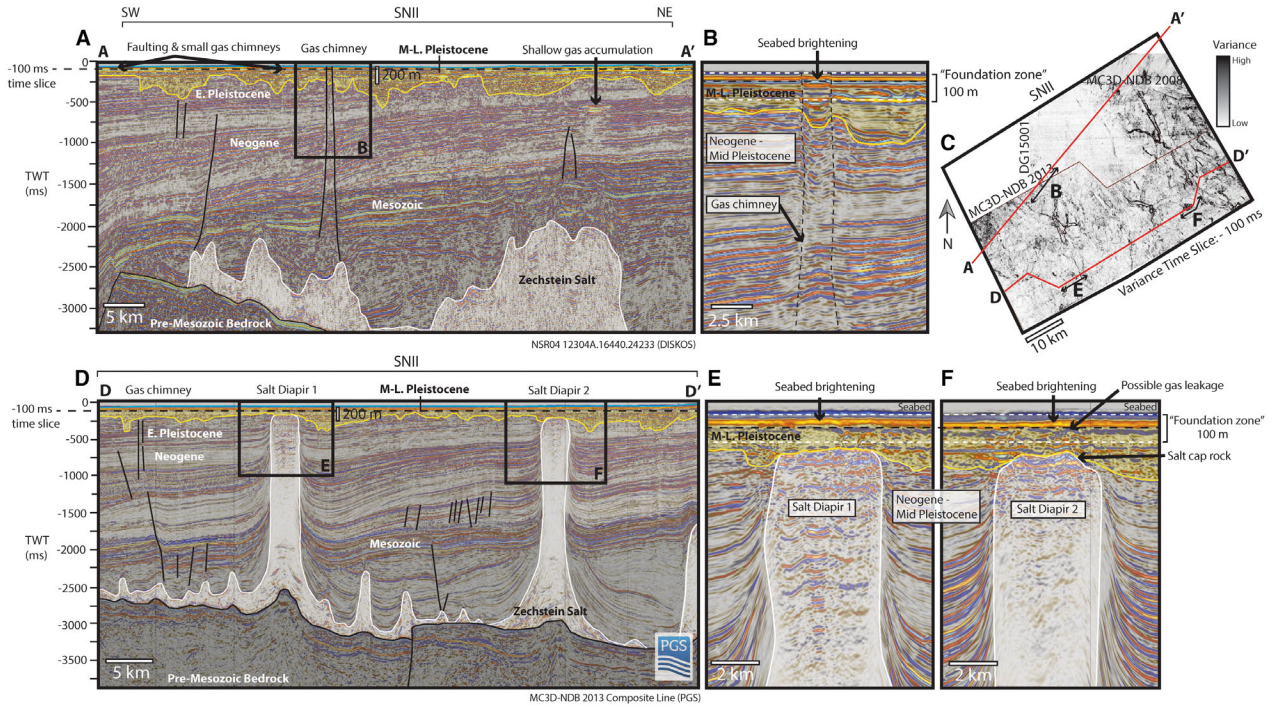

Fig. 4. A. Annotated 2D seismic profile A–A′ from survey NSR04 showing gas migration pathways (faulting, gas chimneys) from the deep subsurface into the shallow (Neogene and Pleistocene) stratigraphy. B. Close-up of a gas migration structure originating from the Jurassic source rock, extending up to a possible shallow gas accumulation close to the seabed. C. −100 ms variance time slice from 3D seismic surveys DG15001 (DISKOS) and MC3D-NDB2013 (PGS) showing key seismic anomalies close to seabed and the location of seismic profiles A–A′ and D–D′. D. Annotated seismic profile D–D′ showing Salt Diapirs 1 and 2 in southern SNII. E. Close-up of Salt Diapir 1 in southwestern SNII. F. Salt Diapir 2 in southeastern SNII, showing high-amplitude, chaotic seismic reflections above the diapirs, within overlying Late Pleistocene sediments. For versions without annotations and interpretations, see Fig. S2. E. Pleistocene = Early Pleistocene; M.-L. Pleistocene = Mid- to Late Pleistocene; TWT = two-way travel time.

with gravel, cobbles and boulders within the upper 50 cm of the surficial seabed sediment in the northeastern part of the site and gravelly–muddy sand in the southeastern part (Fig. 3A, MAREANO/NGU 2021), may represent reworked or exposed subglacial material. In contrast, the deeper (~60–70 m deep) central and southwestern parts of SNII have a smooth bathymetry with gentle changes in slope (Fig. 3A). The seabed in these areas is characterized by sand (in the north) and gravelly–muddy sands (in the south).

Seismic stratigraphy

In this section, an overview of the seismic stratigraphy observed on conventional 2D and 3D seismic data (down to ~3500 ms) is first given in order to give context to shallow geohazards observed within the foundation zone (~0–100 m below the seabed). The late Quaternary to Holocene stratigraphy is then described in greater detail.

Observations from legacy 2D and 3D seismic data. – At depths of ~2500–3500 ms below the seabed, the basement rock at SNII comprises Permian fault blocks, overlain by Zechstein Group evaporites. These form salt pillow and diapir structures of varying height and width within the subsurface (Figs 4, S2). At SNII, most of the diapirs are restricted to within the deeply buried Mesozoic stratigraphy, with the exception of two particularly tall diapirs located in the southwestern part of the site (Salt Diapir 1) and the southeastern part of the site (Salt Diapir 2) (Fig. 4C–F).

The tops of the diapirs occur below an undulating regional erosion surface (the Mid-Pleistocene glacial erosion surface, described below), at ~115 m below the seabed and are characterized by very high-amplitude, chaotic reflections (Fig. 4E, F). Although the diapir tops occur below the ~100 m depth of the so-called 'foundation zone' for offshore wind foundations, the seismic facies between the diapir tops and the seabed are more chaotic than the surrounding Mid–Late Pleistocene sediments. The seismic facies above the diapirs also exhibit higher variance (Fig. 4C) and stronger amplitudes (Fig. 4E, F), while the seabed reflection is also stronger and slightly shallower in the zones directly above the diapirs (Fig. 4E, F). The character of the seismic facies above Diapirs 1 and 2 could be related to a number of potential geohazards including diagenetically altered, fractured or deformed sediments owing to previous

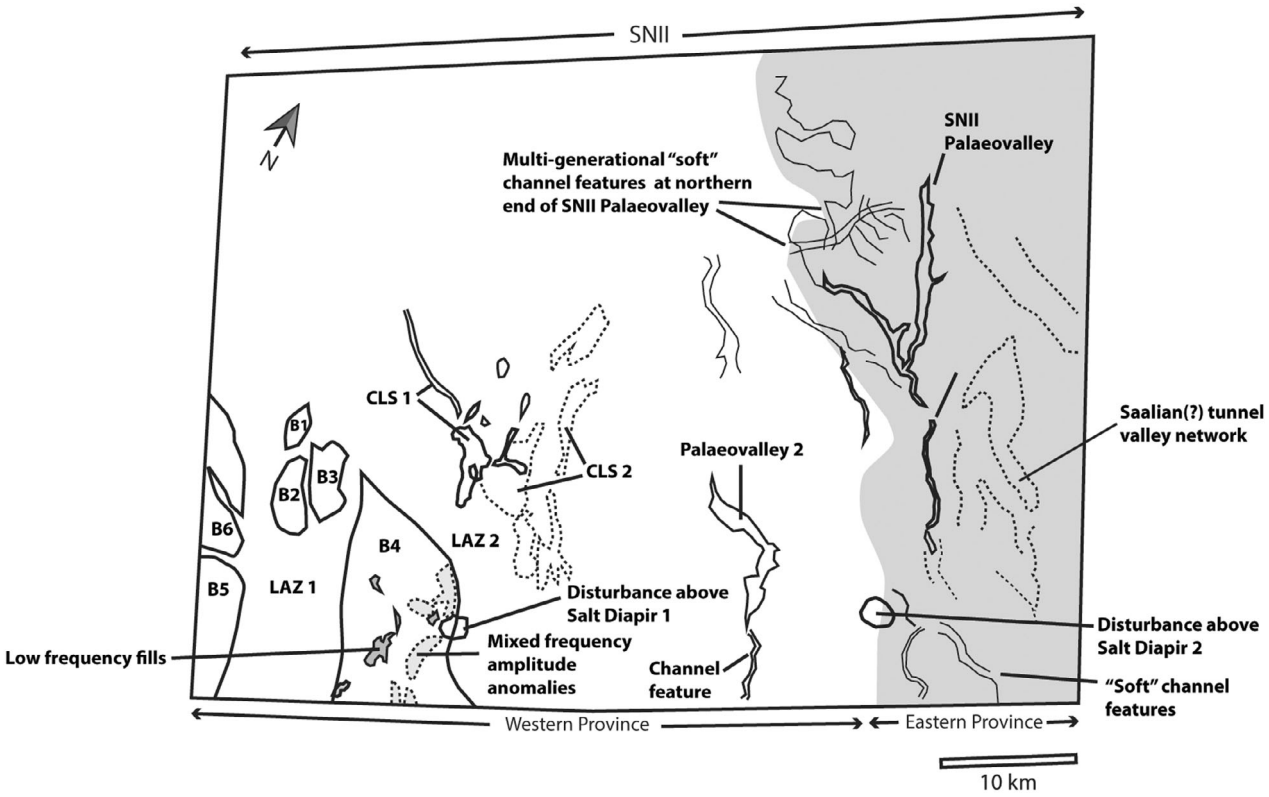

Fig. 5. Summary sketch map of main geomorphic features identified at seabed and near-seabed time slices on SNII 3D seismic data set.

weathering or movement of the salt, in addition to the presence of shallow hydrocarbons and/or other fluid leakage. Above some of the deeper salt structures, faulting, gas chimneys and shallow gas accumulations are clearly visible within the Neogene to Pleistocene stratigraphy (Fig. 4A, B, D), indicating that at least some of the salt structures in the area represent hydrocarbon migration pathways.

In the SNII area, the base Quaternary surface known as the Upper Regional Unconformity (Ottesen *et al.* 2014) is conformable and not easy to identify without deep borehole data. Instead, the Mid-Pleistocene glacial erosion surface (yellow horizon, Figs 5–7) was interpreted. This is characterized by large-scale, U-shaped incisions, interpreted as tunnel valleys, which cut down into the gently southward-dipping upper Neogene (Pliocene) and Lower Pleistocene reflections. The depth of the Mid-Pleistocene glacial erosion surface (and thus the thickness of the Mid–Late Pleistocene section) varies from ~85 m (where incisions are not present) to ~400 m below the seabed. Detailed 3D mapping of this surface is recommended for the installation of longer-piled foundations but was outside the scope of this study.

Within the Mid–Late Pleistocene section, around seven generations of incisional surfaces are present (Figs 6, 7, S3, S4), although these are difficult to correlate laterally owing to the highly variable seismic character of the valley infills and the substrates into which they are incised. Owing to a lack of age-constraining data, we group these incision surfaces tentatively under the Elsterian (the Mid-Pleistocene glacial erosion surface and incisions near the base of the tunnel valleys defined by this surface), Saalian (incision surfaces occurring near the middle and top of the tunnel valleys defined by the Mid-Pleistocene erosion surface) and Weichselian (near seabed incision surface which is mainly defined by the seabed reflection) glaciations (Figs 6A, 7A). The Mid-Pleistocene glacial erosion surface is mainly represented by a strong continuous hard reflection down to a maximum two-way-time depth of ~450 ms and defines the base of the deepest tunnel valley incisions (up to 100 s m deep and ~10 km across). Time-slice intersections show that this generation of tunnel valleys forms a complex cross-cutting network with a wide, slightly sinuous valley trending from W to E in the southern part of the site (E–W TV; Fig. 7D). In places, the steep sides of these older valleys (yellow line, Fig. 7A) can be traced to about 100 ms below the seabed. The ages of the deepest tunnel valleys are uncertain, but various investigations in the nearby Danish and UK sectors of the North Sea propose an Elsterian (Cotterill *et al.* 2017b) or Saalian (Huuse *et al.* 2001) age for the oldest tunnel valley generations in this part of the North Sea.

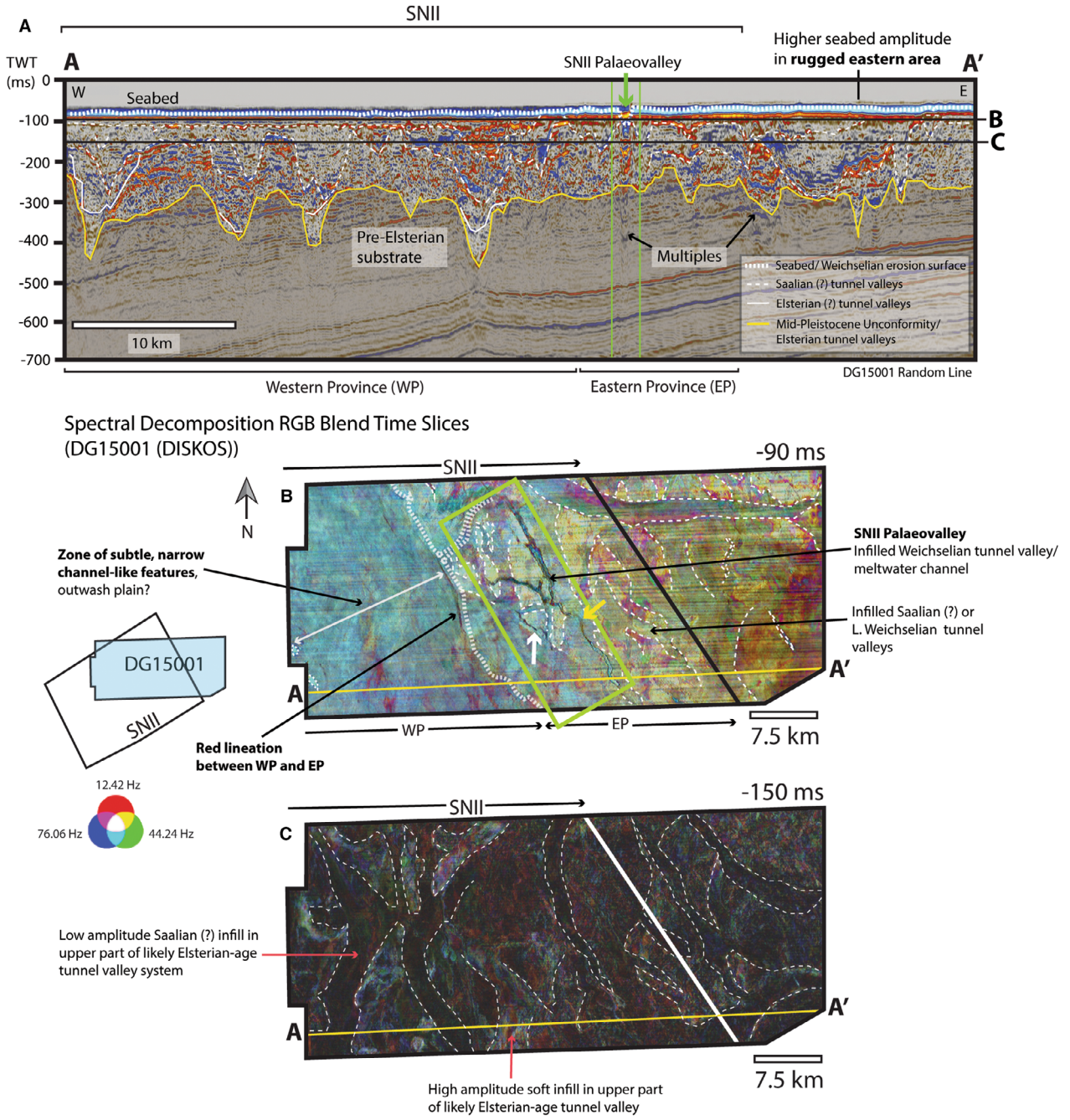

Fig. 6. A. Seismic profile through central SNII from seismic survey DG15001 (DISKOS) showing multigenerational Mid–Late Pleistocene erosional surfaces (tunnel valleys) within the upper ~400 m of the subsurface. B. −90 ms frequency decomposition blend time slice showing near-seabed Saalian to Holocene geomorphic features. C. −150 ms frequency decomposition blend time slice showing the network of multigenerational (Elsterian to Saalian?) tunnel valley incisions and infills located within the lower part of the 'foundation zone'. For versions without annotations and interpretations, see Fig. S3. L. Weichselian = Late Weichselian; TWT = two-way travel time.

Several generations of smaller-scale incised valleys occur within the lower parts of the Elsterian (?) tunnel valley infills (white solid lines; Figs 6A, 7A) which may represent additional smaller-scale Elsterian sub-glacial or fluvial incisions.

Several generations of shallower erosion surfaces occur within the middle to upper parts of the Elsterian (?) tunnel valley infills (thin white stipple; Figs 6A, 7A). These are interpreted as possible Saalian tunnel valleys given their position near the top of the infill of the larger Elsterian (?) aged valleys, but below the youngest incision surface (thick white stipple; Figs 6A, 7A). The youngest incision surface, which mainly coincides with the seabed reflection but also defines the base of many smaller-scale

V-shaped features, e.g. the SNII Palaeovalley (Fig. 7A), is most probably related to the most recent glaciation, the Late Weichselian. Dating from the 3/6-1 core (Hammer *et al*. 2016) confirms the presence of Late Weichselian sediments in at least the southwestern part of SNII.

Shallow geomorphic features in SNII. – Based on the generally shallow, rugged geomorphology and higher seismic amplitudes of the seabed reflection in the eastern part of SNII (Figs 5A, B, 6A, B), indicating a likely harder seabed/shallow stratigraphy than in the deeper, smoother western part of the site, we have subdivided SNII into an 'Eastern Province', where generally harder, more variable seabed conditions are expected and a 'Western Province,' where generally softer conditions, more uniform seabed conditions are expected.

Geomorphic features in each of the defined provinces, represented by subtle changes in the amplitude and frequency of the seabed reflection, were distinguishable on frequency decomposition blend time slices at and around −100 ms (~40 ms below the top of the seabed reflection) (Figs 6B, 7B) and to a lesser degree on the seabed depth map (Figs 8A, S5) and seismic time slices intersecting the seabed reflection (Fig. 8B, which mainly intersects the trough part of the seabed reflection). The key geomorphic features identified are summarized in Fig. 5 and described in detail below.

Eastern Province. – The most prominent geomorphic feature in eastern SNII is a ~20-km-long channel-like feature which we have named the SNII Palaeovalley (green box; Figs 6A, B, 7A, B, 8B, C). It is straight to slightly sinuous and comprises a single trunk valley in its southern half which splits into two branches in its northern half (Figs 6B, 7B, C). A shorter and narrower valley is also present south of the western branch (thick white arrow; Fig. 6B). In cross-section, each branch of the SNII Palaeovalley spans about 500 m across. The seabed reflection is significantly dimmer at the top of the valley infill (green arrow; Fig. 6A), while the valley base is defined by a very strong peak, indicating that the infill of the valley is much softer than the surrounding substrate into which the valley has incised. The middle part of the valley, a few kilometres south of where it branches, is narrower and less deeply incised than the southern and northern parts of the system (thick yellow arrow; Fig. 6B).

To the north and NW of the SNII Palaeovalley, seismic time slices and the MC3D-NDB2008 seabed depth map reveal additional 'soft' channel-like features with easterly and northwesterly orientations (thick white arrows; Fig. 8A, B). Some of these appear to connect with the northern branches of the SNII Palaeovalley, for some, this can only be inferred. The −80 ms seismic time slice with variance overlay also shows three sinuous, low-amplitude, channel-like features connecting to the southern end of the system (thick pink arrows; Fig. 8B). The plan-view geomorphologies of the main trunk and two main branches of the system, which are very straight overall, start and terminate abruptly, and vary in depth along their lengths, are typical of subglacial tunnel valleys observed across much of the North Sea (e.g. Ó Cofaigh 1996; Huuse & Lykke-Andersen 2000; Praeg 2003; Lutz *et al*. 2009; Stackebrandt 2009; van der Vegt *et al*. 2012; Ottesen *et al*. 2020). However, the presence of additional, shallower branches in the southern and northern parts of the system may indicate that it has been reused by fluvial and/or shallow marine systems after the Late Weichselian ice sheet had retreated from the area. It is for this reason that we refer to the system as a palaeovalley rather than a tunnel valley. A more detailed examination of the seismic facies within the SNII Palaeovalley is presented in the Shallow seismic stratigraphy section.

The SNII Palaeovalley runs parallel to the boundary between the earlier defined Eastern and Western Provinces of SNII (Figs 6B, 7B, 8A, B) On the DG15001 frequency decomposition blend, the near-seabed (−90 ms) time slice exhibits mostly red, yellow and white colours (low to mixed frequencies) in the Eastern Province, while the Western Province exhibits lower amplitudes and mostly pale blue (medium to high frequency) colours. The Eastern Province is characterized by a complex network of cross-cutting valleys of ~3–5 km width (thin white stipple; Fig. 6B), into which the SNII Palaeovalley has incised. The older valleys are wider, with much straighter sides and lower sinuosities, appearing geomorphically similar, in plan view, to the many subglacial tunnel valley systems previously mapped in the region (e.g. Jørgensen & Sandersen 2006; Kristensen *et al*. 2007; Ottesen *et al*. 2020). In seismic cross-section (Fig. 6B), these older valleys also show the typical U-shaped geometries of tunnel valleys. The remnants of older sediments located between the valleys are clearly distinguishable from the blue-green colours (medium to high frequencies) of the valley fills by their white-yellow colours (low-medium to mixed frequencies) on the frequency decomposition blend (Fig. 6B). The age of the valleys is uncertain, although given their shallow position they are probably related to either Saalian or Late Weichselian glacial erosion.

Western Province. – The western edge of the Eastern Province is defined ~5 km W of the SNII Palaeovalley (Fig. 6B). Beyond this, a broad zone of subtle, narrow channel-like features striking roughly N–S are observed on the DG15001 frequency decomposition blend (Fig. 6B). This zone is interpreted as a broad erosive area in which the more rugged topographic features seen in the Eastern Province have been removed. It is tentatively suggested that this could relate to the catastrophic drainage of the Late Weichselian North Sea Lake through the area (Hjelstuen *et al*. 2018), although this is speculative. An alternative interpretation

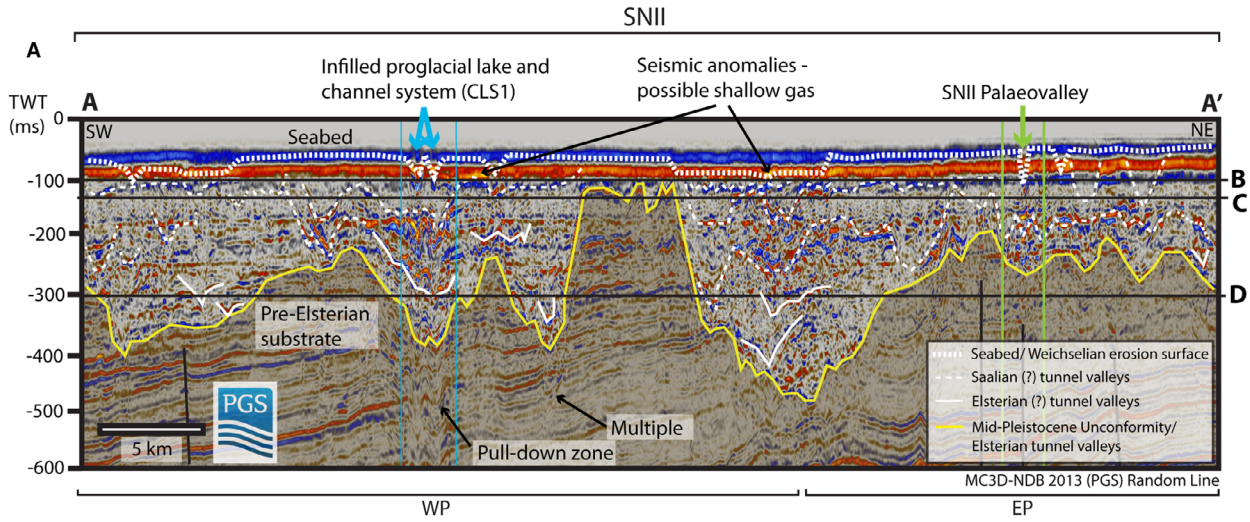

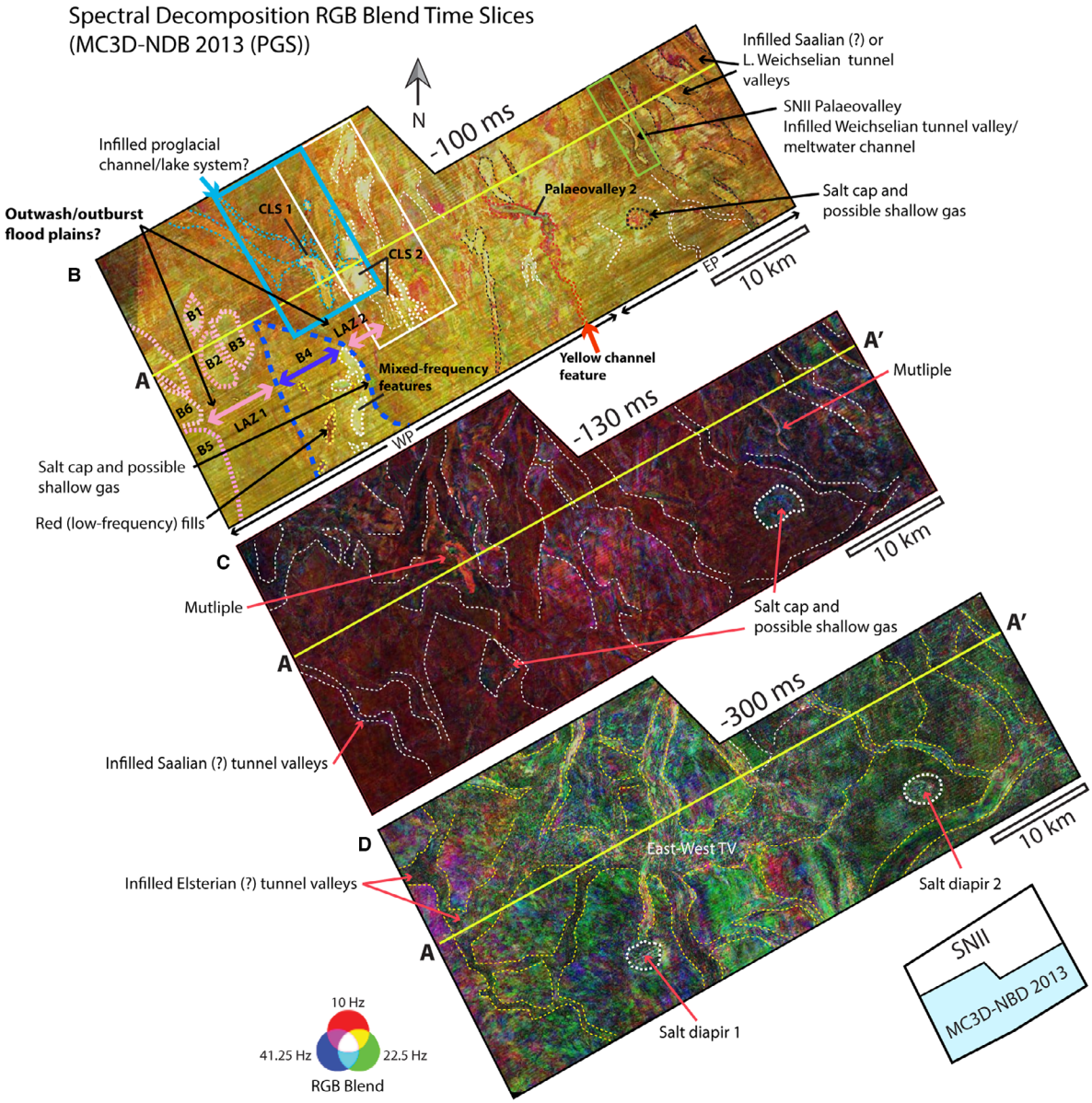

Fig. 7. A. Seismic profile through central SNII from seismic survey MC3D-NDB2013 (PGS) showing multigenerational Mid to Late Pleistocene erosional surfaces within the upper ~400 m of the subsurface. B. −100 ms frequency decomposition blend time slice showing near-seabed Saalian to Holocene geomorphic features. C. −130 ms frequency decomposition time slice showing salt cap rock outlines in southern SNII and D. −300 ms frequency decomposition time slice showing probable Elsterian tunnel valleys and Salt Diapirs 1 and 2. For versions without annotations and interpretations, see Fig. S4. L. Weichselian = Late Weichselian; TWT = two-way travel time.

is that glacifluvial erosion from the retreating Late Weichselian ice sheet formed the deeper, smoother topography of the Western Province. Postglacial fluvial erosion by rivers sourced from the EPV is another possibility.

The most prominent amplitude anomaly in western SNII is a N–S-trending, high-amplitude incisional feature, connected to several high-amplitude channel-like features to the north (Channel/Lake system (CLS) 1, light blue box; Figs 7A, B, 8A, B). Like in the SNII Palaeovalley, the seabed reflection is significantly weaker above CLS 1, while the trough below is significantly stronger, indicating an infill that is much softer than the surrounding substrate. A zone of pull-downs and a prominent multiple of the high-amplitude features are also present in the seismic beneath it (light blue box, Fig. 7A). A zone of high-amplitude reflections within the Elsterian tunnel valley fill at ~200 ms (light blue box, Fig. 7A) could also indicate that the very soft signature at the seabed is related to an accumulation of shallow hydrocarbons migrating from below CLS 1. The size and plan-view morphology of CLS 1 are similar to those of a modern proglacial lake system (e.g. Lake Tasman in Dykes *et al.* (2010) and Lake Mueller in Fitzsimons & Howarth (2017)). A less prominent but similarly shaped white (mixed frequency) feature, and several other white channel and splay-like features are also observed to the east of CLS 1 (CLS 2, white box, Fig. 7B) and may represent deposits from an earlier proglacial channel and lake system. Based on the channel features feeding into CLS 1 and CLS 2t from the NW and the NE, it is assumed that their formation is probably related to the outpouring of glacial meltwater ahead of the retreating Late Weichselian ice sheet, although additional input channels from other directions may have existed but have subsequently been removed by marine erosion. Without mapping out a larger area and additional features as CLS 1 and CLS 2, it is not possible to be certain if these were likely to have been formed by meltwater sourced from the retreating ice margin, although this is the depositional model for the 0.5–1 km wide channel features mapped between Late Weichselian moraine ridges north of Dogger Bank (Phillips *et al.* 2018).

In the southwestern part of SNII, frequency decomposition blend time slices and to a lesser degree seismic amplitude time slices also reveal a straight, ~7-km-wide, lower amplitude zone, that runs parallel to the western edge of the site (low amplitude zone (LAZ) 1; Fig. 7B), splitting into several straight branches separated by higher amplitude yellow-white bars (B1–3; Fig. 7B) about 10 km south of Greater Fish Bank. A similar lower amplitude zone is also observed in the central part of the site (LAZ 2; Fig. 7B), separated from the LAZ 1 by a higher amplitude, ~10-km-wide, lozenge-shaped area (B4; Fig. 7B). Bars B1–B4 have geometries similar to the bars that form within braided rivers (cf. Bridge & Lunt 2006) or catastrophic outburst floodwater channels (e.g. Bretz *et al.* 1956; Bellwald *et al.* 2021). We therefore tentatively interpret B1–4 as bar-shaped remnants of older sediments left within the two broad zones of erosion (LAZ 1 and LAZ 2). The mechanism by which this erosion was achieved is uncertain, although a possible candidate would be the Late Weichselian North Sea Lake outburst flood from the south (Hjelstuen *et al.* 2018) or glacifluvial action related to the former Late Weichselian ice sheet to the north.

B4 mainly exhibits yellow colours on the frequency decomposition blend, indicating low to medium frequencies in the data (Fig. 7B). However, there are four small (<4-km-long), red-coloured (low-frequency), elongated to crescent-shaped features in the southern half of B4 (yellow stipple; Fig. 7B). These are interpreted as possible small, infilled lake basins preserved between the erosive zones on either side of B4. In contrast, the eastern side of B4 is characterized by five high-amplitude, white (mixed frequency) features (white stipple; Fig. 7B). These represent amplitude anomalies located close to the cap rock zone of the shallowly buried (~115 m below the seabed) Salt Diapir 1 (Figs 7D, 8B), which could represent shallow hydrocarbon accumulations.

Within the easternmost part of the Western Province, an elongated, NW–SE-trending feature exhibits red–green (low-medium frequencies) on the −100 ms frequency decomposition blend time slice (termed Palaeovalley 2, red stipple; Fig. 7B). It has a similar geomorphology to the interpreted proglacial lake system CLS 1 to the west, although it is longer, with rougher sides and may have had a southern rather than northern source, indicated by a sinuous, yellow, channel-like feature connecting to its southern end (red arrow; Fig. 7B). Another difference is that this system has a much lower impedance contrast to the surrounding substrate into which it is incised, as indicated by its more subtle appearance on the −80 ms seismic time slice (profile G–G′; Fig. 8B) where it is only revealed by variance and not by any strong amplitude anomaly as is the case for CLS 1. The frequency properties of Palaeovalley 2 are more similar to the smaller isolated lake infills located within the B4 bar in the southwestern part of the site (yellow stipple; Fig. 7B) and could perhaps

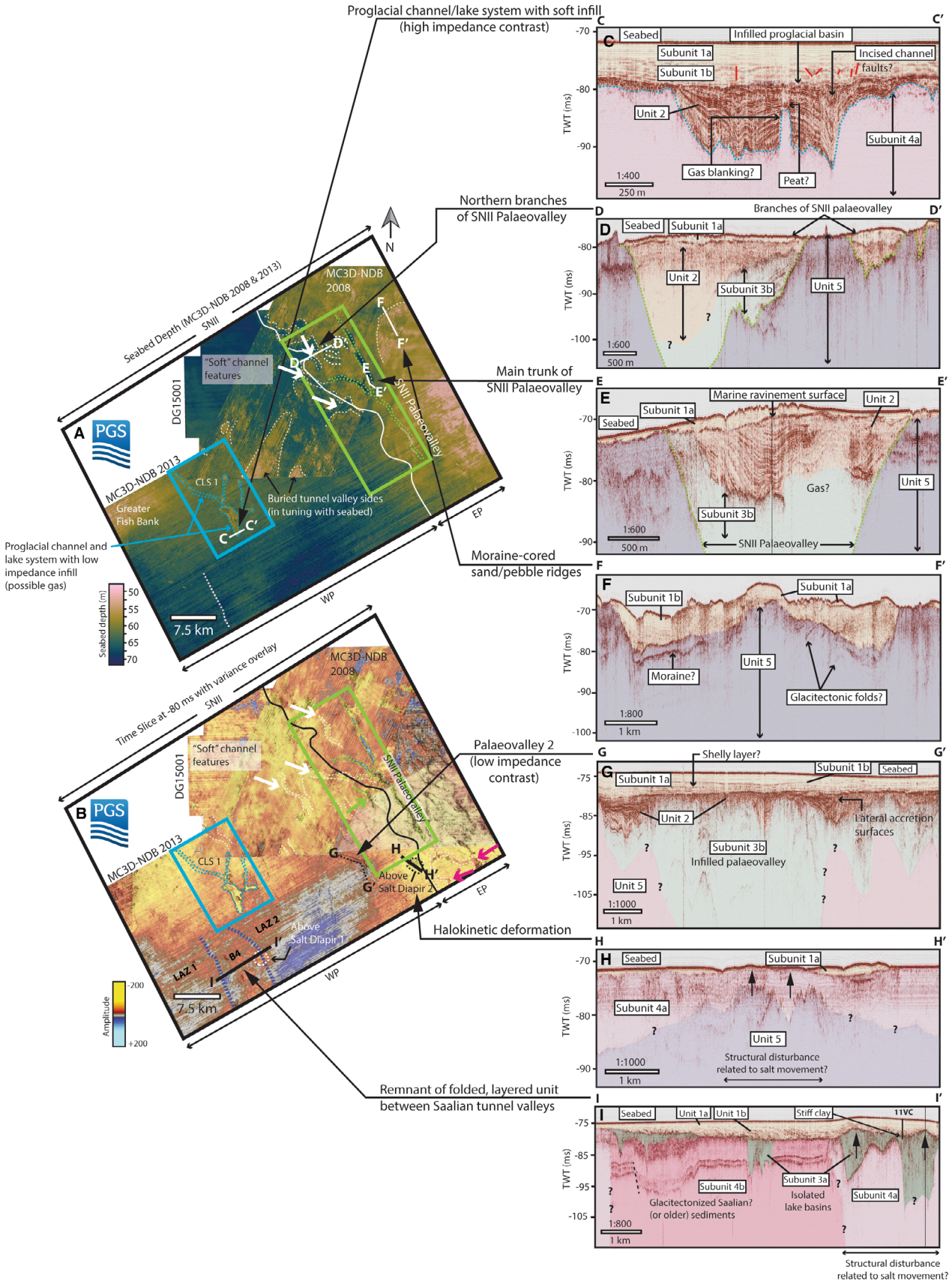

Fig. 8. A. Seabed depth from MC3D-NDB2008 (PGS), MC3D-NDB2013 (PGS) and DG15001 (DISKOS) (background). B. −80 ms seismic time slices with variance overlays from DG15001 (DISKOS), MC3D-NDB2013 (PGS) and MC3D-NDB2008 (PGS) (background). TOPAS profiles through: C. An infilled proglacial lake system interpreted in western SNII, D. Northern branches of the SNII Palaeovalley, E. Main trunk of the SNII Palaeovalley, F. Ridges of surficial sand in northeastern SNII overlying moraines and glacitectonized deposits, G. Smaller infilled palaeovalley system SW of SNII Palaeovalley, H. Possibly structurally disturbed sediments above Salt Diapir 2, I. Infilled isolated incisional basins containing overconsolidated glacilacustrine clays, possibly pushed up in the eastern part of the profile by movement of Salt Diapir 1 after the LGM. For versions without annotations and interpretations, see Fig. S5. EP = Eastern Province; LGM = Last Glacial Maximum; TWT = two-way travel time; WP = Western Province.

have more similar properties to these, i.e. could be filled by stiff rather than soft sediments.

Integrated shallow seismic stratigraphy and core observations

In this section, seismic units mapped on the SNII sub-bottom profiler data set are presented (Figs 8, 9, S5, S6). Five units (and associated subunits) are described and integrated with 3D seismic observations, sedimentological and geotechnical information from borehole (3/6-1) and multisensor core logger, shear strength and visual analysis from the SNII vibrocore data set (Figs 9–12, S7–S9). They are also summarized in Table 1.

Unit 5, chaotic high-amplitude facies (eastern SNII). – Subunit 4a and Unit 5 are defined separately on the basis of their contrasting seismic characters and probably geotechnical differences. Unit 5 is an acoustically transparent to chaotic, highly heterogeneous seismic unit comprising multiple rugged, high-amplitude internal reflections of variable lateral continuity (Figs 8D, E, F, 9A, 10). In the Eastern Province, the top of the unit is mainly, but not exclusively, characterized by strong amplitudes. It mainly occurs tens of centimetres to several metres below the seabed but is also locally exposed at the seabed (Fig. 8D, F). A prominent exception to this is where Unit 5 is deeply incised (down to ~20 m) by the SNII Palaeovalley described in the previous section (Fig. 8D, E). In general, however, top Unit 5 is a shallowly buried, rugged surface characterized by ridges and troughs, which have influenced the thicknesses of the overlying (Unit 1) seafloor sediments (Figs 8F, 9A, 10D). The base of Unit 5 is not visible on the TOPAS data set (which penetrates down to ~40 m).

A range of seismic facies are observed within Unit 5. The upper 5–10 m are characterized by rugged, medium- to high-amplitude reflections which define a complex network of buried ridges and troughs (Fig. 9A), which correlate spatially to the network of Saalian (?) tunnel valleys observed on near-seabed frequency decomposition blend time slices from the 3D seismic data set (Figs 5A, B, 9C). The infill facies of the valleys are generally seismically transparent to chaotic, but gently dipping parallel-layered infill facies are also observed. In one of the profiles, the layering appears to be affected by near upright, antiform, close, similar folding (Fig. 8F) similar to that found within proglacial thrust wedges (Phillips 2018).

The buried valley landscape within Unit 5 is truncated in places by high-amplitude, subhorizontal reflections (e.g. the reflection marked with a black line in Fig. 10D) and overlain by a chaotic to transparent seismic facies of variable thickness (~0–3 m). In vibrocore 02VC, the high-amplitude reflection shown in black (Fig. 10D) was found to represent the top of a 40-cm-thick diamicton layer comprising clay, sand, gravel, pebbles and shell fragments characterized by a higher gamma density (2.4–2.6 g cm^{-3}) than the underlying and overlying gravelly sand deposits (with densities of 2.0–2.2 g cm^{-3}). This is interpreted as a till, probably deposited during the Late Weichselian glaciation, given its shallow position. The gravelly sands below the till have not yet been dated but given the Saalian to Eemian age of the sands encountered in the 3/6-1 boring in the southwestern part of SNII (Hammer *et al.* 2016), it is possible that the deeper parts of Unit 5 represent glacially reworked/glacitectonized Saalian to Mid-Weichselian aged marine sands or possibly older deposits. The seismically transparent to chaotic gravelly sand layer above the till probably represents a late glacial proglacial or postglacial marine deposit. The coarseness of the deposit overlying the till may suggest that it was reworked locally from the till and the gravelly sand deposits that lie beneath it, within the shallow marine environment that occupied the area prior to full marine inundation. Alternatively, the gravelly sands could have been transported by glacial outwash, prior to marine inundation, during the retreat of the Late Weichselian ice sheet. A postglacial fluvial origin for the gravelly sands cannot be ruled out, but seismic evidence for fluvial channels in the Eastern Province is largely lacking, with the exception of the 'soft' channel features at the southern and northern ends of the SNII Palaeovalley (pink arrows and white arrows; Fig. 8B). The high-amplitude reflections at top Unit 5 were found to represent a 60-cm-thick, loose, clast-supported pebble layer. It is uncertain how laterally extensive or common such deposits may be across the Eastern Province, although a similar density log signature is observed at the top of Unit 5 in northeastern SNII from vibrocore 08VC. This layer is described in more detail in the section 'Subunit 1b, layered facies in western SNII, chaotic facies in eastern SNII'.

Below the smoother, deeper seabed bathymetry of the Western Province, the top Unit 5 reflection becomes increasingly difficult to identify on the sub-bottom profiles (Fig. 9A). A weak, patchy reflection at ~10 m below the seabed below the eastern part of the Western

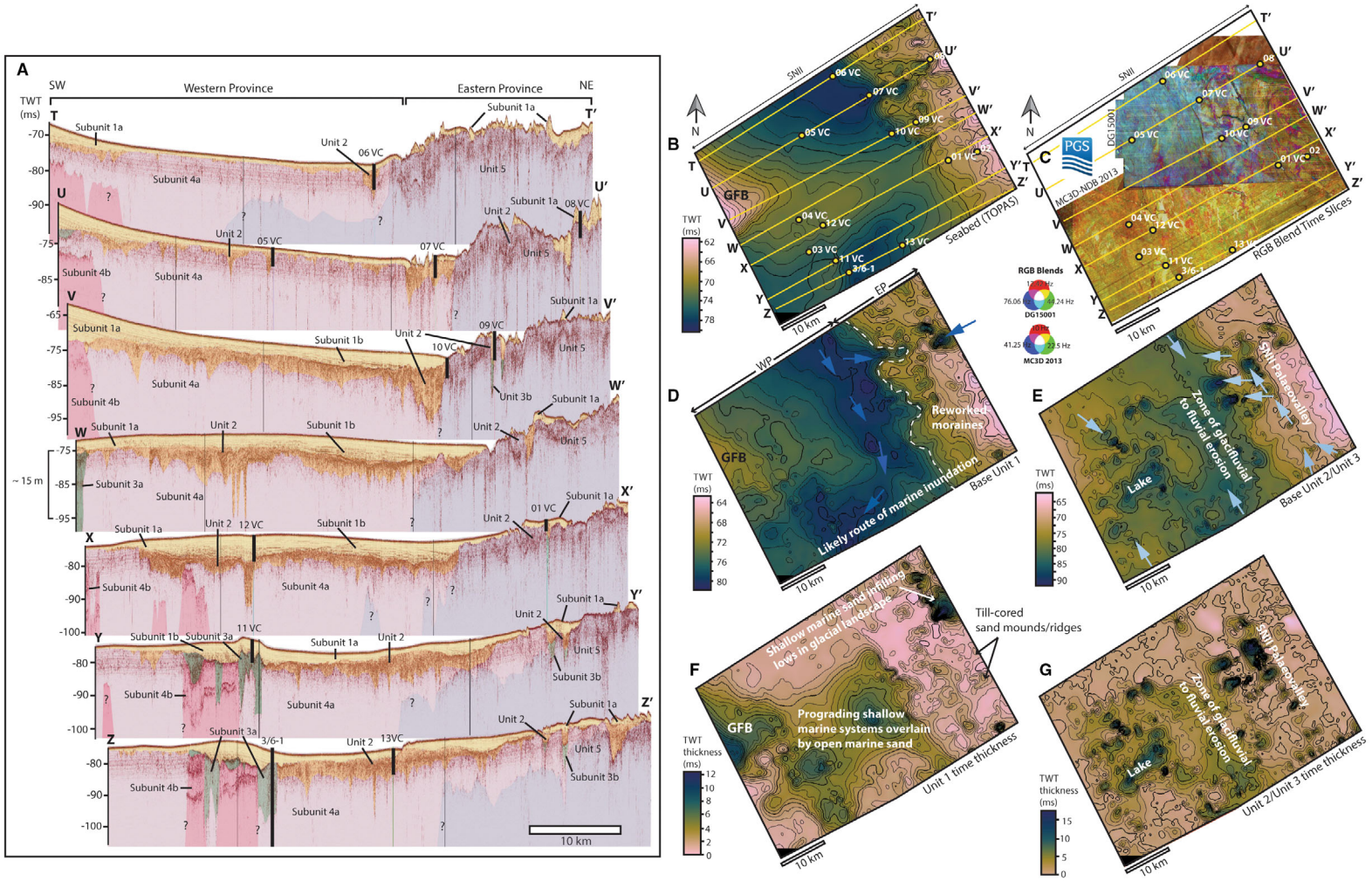

Fig. 9. A. Southwest- to NE-trending sub-bottom profiles through SNII showing interpreted seismic units, vibrocore locations and location of geotechnical boring 3/6-1 (unit colours correspond to preliminary ground model, Fig. 13). B. Seabed time map interpreted on sub-bottom profiler data set showing sub-bottom profile locations (yellow lines) presented in A and core locations (yellow circles). C. −100 ms time slice through frequency decomposition blends extracted from MC3D-NDB2013 (PGS) and DG15001 (DISKOS) with time slice from MC3D-NDB2008 (PGS) in the background for comparison between geomorphic features resolved on conventional 3D seismic time slices vs. those resolved on sub-bottom profiles. D. Annotated base Unit 1 (Holocene marine sand) time map interpreted on sub-bottom profile data set. E. Combined base Unit 2 and base Unit 3 (basal Late Weichselian subglacial/proglacial erosion surface) time map based on sub-bottom profile data set. F. Annotated Unit 1 time thickness map (Holocene sediments). G. Unit 2/3 time thickness map (Late Weichselian to Holocene sediments). For versions without annotations and interpretations, see Fig. S6. TWT = two-way travel time.

Table 1. A summary of seismic facies descriptions and genetic interpretations for each of the seismic units/subunits identified on the Sørlige Nordsjø II offshore wind site (SNII) sub-bottom profiler data set.

Sub-bottom profiler units/subunits	Seismic facies description	Genetic interpretation
Subunit 1a	Transparent drape in west, ridges in east	Holocene to modern open marine deposition
Subunit 1b	Localized to chaotic facies	Localized shallow marine systems (shorefaces, beaches, tidal bars?)
Unit 2	High- to very-high-amplitude, strongly layered, occurring within near-surface incisions	Transitional facies from proglacial outwash to postglacial transgressive fluvial/lacustrine
Subunit 3a	Transparent to chaotic, occurring within isolated basins	Glacial lake infills
Subunit 3b	Transparent to chaotic to weakly layered, occuring at base of palaeovalleys	Subglacial to proglacial palaeovalley infill
Subunit 4a	Transparent with occasional weak internal reflections and medium-amplitude vertical features	Pre-LGM marine deposits
Subunit 4b	Localized folded (and faulted?), parallel to subparallel layered facies	Eroded remnant of glacitectonized deposits (original depositional environment uncertain)
Unit 5	Transparent to choatic, occasionally layered, with internal erosion surfaces	Subglacial and glacitectonized/glacially eroded deposits

Province may represent a deeper, westward continuation of top Unit 5, although this is highly uncertain. Several possible explanations for the apparent absence or increase in burial depth of Unit 5 in the Western Province are considered. One possibility is that Unit 5 was more deeply eroded by glacial action in the Western Province, with a younger sediment unit (Subunit 4a) now juxtaposed with Unit 5 (Fig. 9A). A second explanation is that Subunit 4a and Unit 5 actually comprise a single sedimentary unit that have experienced different degrees of subglacial erosion and glacitectonic compression, with erosion and deformation having been focused on the eastern part of the site, creating a more chaotic and heterogeneous seismic facies there. A third explanation is that the strong reflections and chaotic seismic facies observed in the upper part of Unit 5 were once also present in upper Subunit 4a but were subsequently removed by glacial or postglacial erosion which affected the Western Province more strongly owing to its lower elevation.

Unit 4, layered and structureless facies (western SNII). – Unit 4 comprises two subunits, Subunit 4b, a layered, folded seismic facies only present locally in the south-western and western parts of SNII and Subunit 4a, a largely transparent seismic facies with a wide distribution in the Western Province (Fig. 9A; Table 1), described separately below.

Subunit 4b, deformed, layered facies (patchy distribution, southwestern SNII). – Subunit 4b comprises a seismic facies containing folded and possibly faulted high-amplitude reflections only present in western and southwestern SNII (Figs 8I, 9A). The strong, broadly parallel reflections within Subunit 4b terminate abruptly, apparently truncated, and are juxtaposed with the transparent facies of Subunit 4a (Fig. 8I). The occurrence of this folded, layered facies was found to correlate with subtle amplitude and frequency changes on 3D seismic time slice attribute maps (Figs 8B, I, 9C), with occurrences of Subunit 4b in sub-bottom profiles correlating to the features B1–B6 outlined in the previous section (Fig. 7B). Occurrences of Subunit 4b are therefore interpreted as remnants of once laterally extensive, layered deposits which have largely been removed by erosion. The age of Subunit 4b is highly uncertain. The juxtaposition of Subunit 4b with Subunit 4a (which dates on the 3/6-1 core by Hammer *et al.* (2016) indicate to be of Saalian to Mid-Weichselian age) indicates that Subunit 4b could be as old as Saalian age, with much of it being removed by the Saalian glacial erosion and Saalian, Eemian and Weichselian marine deposits subsequently infilling the valleys between the Subunit 4b remnants. However, the braid-bar-like appearance of features B1–B4 indicate that Subunit 4b could in fact be younger Weichselian-aged deposits largely removed by late glacial to postglacial fluvial processes such as outwash drainage or the outburst flood of the Late Weichselian North Sea Lake.

Subunit 4a, structureless facies (widespread, western SNII). – Subunit 4a is mainly seismically transparent, with sparse, low-amplitude internal reflections and a weak top reflection (Fig. 9A). It occurs ~1 m below the seabed in the northern part of the Western Province, occurring progressively deeper southwards owing to the presence of thicker surficial seabed sediments (Unit 1) and infilled incisions (Unit 2 and Subunit 3A) which occur in the central and southern parts of the Western Province (Fig. 9A). Where it has not been heavily incised by base Unit 2/base Subunit 3a, the upper few metres of Subunit 4a are characterized by narrow, medium amplitude, vertical features (e.g. profiles T–T′ and U–U′; Fig. 9A), which may represent subaerial, periglacial weathering features such as ice-wedge casts (e.g. Svensson 1988) or sand wedges (e.g.

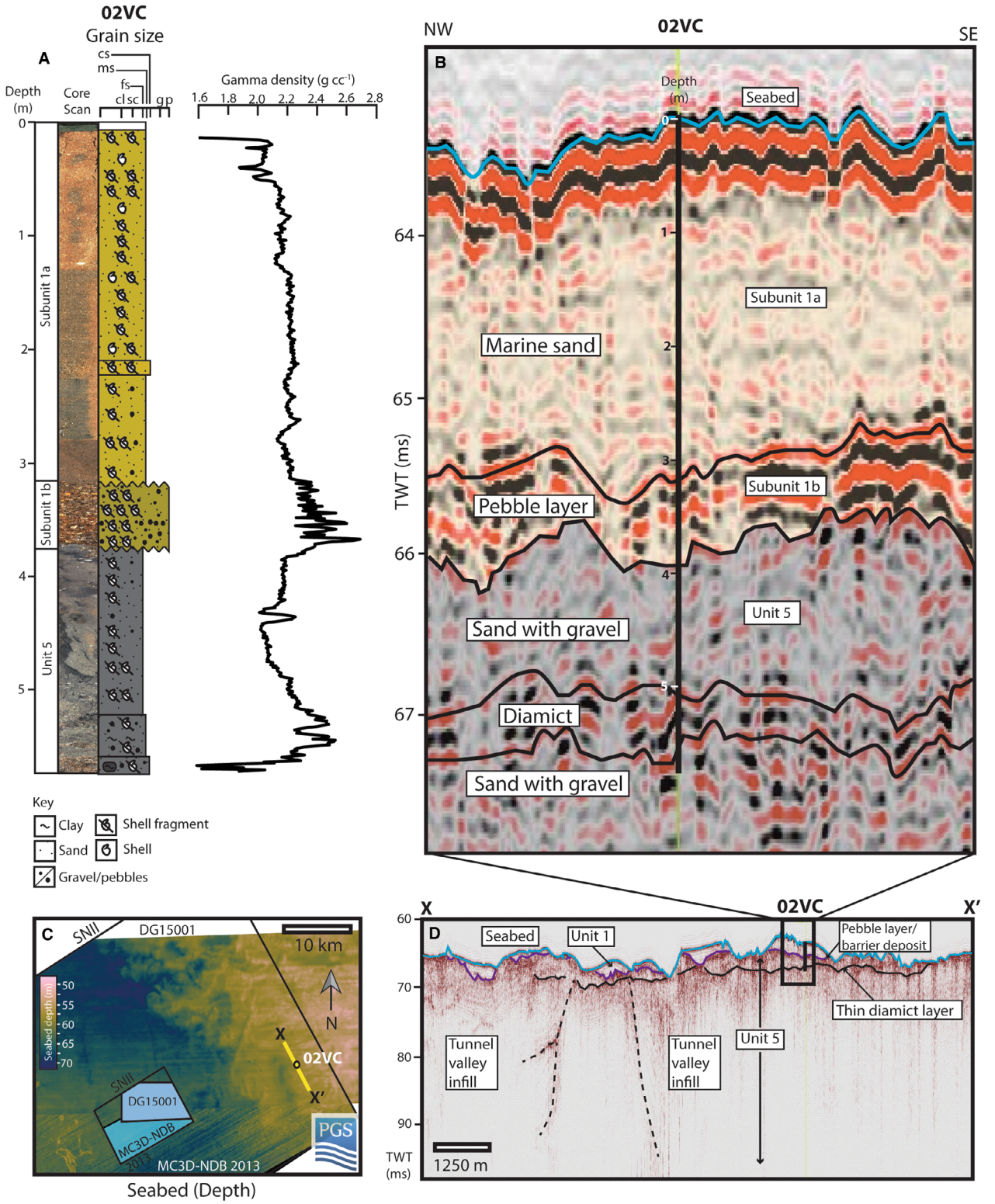

Fig. 10. A. Core scan photograph, sedimentary log and gamma density log for vibrocore 02VC. B. Northwest–SE sub-bottom profile correlated to 02VC. C. Seabed depth map from surveys DG15001 (DISKOS) and MC3D-NDB2013 (PGS) showing the location of profile X–X′. D. Northwest–SE sub-bottom profiler cross-section through 02VC location, showing high-amplitude reflections present locally in upper Unit 5 and at base Unit 1 which are interpreted to correlate with the 02VC diamict and pebble layers respectively. For versions without annotations and interpretations, see Fig. S7. Cl = clay; sc = silty clay; fs = fine sand; ms = medium sand; cs = coarse sand; g = gravel; p = pebbles; TWT = two-way travel time.

Washburn 1980). These features are largely absent from Subunit 4a where Unit 2 overlies it (e.g. Fig. 8C) and have probably been removed by postglacial erosion processes. In southern SNII, Subunit 4a is also tentatively mapped into parts of the Eastern Province where the transparent seismic facies appears to continue eastwards and drape the weak, rugged reflection interpreted as top Unit 5 (profiles Y–Y′ and Z–Z′; Fig. 9A). Generally, the base of Subunit 4a is not visible on the sub-bottom profiler data set, with the exception of where it is underlain by or juxtaposed to older seismic units (Subunit 4b, Unit 5).

In southwestern SNII, Subunit 4a is sampled by the 3/6-1 core (Fugro 2000) (profile Z–Z′; Fig. 9A), which is summarized in Fig. 2. We correlate our Subunit 4a with the largely sandy Fugro lithostratigraphic units IV, V and VI on the basis that our Subunit 3a, the transparent to chaotic facies infilling a small basin which incises into Subunit 4a, most likely correlates with hard glacilacustrine clays of Fugro Unit III (Fig. 2, profile Z–Z′; Fig. 9A). The penetrated section of Subunit 4a therefore probably largely comprises loose to medium density, Saalian to Eemian age, silty sand (Unit VI), overlain by 1 m of hard clays (Unit V) and 1 m of loose, silty, marine sand of Mid Weichselian age (Knudsen 2000; Hammer *et al*. 2016). The interpreted top Subunit 4a boundary is a weak, undulating to chaotic reflection which most likely correlates to the acoustic impedance contrast between the hard glacilacustrine clays of Subunit 3a (Fugro Unit III) and the underlying sand-dominated succession of Subunit 4a (Fugro units IV, V and VI) (profile Z–Z′; Fig. 9A).

Despite the largely homogeneous appearance of Subunit 4a in sub-bottom profile, the correlated lithostratigraphic Units IV, V and VI (Fugro 2000) vary significantly in grain size and age. Within Unit VI, the upper part of the unit comprises silty, fine to medium sand, with pockets of hard clay, assigned an Early Weichselian age (Hammer *et al*. 2016). Between 14 and 24 m, the sands of Eemian age, while below 24 m, are Saalian age (Hammer *et al*. 2016). Below 28 m, the Saalian-aged sands are coarser and contain rounded gravel and shell fragments. At 30 m depth, the sand becomes finer again, comprising a silty, fine sand, with a ~1-m-thick layer of sandy silt. Although there do not appear to be large acoustic impedance contrasts between the Saalian, Eemian and Early to Mid-Weichselian deposits, significant variability in friction angle measurements is documented (from 20 to 45° between 15 and 22 m depth within the Eemian sands vs. 26° within the Mid Weichselian sands). These indicate that there are important geotechnical variations within Subunit 4a which cannot necessarily be mapped out on standard shallow acoustic data sets.

Unit 3, transparent to layered facies (localized incisions, eastern and western SNII). – Unit 3 comprises two seismic subunits (Table 1). They are tentatively interpreted to be of similar age (Late Weichselian), although their differences in seismic and geomorphic character indicate deposition within separate subglacial to proglacial drainage systems as outlined below.

Subunit 3b, variable facies in lower tunnel valley fills (eastern SNII). – Subunit 3b comprises transparent, chaotic and weakly layered seismic facies which infill the lower parts of the SNII Palaeovalley system (Figs 8D, E, 9A, 11D) and the Palaeovalley 2 (profile G–G′; Fig. 8G). These basal valley fills are both incised by younger erosion surfaces and overlain by the more strongly layered facies of Unit 2. The top Subunit 3b erosion surface varies from a very strong reflection in some parts of the valleys to a completely invisible boundary in other parts. In some cases (Fig. 8D), this is probably due to a low acoustic impedance contrast between Subunit 3b and Unit 2, but in other parts of the SNII Palaeovalley, zones of blanking affecting both Subunit 3b and Unit 2 appear to obscure the top Subunit 3b reflection (Fig. 8E). The blanking zones are relatively common within the SNII Palaeovalley and are interpreted as being related to possible shallow biogenic gas accumulations.

Within the SNII Palaeovalley, the base of Subunit 3b represents the erosive base of the valley, which also varies from a very hard to absent reflection. The valley sides truncate subhorizontal reflections with the substrate, Unit 5, into which the valley is incised (Figs 8D, E), down to a maximum of ~30–35 ms (~20 m) below the seabed (Fig. 11D). Along the southwestern side of one of the northerly branches of the valley system, a transparent part of Subunit 3b was penetrated by the 09VC vibrocore (Figs 11B, D). The transparent facies was found to comprise low shear strength (20–50 kPa), strongly laminated, grey and black (organic rich) clays (containing brackish cold-water foraminifera *Elphidium*). The transition into the overlying Unit 2 sediments is subtle, marked only by a weak reflection and a slight colour change into overlying, slightly less organic-rich, slightly weaker clay (Fig. 11A, B). Strongly laminated clays associated with cold (glacial settings) are often referred to as rhythmites, with the laminations forming seasonally in correspondence with pulses of meltwater input from a nearby retreating ice mass (e.g. Evenson *et al*. 1977; Powell & Molnia 1989). The cored part of Subunit 3b is therefore tentatively interpreted as a proglacial or glacimarine deposit, similar to the overlying Unit 2.

In deeper, more central parts of the SNII Palaeovalley system unreachable by vibrocorer, Subunit 3b is characterized by much higher amplitude layers than those encountered in vibrocore 09VC, including a seismic facies comprising discontinuous clusters of very-high-amplitude reflections near the top of Subunit 3b and the base of Unit 2 in the northeastern part of the valley system (Fig. 11E). As TOPAS profiles do not distinguish between very hard or very soft signatures, this facies could represent very hard, discontinuous layers (such as

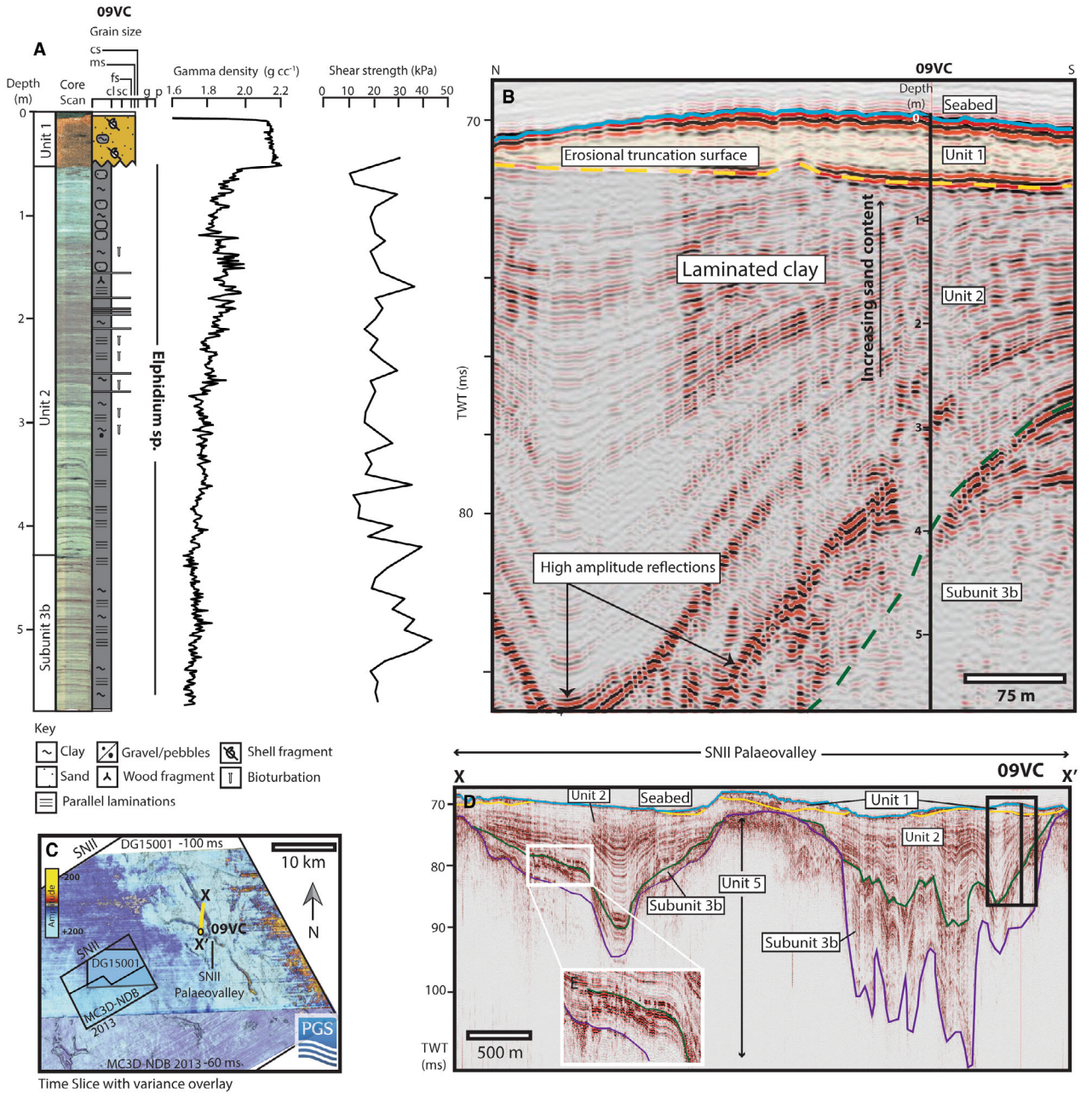

Fig. 11. A. Core scan photograph, sedimentary log, gamma density log and shear strength measurements for vibrocore 09VC. B. North–south sub-bottom profile correlated to 09VC showing multiple generations of soft, laminated clays (rhythmites) truncated and overlain by medium-grained marine sand. C. Seabed depth map from surveys DG15001 (DISKOS) and MC3D-NDB2013 (PGS) showing the location of profile X–X′. D. North–south TOPAS profile through 09VC showing the multigenerational infill of the northwestern and northeastern branches of the SNII Palaeovalley. E. Zoomed in section of high amplitude, discontinuous seismic facies in upper part of Subunit 3b and lower part of Unit 2 in SNII Palaeovalley. For versions without annotations and interpretations, see Fig. S8. Cl = clay, sc = silty clay, fs = fine sand, ms = medium sand, cs = coarse sand, g = gravel; p = pebbles; TWT = two-way travel time.

an eroded desiccation surface, or coarse deposits such as ice-rafted debris) or very soft, discontinuous layers (such as eroded organic rich deposits). The presence of organic-rich layers within upper Subunit 3b is consistent with the presence of minor gas blanking zones in upper Subunit 3b/lower Unit 2, and similar blanking above high-amplitude incision infills are recorded in other palaeovalleys in the region, such as the EPV (Özmaral *et al*. 2022).

The presence of Subunit 3b within Palaeovalley 2 (Fig. 8G) is interpreted tentatively. Palaeovalley 2 is resolved well on frequency decomposition time slices

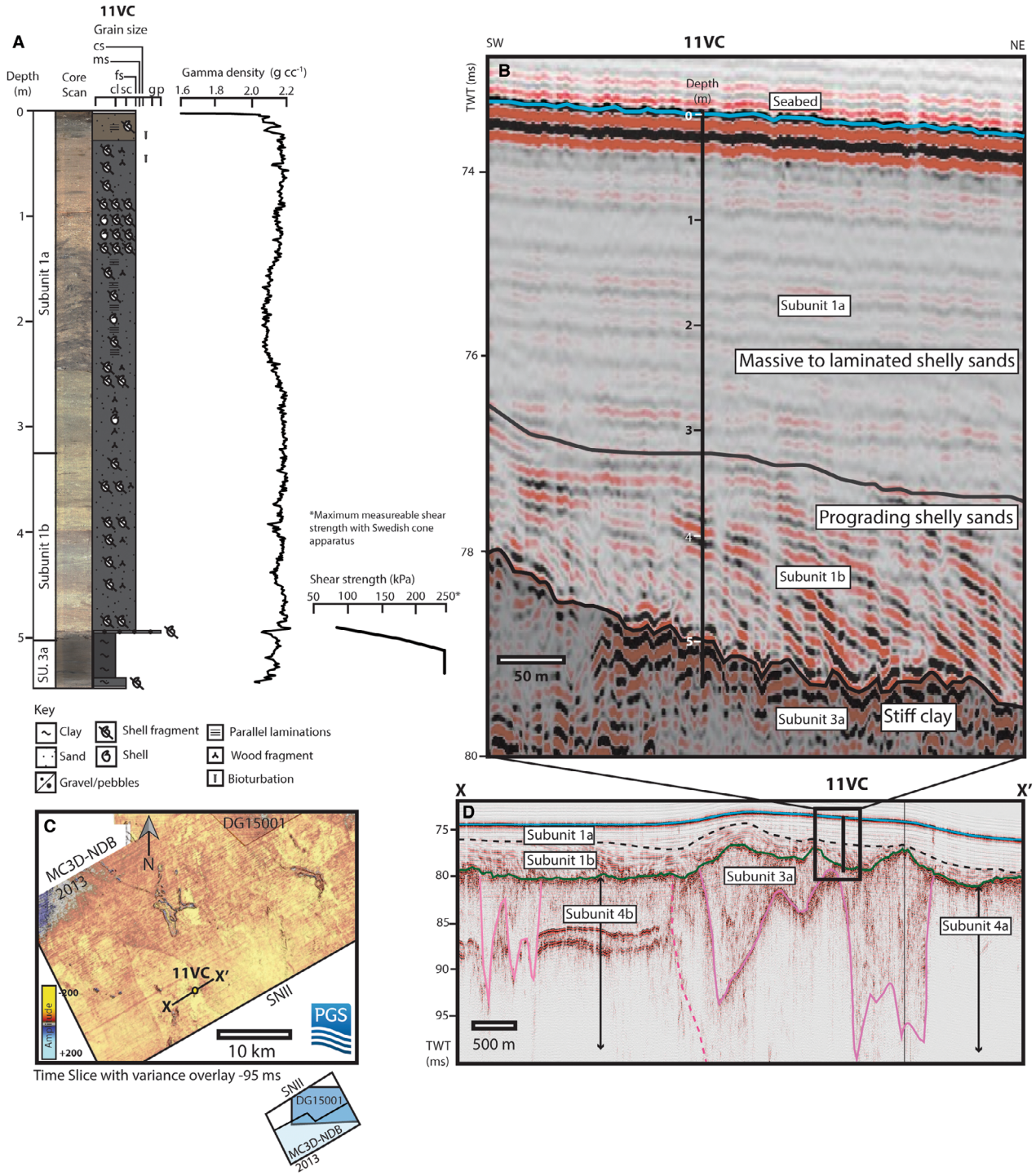

Fig. 12. A. Core scan photograph, sedimentary log, gamma density log and shear strength measurements for vibrocore 11VC. B. Southwest–NE sub-bottom profile correlated to 11VC showing desiccated glacilacustrine clays overlain by prograding shallow marine sands and acoustically transparent marine sands (e.g. Fig. 13D). C. Seabed depth map from surveys MC3D-NDB2013 (PGS) and DG15001 (DISKOS) showing the location of profile X–X′. D. Southwest–NE sub-bottom profile through 11VC showing the zone of shallow stratigraphy located above Salt Diapir 1 (the diapir is located below the penetration depths of the sub-bottom profiler). For versions without annotations and interpretations, see Fig. S9. Cl = clay; sc = silty clay; fs = fine sand; ms = medium sand; cs = coarse sand; g = gravel; p = pebbles; TWT = two-way travel time.

(Fig. 7B), but lacks a strong base reflection like that observed at the base of the SNII Palaeovalley (Fig. 10D). 3D seismic time slices also indicate that the infill of Palaeovalley 2 possesses similar seismic amplitudes to the surrounding substrate, unlike the fill of the SNII Palaeovalley, which is significantly softer than the

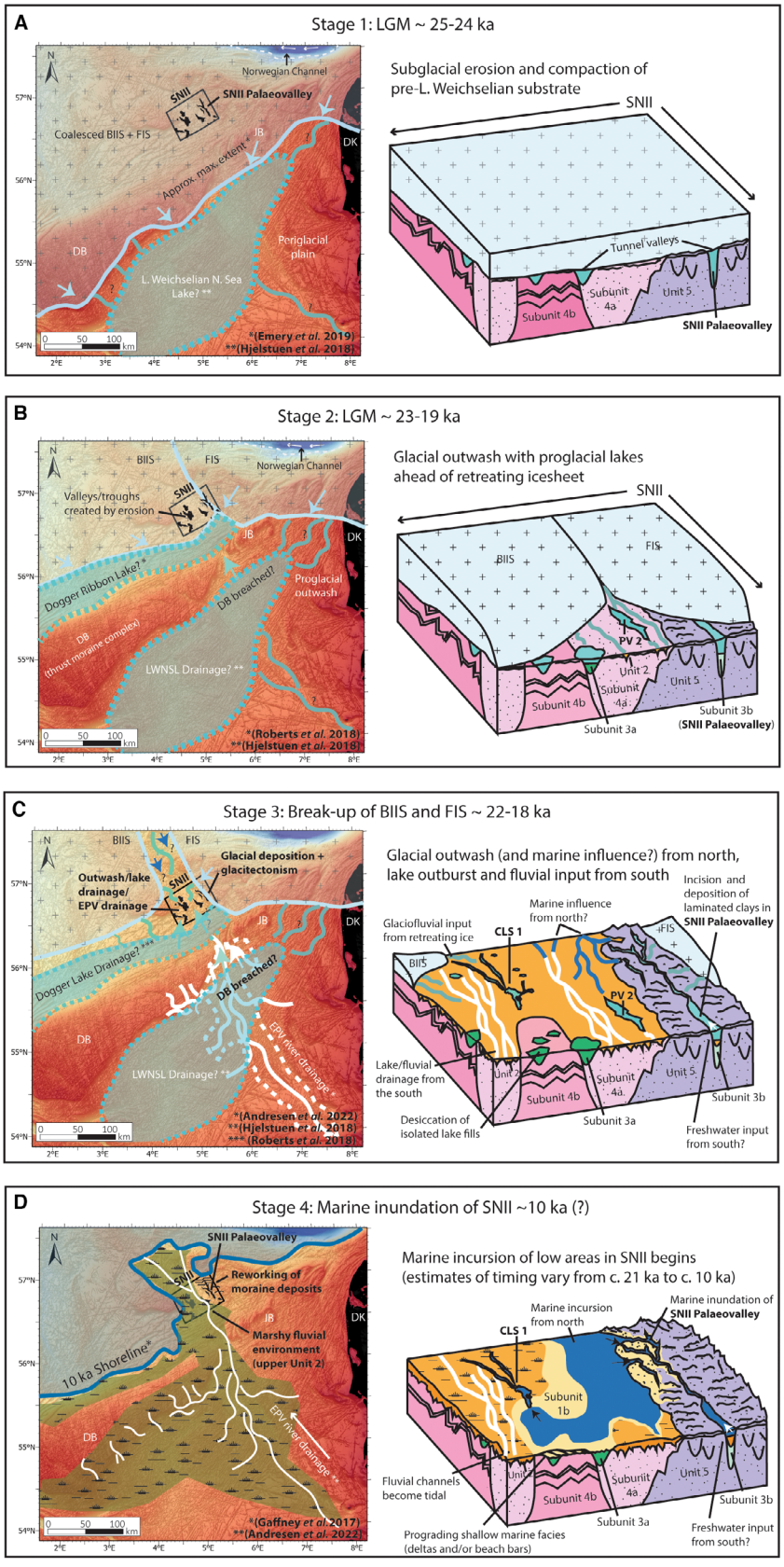

Fig. 13. Model of depositional environment evolution at SNII showing: A. Subglacial erosion and compaction of pre-Late Weichselian sediments at ~25–24 ka during the Late Weichselian glaciation. B. The onset of Late Weichselian deglaciation with the separation of the BIIS and FIS, the creation of proglacial and ice-dammed lake systems, glacifluvial/lake outburst erosion and deposition of glacial outwash sediments onto the proglacial plain and possible fluvial erosion/deposition from the Elbe river system. C. Glacifluvial/fluvial erosion and deposition within an increasingly warm and wet marshland environment with encroaching coastline. D. Estuarine environment with tidal channels, gradual marine inundation and establishment of prograding shallow marine depositional systems prior to full marine inundation at ~9 ka (Gaffney *et al.* 2017). Approx. max. extent =approximate maximum extent; BIIS = British Irish Ice-sheet; DK = Denmark; EPV = Elbe Palaeovalley; FIS = Fennoscandian Ice-sheet; DB = Dogger Bank; JB = Jutland Bank; L. Weichselian = Late Weichselian; LWNSL = Late Weichselian North Sea Lake; N. Sea = North Sea.

substrate. It is therefore likely that the layered facies at the base of the smaller palaeovalley is harder and therefore probably older than the SNII Palaeovalley infill. This is also supported by the presence of possible glacitectonic folds within the Palaeovalley 2 (Fig. 8G) fill vs. a lack of folding within the SNII Palaeovalley fill.

Subunit 3a, transparent to chaotic facies (localized incisions, SW SNII). – Subunit 3a is characterized by transparent to low-amplitude chaotic seismic facies, occurring locally within isolated basins of 2–4 km width and depths of around 5–10 m (shown in dark green; Fig. 9A). The top reflection of the basin infills is characterized by a layer of medium- to high-amplitude, chaotic reflections, penetrated by both vibrocore 11VC (profile Y–Y′; Fig. 9A) and core 3/6-1 (profile Z–Z′; Fig. 9A). Base Subunit 3a is mainly characterized by low- to medium-amplitude, slightly chaotic reflections. The basal surface is clearly erosive and incises locally into both Subunits 4a and 4b. On both 3D seismic variance (Fig. 8B) and frequency decomposition time slices (yellow stipple; Figs 7B, 9C), the basins are mainly resolved as oval to crescent-shaped high variance features and red colours representing low seismic frequencies, although some of the basins have a more subtle appearance on the 3D seismic (e.g. the basin penetrated by 3/6-1; Fig. 9A, C).

We correlate Subunit 3a to the stiff clays documented between 2.6 and 10 m in the 3/6-1 core (lithostratigraphic Unit III; Fugro 2000). The unit comprises a stiff to hard, grey clay, with numerous bands and pockets of fine sand in the upper part, and numerous silt partings and occasional black staining in the middle parts. It is almost barren of foraminifera and interpreted as a glacilacustrine clay (Knudsen 2000) and assigned a Late Weichselian age (Hammer *et al.* 2016). The upper part of a separate occurrence of Subunit 3a further north was penetrated by vibrocore 11VC (Fig. 12). Strong reflections at the top of the Subunit were found to represent the boundary between loose shelly sands (Subunit 1b) and a 40-cm-thick layer of stiff, dark grey clay with shear strengths exceeding 250 kPa (the maximum measurable shear strength for the Swedish cone apparatus) (Fig. 12A). This stiff layer could represent a desiccation surface formed through subaerial exposure of the clays (e.g. Mesri & Ali 1999; Cotterill *et al.* 2017b; Emery *et al.* 2019b, 2020), when the presumably proglacial lacustrine basins dried up during the retreat of the Late Weichselian ice sheet.

The apparent lack of truncation surfaces or glacial deposits overlying Subunit 3a preclude an interpretation of overconsolidation by ice loading. Indeed, Subunit 3a appears to have been more resistant to the subsequent marine erosion represented by the base Unit 1 surface than the surrounding Subunits 4a and 4b and retained a higher relief prior to marine inundation (profiles Y–Y′, Z–Z′; Fig. 9A). This is particularly apparent for the basin fill shown in Fig. 12D, which is located directly (~115 m) above the top of Salt Diapir 1 (Fig. 7D). It is therefore tentatively suggested that the lake basins within the vicinity of buried Salt Diapir 1 may have been preferentially preserved owing to desiccation caused by movement of the underlying salt diapir at the end of the last glaciation. The surrounding sandy sediments of Subunits 4a and 4b which form the substrate into which the basins are incised would not have suffered over-consolidation through desiccation and so would have been more susceptible to marine erosion than the desiccated lake fills.

Unit 2, layered high-amplitude facies (widespread in western SNII, present locally in the east). – Seismic Unit 2 comprises medium- to very-high-amplitude, generally layered, seismic facies. It occurs within a range of incisional features found mainly within the Western Province (Figs 8C, G, 9A), but also within the upper part of the SNII Palaeovalley system (Figs 8D, E, 11) and smaller erosive troughs in the Eastern Province (Fig. 9A). Top Unit 2 is of variable character. In much of the Western Province, it comprises an undulating conformable surface between the high-amplitude layered Unit 2 facies and the overlying transparent to low-amplitude facies of Unit 1 (e.g. Fig. 8C). In some parts of the Western Province, the low-amplitude reflections of the layered Subunit 1b onlap top Unit 2 from the north (Fig. 8G).

Within the SNII Palaeovalley, Unit 2 is truncated by the base Unit 1 surface (Figs 8E, 11B, D), while the base of Unit 2 incises the older infill of the valley (Subunit 3b), indicating that the valley was used by at least two different generations of depositional systems after its formation and prior to marine inundation (represented by base Unit 1). Within one of the branches in the northern part of the system, this second generation of

infill was found to comprise soft, laminated clays (vibrocore 09VC; Fig. 11). In the lower part of the unit, the black and grey clay layers are very distinct, and very similar in appearance to the underlying Subunit 3b, which we interpret as proglacial rhythmites. In the upper part of the unit, the laminations become less distinct and appear slightly mixed, possibly as a result of bioturbation. In the middle and upper part of Unit 2, the clays are interbedded with laminations of fine sand and contain abundant sand lenses, corresponding to an upwards increase in gamma density (Fig. 11A). A wood fragment observed at 1.6 m indicates a depositional environment in proximity to terrestrial vegetation. Benthic foraminifera *Elphidium* sp., were also identified throughout Unit 2 in the 09VC core (Fig. 11A). The brackish, cold-water foraminifera indicate that a connection between the SNII Palaeovalley and the sea was established relatively soon after the initial retreat of the Late Weichselian ice sheet, while the climate remained cold. The wood fragment, indications of bioturbation and increasing input of sand to the upper part of the valley then indicate an increasingly temperate and more strongly marine influenced environment. The truncation of Unit 2 by the base Unit 1 reflection in the upper part of the palaeovalley (Fig. 11B) indicates that part of Unit 2 was then subsequently removed when the Eastern Province became fully inundated by the sea.

In the Western Province, base Unit 2 is not characterized by a strong, mappable reflection, but rather a transition from the transparent facies of Subunit 4a into the strongly layered Unit 2 facies (Fig. 8C). The base Unit 2 surface incises into the Saalian to Mid-Weichselian sandy substrate (Subunit 4a) across a 20–30 km wide, NW–SE-trending zone in the central and southern parts of the Western Province (Fig. 9E), focused between the zones of presumably greater resistance and/or higher topography represented by Subunits 4b and 3a in the southwestern part of the site and Unit 5 in the eastern part of the site (Fig. 9A).

Within the Western Province, Unit 2 is thickest (up to 20 ms thick) where it infills the deepest zones of erosion, such as the CLS 1 system identified on 3D seismic data in the previous section (e.g. CLS 1; Fig. 8A–C) and an overdeepened zone located west of the SNII Palaeovalley, along the boundary between Subunit 4a and Unit 5 (profile V–V′; Fig. 9A). The presence of apparently laterally accreting dipping reflections within the incision infills (e.g. Figs 8G, 9A) indicates that Unit 2 probably has a partly fluvially influenced genesis, although the succession may have an increasingly marine-influenced succession in its upper parts in the Western Province, as is the case within the SNII Palaeovalley in the Eastern Province (Fig. 11). In the 3D seismic data set, the large acoustic impedance contrast between the CLS 1 and the rest of Unit 2 is probably due to the greater thickness of the CLS 1 infill, although the presence of very soft organic-rich material and shallow gas may also contribute. Moreover, a zone of possible gas blanking is observed in the lower part of the laminated infill of the southern part of CLS 1 (Fig. 8C).

Unit 1, layered to transparent facies (widespread in western SNII, patchy in eastern SNII). – Unit 1 comprises an upper transparent seismic facies (Subunit 1a) present at the seabed across almost all of SNII (Fig. 9A, F) with localized occurrences of a layered, prograding seismic facies in the lower part of the unit (Subunit 1b) in the Western Province (Figs 9A, 12) and a basal high-amplitude facies occurring locally at the top of Unit 5 in the Eastern Province (Fig. 10). The generally homogeneous character of Unit 1 (with local variations in the seismic character of the basal parts) is typical of Holocene marine sands in the region including the Ling Bank, Dogger Bank and the EPV (Hjelstuen *et al.* 2018; Prins & Andresen 2019; Emery *et al.* 2020; Özmaral *et al.* 2022). Foraminiferal analysis of the 3/6-1 core (Knudsen 2000) also confirms a warm marine (i.e. postglacial) depositional environment for Unit 1.

Unit 1 is thickest in the central and southern parts of the Western Province, in the northwestern corner of the site (Greater Fish Bank), and locally within troughs and on top of ridges at top Unit 5 in the Eastern Province (with a time thickness of 3–12 ms, ~1.5–6 m) (Fig. 9F). The thicker accumulations of Unit 1 broadly correlate to where the inherited bathymetry was deepest (base Unit 1; Fig. 9D), although this is not the case for Greater Fish Bank, a sand bank which overlies a buried topographic high.

In the Eastern Province, Unit 1 is generally thinner and patchier, with large variations in thickness (Fig. 9A, F). This is most likely related to the rugged topography of the top Unit 5 palaeosurface, which is characterized by troughs and ridges. The troughs sometimes correspond to thicker Holocene packages, e.g. in the northeastern part of the site, where a 10–12 ms deep trough between mounds of glacitectonized sediments is infilled by transparent to chaotic Unit 1 seismic facies (Fig. 8F). The ridges have probably formed barriers or high-friction surfaces onto which thicker dune-like mounds have formed. A similar relationship between rugged morainal ridges and Holocene sand ridges has also been observed at Dogger Bank (Emery *et al.* 2020).

Subunit 1b, layered facies in western SNII, chaotic facies in eastern SNII. – In the Eastern Province, a semi-continuous, chaotic, high-amplitude seismic facies occurs locally at the base of Unit 1 (Fig. 10). In cores 02VC and 08VC, this facies exhibits higher densities (up to 2.8 g cm^{-3}) and magnetic susceptibilities than the overlying transparent facies (Subunit 1a). This was initially interpreted to be part of glacitectonized Unit 5, but was found to comprise a bed of loose, rounded pebbles, gravel, sand and shell fragments, typical of a high-energy coastal environment. Occurrences of

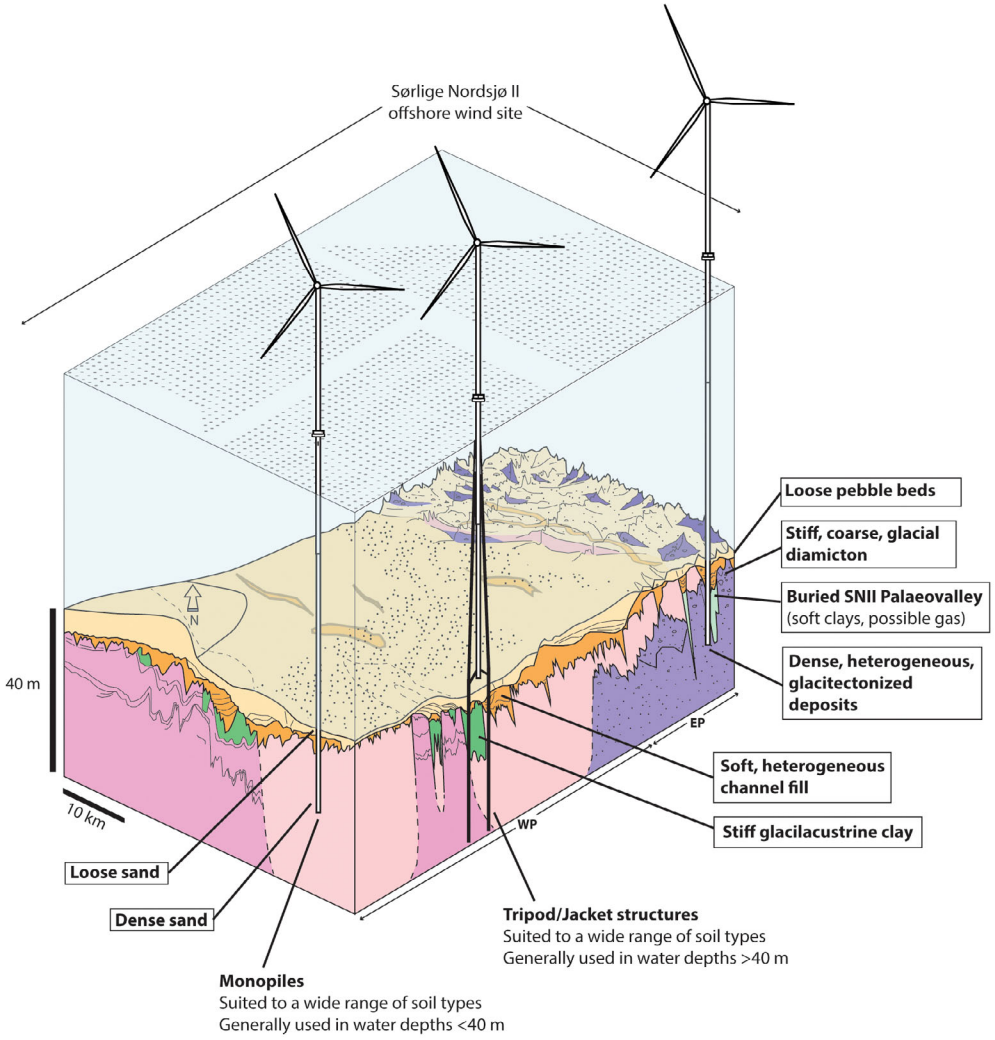

Sub-bottom profiler units	Geotechnical Properties	
Subunit 1a Silty fine sand (homogeneous)	**Angle of friction:** 15 **(loose)*** **Submerged unit weight:** 7.8-9.8 kN/m³*	Soft
Subunit 1b Layered, prograding marine sand to pebbly deposits	More heterogeneous than Unit 1a	
Unit 2 Layered fluvial (peat, clay, silt, sand)	Low shear strength laminated clays with fine sand layers and organic rich layers.	
Subunit 3a Homogenous glacilacustrine clay	**Shear strength:** 160-280 kPa (**stiff - hard**)* Submerged unit weight: 9.2 kN/m³*	Hard
Subunit 3b Chaotic - layered (base valley infill)	Upper part - low shear strength clay (09VC). Lower parts uncertain - may be **more consolidated** and contain **coarser deposits**.	Soft to variable
Subunit 4a Fine sand (homogeneous)	**Angle of friction:** 30 (**medium dense**)* Submerged unit weight: 9.8 kN/m³*	Medium
Subunit 4b Glacitectonized (layered)	Possibly overconsolidated. Faulting and folding could represent **planes of weakness**.	Hard
Unit 5 Glacitectonized (heterogeneous)	As above + contains **boulders** (MAREANO/NGU (2021)	

Fig. 14. Preliminary ground model for SNII showing distribution and likely properties of the five sub-bottom profiler-based geological units (1–5) and their associated subunits. The site is divided into two geotechnical provinces, East (EP) and West (WP), within which Unit 5 and Unit 4 respectively form the main glacially deformed/compacted substrate beneath glacially influenced to postglacial sedimentary cover of highly variable geotechnical properties. *Fugro (2000).

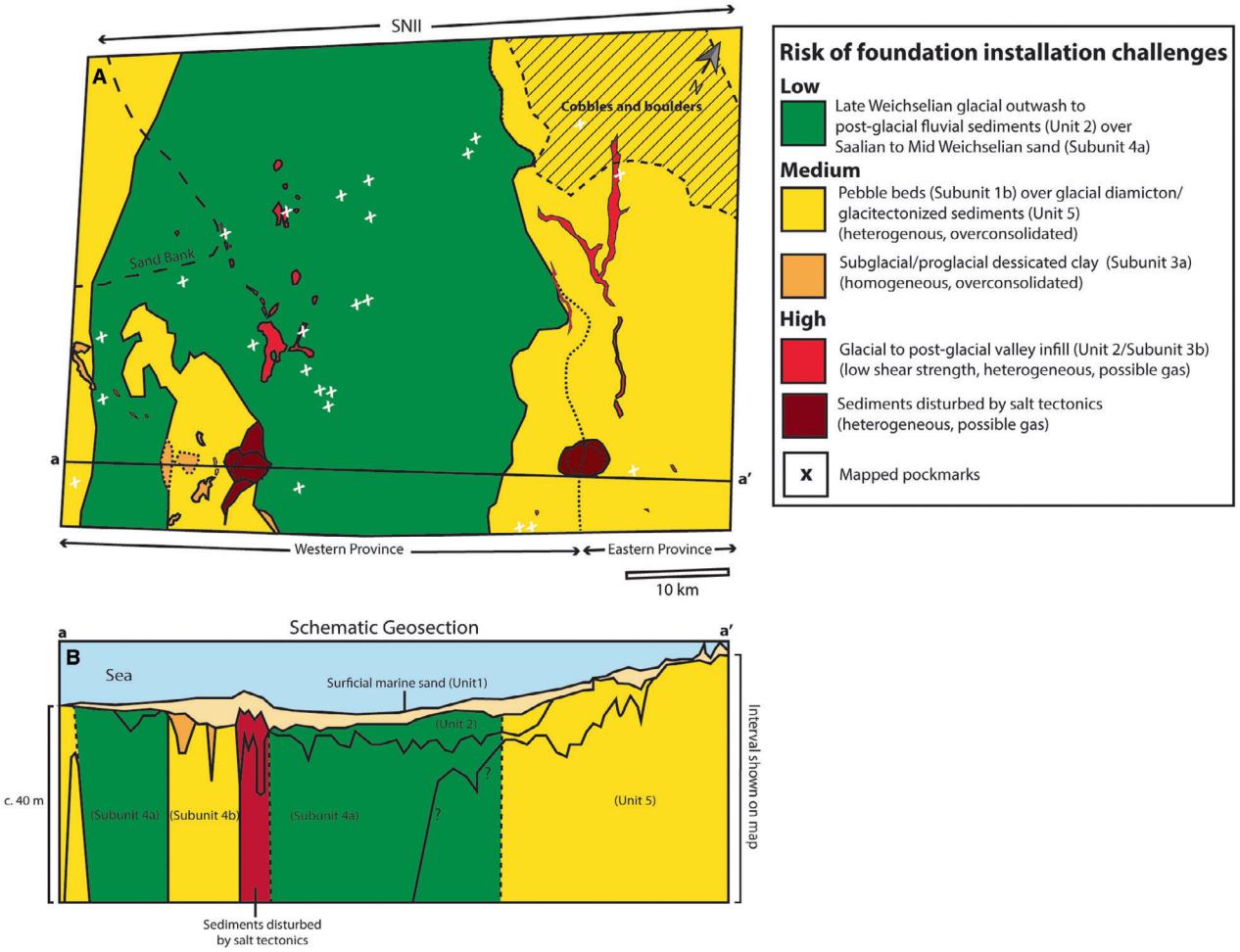

Fig. 15. A. Risk map highlighting zones with different likelihoods for causing challenges during installation of offshore wind infrastructure at SNII. Areas underlain by salt diapirs, representing an increased risk of shallow gas and instability are shown in dark red. Areas with buried valleys, channels and lake basins with very soft, layered infill and increased risk of peat deposits and shallow gas are shown in red. Areas with buried lake basins containing desiccated glacilacustrine clay deposits with high shear strengths are shown in orange. Areas with exposed/reworked or shallowly buried, potentially overconsolidated/coarse subglacial/glacitectonized deposits are shown in yellow. Areas with glacifluvial to fluvial deposits and fine-grained Holocene marine deposits overlying medium density Eemian sands are shown in green. Possible pockmarks identified on seismic profiles, indicative of possible shallow gas accumulations or gas seepage, are marked as white crosses. B. Schematic geosection through southern SNII showing the relationship between mapped sub-bottom profiler units and assigned risk.

Subunit 1b in the Eastern Province are therefore interpreted as beach or tidal bar type deposits, comprising coarse material reworked from the underlying and nearby exposures of coarse Unit 5 sediments. Owing to the chaotic nature of upper Unit 5 and Subunit 1b, it was difficult to map out other occurrences of the pebble deposits with confidence. This should be investigated further as part of detailed ground investigations for wind developments in the Eastern Province, as thicker and potentially coarser occurrences of Subunit 1b could pose potential foundation and cable installation challenges.

In the Western Province, Subunit 1b is locally characterized by medium-amplitude, layered to progradational seismic facies (Figs 8G, I, 9A, 12B, D). These occur within the central and southern parts of the Western Province, with an apparent northeastward direction of progradation from shallower parts of the base Unit 1 surface towards the deeper parts. At top Subunit 1b, the progradational reflections are truncated in some places, with a more conformable top surface in others (Figs 9A, 12D).

Above Salt Diapir 1, the internal geometries within Subunit 1b are more complex than in other parts of the site, with internal truncational surfaces and onlapping/-down lapping relationships, perhaps owing to the uneven topography of top Subunit 3a (Fig. 12D) or perhaps owing to movement of the diapir pushing the overlying sediment units upwards. Within Subunit 1b, the reflections in some places appear disrupted by what looks like small normal faults with an offset of about 30 cm. They do not appear to continue upwards into the overlying transparent Subunit 1a (Figs 8C, 12D).

Subunit 1a, transparent to chaotic facies (widespread in western SNII, patchy in eastern SNII). – Subunit 1a comprises a transparent seismic facies that drapes over Subunit 1b, Unit 2 and Subunit 4a in the Western Province and Subunit 1b, Unit 2 and Unit 5 in the Eastern Province (Fig. 9A). It generally exhibits gamma densities of 2.1–2.2 g cm^{-3} in the Western Province, where it is dominated by fine-grained, silty sands (Fig. 12) and gamma densities of 2.3–2.4 g cm^{-3} in the Eastern Province, where medium-grained, pebbly sands are encountered (Fig. 10). In the Western Province, there are no major density differences between Subunits 1a and 1b (Fig. 12A). In core 12VC in the southwestern part of the site, Subunits 1a and 1b both exhibit densities of 2.1 g cm^{-3}. In core 11VC further south, Subunit 1a shows slightly higher densities of 2.1–2.2 g cm^{-3}. In the Eastern Province, Subunit 1b is much coarser than Subunit 1a and displays much higher gamma densities (Fig. 10).

Discussion

In this section, sub-bottom profiler Units 1–5 are discussed in the context of the regional stratigraphic framework of the Dogger Bank–SNII–EPV region of the southern North Sea (Fig. 13), with a focus on how late Quaternary depositional environment changes may have influenced the geotechnical properties of the shallow subsurface at SNII. The distribution and likely geotechnical properties of Units 1–5 are summarized as a preliminary ground model for the site (Fig. 14), with an accompanying risk map (Fig. 15) indicating zones assigned a low (green), medium (yellow/orange) or high (red) risk of offshore wind foundation installation challenges. A brief discussion about the potential geotechnical properties of the underlying pre-Saalian stratigraphy present below the signal penetration depth of the sub-bottom profiler data set (below ~40 m) but identified within the upper ~100 m of the shallow subsurface on the conventional 3D seismic data set follows. In the final sub-section, offshore wind turbine foundation options suitable for the predicted SNII ground conditions are then discussed.

Preliminary ground model for SNII

Unit 5, subglacial and glacitectonized sediments. – Vibrocore 02VC (Fig. 10) indicates that at least some parts of upper Unit 5 comprise till, which sets up a strong reflection at or close to the seabed in the Eastern Province. Given its relatively flat-lying and semi-continuous distribution around 02VC, the till is interpreted as a thin layer of ground moraine, deposited by the coalesced Late Weichselian BIIS–FIS ice sheet which is commonly interpreted as having extended south of the SNII area to the Dogger and Jutland Banks (Fig. 13A; Bradwell *et al.* 2008; Ballantyne 2010; Sejrup *et al.* 2016; Phillips *et al.* 2018; Roberts *et al.* 2018; Emery *et al.* 2019b). The SNII Palaeovalley which incises Unit 5 down to ~20 m below the seabed is also thought to be linked to the Late Weichselian ice sheet, with the geomorphological characteristics typical of a subglacial tunnel valley system carved out by pressurized, subglacial meltwater close to the ice-sheet margin (Ó Cofaigh 1996; Huuse & Lykke-Andersen 2000; Stewart *et al.* 2013; Stewart 2016).

The base of the SNII Palaeovalley and the till horizon (shown in black; Fig. 10D) also truncate older, buried tunnel valley systems which may date from earlier in the Late Weichselian glaciation or as far back as the Saalian glacial period. It is uncertain whether the deeper parts of Unit 5 are of similar age to the Saalian to Mid-Weichselian marine sands of Subunit 4a or are older; however, the shallower bathymetry of the Eastern Province would seem to suggest that Unit 5 comprises sediments that were more resistant to the erosive power of the Late Weichselian ice sheet and its subsequent proglacial meltwater systems. This, along with the lack of buried tunnel valleys within Subunit 4a, supports an interpretation of Unit 5 as a remnant from an older glaciation, no longer present within the shallow subsurface of the Western Province, perhaps removed by Saalian glacial erosion. Subunit 4a is therefore tentatively interpreted as the postglacial marine infill of a Saalian or older tunnel valley system, of which the lower parts of Unit 5 and (possibly) Subunit 4b form the valley sides (Fig. 13A).

A possible geological analogue (a distant but comparable geological unit, e.g. Howell *et al.* (2014) and references therein) to the upper parts of Unit 5, certainly the till layer, is the Late Weichselian Dogger Bank Formation, a variable but often predominantly stiff to very stiff, clay-rich diamicton with sand lenses and thin gravel beds, found at the Dogger Bank offshore wind zone (Cotterill *et al.* 2017a, b; Roberts *et al.* 2018; Emery *et al.* 2019b, 2020; Phillips *et al.* 2022). Like Unit 5, the Dogger Bank Formation contains high-amplitude internal reflection surfaces separating acoustically structureless to layered and deformed seismic units. The high-amplitude reflection at the top of the Basal Dogger Bank Formation is interpreted as a possible desiccation surface with overconsolidated soil properties owing to subaerial exposure. This might also be the case for some of the rugged, high-amplitude reflections within the upper parts of Unit 5. Seismically, Unit 5 seems to be most similar to the Older and Younger Dogger Bank Formations, which comprise acoustically structureless, internally deformed ridges attributed to thin-skinned, glacitectonic folding and thrusting at the oscillating margin of the Late Weichselian North Sea ice sheet, and an overlying acoustically well-layered subunit, whose thickness is influenced by the underlying surface of the Older Dogger Bank Formation. Unit 5 is not as severely deformed as the Older Dogger Bank Formation but does

have one area with a ridge-like feature containing folded reflections in the northeastern part of the Eastern Province (Fig. 8F). Lows within the more acoustically structureless parts of Unit 5 are also infilled by an acoustically layered infill at many locations within the Eastern Province (e.g. Fig. 10D). At Dogger Bank, these layered infills comprise mainly stiff to very stiff clays; however, similar infills observed at SNII were not sampled in this study. Each of the subunits of the Dogger Bank Formation reportedly contains laterally continuous loess, hard desiccation surfaces and channels, indicating a highly heterogeneous geotechnical character. Given a similar degree of seismic facies heterogeneity within Unit 5, a similar degree of sedimentological heterogeneity should be anticipated within the Eastern Province of SNII.

Although the Dogger Bank Formation and Unit 5 have seismic similarities and indications of glacitectonism, they have probably experienced rather different evolutions owing to their different positions relative to the line of maximum extent of the Late Weichselian ice sheet. Based on the lack of a major morainal fold and thrust belt at SNII, it does not appear that the southern margin of the last North Sea ice sheet spent significant time oscillating there, as it did at Dogger Bank to form the Dogger Bank Formation glacitectonic complex. This probably occurred further SW and SE of SNII, forming the northeastern part of Dogger Bank and the Jutland Bank. Unit 5 may largely, beneath the shallow till horizon, comprise older deposits than the Dogger Bank Formation, compressed and deformed by the last Late Weichselian ice sheet, but perhaps deposited during earlier glacial and interglacial periods. The buried and truncated landscape preserved beneath the shallow till horizon within Unit 5 may therefore comprise stiffer, older deposits than the Late Weichselian Dogger Bank Formation (Fig. 15), although this is highly uncertain. Owing to the presence of the coarse, dense, till layer in upper Unit 5, the very coarse-grained shallow marine sediments deposited above it, and the potential for dense, pre-Weichselian glacial and interglacial deposits beneath the till layer, the Eastern Province is assigned a medium risk for foundation installation challenges (Fig. 15).

Subunit 4b, layered, glacitectonized remnants. – Owing to the apparent truncation Subunit 4b's internal layering and its plan-view geomorphic character on 3D seismic attribute time-slices, it is interpreted as either inter-tunnel valley remnants, surrounded by infilled Saalian or older tunnel valley incisions (Fig. 13A), or remnants of a younger depositional unit largely removed by strong glacifluvial or fluvial activity during the Late Weichselian. The lithology and geotechnical properties of the strong reflections a top Subunit 4b and the high-amplitude, folded horizons within it are unknown, but they may represent glacitectonized, overconsolidated, desiccated clay horizons similar to those within the Dogger Bank Formation. Like Unit 5, Subunit 4b is assigned a medium risk for foundation installation challenges, on the basis of potentially containing stiff, glacitectonized soil horizons of unknown lithology.

Subunit 4a, sandy tunnel valley infill (Late Saalian to Early Weichselian). – Radiocarbon dates from the 3/6-1 core (Hammer *et al.* 2016) indicate that between 10 and 37 m depth below the seabed, Subunit 4a represents marine sands with an average friction angle of 30°, deposited after the retreat of the Saalian North Sea ice sheet and before SNII was covered by the Late Weichselian ice sheet. Chaotic seismic facies representing marine sands from the Eemian interglacial period through to the Early- to Mid-Weichselian, overlying infilled pre-Late Weichselian incisional surfaces, are also documented within the shallow subsurface at and south of Dogger Bank (Prins & Andresen 2021). These have a significantly higher recorded friction angle of 42° and high cone resistance and sleeve friction values. In western Dogger Bank, the Eemian (and/or Mid-Pleistocene) sands beneath the Late Weichselian Dogger Bank Formation are described as dense to very dense. In the German sector several hundred kilometres to the south, Eemian sands are not identified, although very dense fluvial sands of Saalian age infilling Saalian tunnel valleys (the Buried Valley and Upper Fluvial Members; Fig. 2) showing friction angles ranging from 29 to 47° and cone tip resistances of 20–60 MPa are considered a suitable substrate for monopile foundations (Fleischer *et al.* 2023).

The upper parts of Subunit 4a, where they have not been heavily eroded by Late Weichselian subglacial erosion or postglacial outwash erosion, may comprise similar outwash plain deposits to those at the base of the Dogger Bank Formation. These comprise channel fills thought to have been deposited by a series of braided river systems originating out of northern Europe and the UK or glacial outwash systems flowing southwards from the BIIS and FIS ice sheets as they advanced towards their maximum Last Glacial Maximum extent (Cotterill *et al.* 2017b). At Dogger Bank, these deposits are a complex sequence of glacifluvial and glacilacustrine sediments deposited across a laterally extensive outwash plain, representing at least in part the Basal and Lower Dogger Bank Formations that later became folded and thrusted by the ice front (Cotterill *et al.* 2017b). As the ice margin retreated after forming the Dogger Bank fold-and-thrust complex, additional bedded outwash sediments were laid down on top of the complex (the Younger Dogger Bank Formation). The upper parts of Subunit 4a may therefore have been deposited within a similar depositional environment to the Basal and Lower Dogger Bank Formations (Fig. 13B), without being subjected to glacitectonism as strong owing to being located north of the maximum southern position of the ice margin, while the lower part of Unit 2 which

infills incisions in upper Subunit 4a, might represent similar deposits to the Younger Dogger Bank Formation outwash plain deposits (e.g. Fig. 13C).

Overall, Subunit 4a probably spans a range of depositional environments from the Saalian late glacial to interglacial marine environment to the pre-Late Weichselian cold marine to periglacial terrestrial environment, although evidence of a well-developed Late Weichselian ground moraine as encountered in the Eastern Province, is lacking. The 3/6-1 boring indicates that Subunit 4a largely comprises medium density sands, suitable for foundation installation, although a 1 m interval of stiff clay is present at 11 m depth. The properties of Subunit 4a in other parts of the Western Province are untested but are considered to probably be relatively similar to those encountered in 3/6-1. The majority of the Western Province, where the shallow subsurface comprises Unit 1, Unit 2 and Subunit 4a, and no seismic anomalies are identified, is therefore defined as having a low risk of foundation installation issues (Fig. 15).

Subunit 3b, tunnel valley infill (Late Weichselian). – The lowermost seismic facies within the SNII Palaeovalley are interpreted as deposits from an early phase of proglacial sedimentation during the retreat of the Late Weichselian ice sheet from the SNII area (Fig. 13B). The interpreted rhythmites encountered in core 09VC indicate that this was probably a proglacial lake environment perhaps connected to the Late Weichselian Dogger Lake (e.g. Roberts *et al.* 2018) with a relatively early connection to the sea becoming established, as indicated by the presence of foraminifera *Elphidium*.

However, the presence of several blank zones within the valley fill would suggest that there are some minor biogenic gas accumulations within it, and thus probably some thicker organic rich layers than the black laminations observed in vibrocore 09VC. 3D seismic data also indicate that the SNII Palaeovalley has an overall very soft infill, which may be purely related to its very soft clay-rich lithology, or partly owing to the presence of shallow gas. The SNII Palaeovalley fill is therefore assigned a high risk of possible foundation installation challenges, related to the softness of the infill and the hazard posed to borehole and other operations by the possible presence of shallow gas. The infill of Palaeovalley 2 in the SE part of the Western Province does not show a significantly softer or harder signature than the surrounding substrate or any indications of gas blanking and so is assigned a low risk of foundation installation issues.

Subunit 3a, stiff glacilacustrine clays (Late Weichselian). – Cores 3/6-1 and 11VC indicate that Subunit 3a comprises stiff glacilacustrine clays of Late Weichselian age. We propose that these relatively small, isolated basins were small proglacial lakes, filled by rock flour-laden meltwater from the retreating Late Weichselian ice-sheet margin (Fig. 13B), which subsequently became cut-off and dried out (Fig. 13C). The reason these are only identified within the southwestern part of the site might be related to preferential preservation caused by halokinetic movement below this part of the site, which overlies Salt Diapir 1. However, the topography in this part of the outwash plain may simply have been higher owing to the higher resistance of Subunit 4b, in which the Subunit 3a deposits mainly occur, to glacial erosion, thus protecting the lakes from removal by subsequent fluvial action during deglaciation (Fig. 13C).

Shear strength measurements in Subunit 3a range from 160 to 240 kPa in the 3/6-1 core to over 250 kPa in vibrocore 11VC. Comparable facies include a more widespread clay interval identified in the Danish sector SE of Dogger Bank (Unit 2, Prins & Andresen 2019) (Fig. 2), which has an average undrained shear strength of 117–156 kPa, and >100 kPa undrained shear strength clays identified within topographic lows in the Younger Dogger Bank Formation termed the Botney Cut Formation (Cotterill *et al.* 2017b). Owing to the high shear strengths and significant thickness (~5–10 m) of these deposits in southwestern SNII, they are assigned a medium to high risk of causing foundation installation challenges (Fig. 15).

Unit 2, layered proglacial to coastal sediments (Late Weichselian to Holocene). – The layered seismic facies of Unit 2 are interpreted as spanning a range of depositional environments from proglacial outwash plains to tidal channel systems (Fig. 13C, D). The broad erosive zone in the Western Province infilled by chaotic to layered, high-amplitude reflections with multiple incision surfaces and lateral accretion geometries are indicative of lateral migration and so are interpreted broadly as fluvial sediments. As in other layered channel fills in the region, such as western Dogger Bank (Emery *et al.* 2019b) and SE of Dogger Bank (Prins & Andresen 2019), the lower parts of Unit 2 may represent part of the proglacial outwash succession deposited across the region as the Late Weichselian ice sheet retreated.

Although glacial outwash from the retreating BIIS and FIS margins is likely to have contributed significantly to fluvial erosion and deposition in the Western Province of SNII, the position of SNII directly north of the Dogger Bank–Jutland Bank Gap make it likely that fluvial input and lake drainage/outburst flooding from south and SW of SNII also played a significant role in eroding the Western Province and depositing the lower part of Unit 2 (Fig. 13C). An outburst flood from the Late Weichselian North Sea Lake and drainage from the Elbe Palaeovalley have both been proposed as the possible mechanisms by which the Dogger and Jutland Bank became breached, although some studies have proposed that the Late Weichselian North Sea Lake may

rather have become infilled by glacial outwash (Andresen *et al.* 2022). On the basis of sub-bottom profiler and shallow sediment core data, Hjelstuen *et al.* (2018) propose that the breach occurred at around 19 cal. ka BP, when a pulse of freshwater entered the Norwegian Channel via an ice-free corridor between the BIIS and FIS ice sheets (Fig. 13C) and a prograding delta system was deposited on the Ling Bank, north of SNII. More recent dating calibration (Brendryen *et al.* 2020) indicates that the breach occurred slightly later, closer to 17.5 cal. ka BP. Other studies have suggested that this ice-free corridor opened as early as 22 cal. ka BP (Roberts *et al.* 2018). Radiocarbon dating of the Unit 2 fluvial to tidal sediments and Unit 1 marine sediments is therefore highly recommended as a means of narrowing down the range of dates during which the Dogger–Jutland Bank was breached vs. when the ice-free corridor formed and began to be exploited by the rising sea.

The middle to upper parts of Late Weichselian channel fills in the region record a change to a vegetated, temperate fluvial plain setting as the climate warmed, permafrost thawed and precipitation increased (Emery *et al.* 2020). As the sea began to encroach, the channel systems would then have become tidal, interspersed perhaps with salt marshes (Fig. 13C, D). At Dogger Bank, the upper parts of the layered channel fills become increasingly organic rich, indicating that the former outwash plain became vegetated, i.e. warmer and wetter. The low densities and very-high-amplitude layered facies encountered in the upper parts of Unit 2 in the Western Province are therefore interpreted as fine-grained, organic rich fluvial to tidal channel deposits. The timing of when the channels in SNII began to experience a marine influence is highly uncertain without radiocarbon dating, which was outside the scope of this study. Various studies in the region have proposed very different timings for when this began to occur, ranging from as early as 21–19 cal. ka BP (Roberts *et al.* 2018) based on geological evidence that the final northward retreat of the 'North Sea Lobe' part of the BIIS past the Durham and Northumberland coast and into the Firth of Forth occurred between 19 and 17 cal. ka BP under glaciomarine conditions in the central and northern North Sea, to as late as ~15 cal. ka BP (Hammer *et al.* 2016), based on radiocarbon dating of bivalves taken from the top of Fugro lithostratigraphic Unit III in the 3/6-1 boring. At Dogger Bank, the peat-bearing intervals within Unit 2 equivalent channels contain salt marsh foraminifera and pollen taxa, which indicate that the peats formed between the high and mean tide levels, representing the first marine influence on Dogger Bank at ~9130 cal. ka BP (Shennan *et al.* 2000).

Foraminifera species within the marine truncated upper infill of the SNII Palaeovalley indicate that the climate was still cold when the valley first became connected to the sea, favouring a Late Weichselian rather than Holocene encroachment of the sea into SNII, in line with the geological model of Roberts *et al.* (2018) (Fig. 13C).

The subtle channel features observed on 3D seismic maps (white arrows; Fig. 8A, B) branching outwards from the northern end of the SNII Palaeovalley and connecting it with the deeper base level of the Western Province (Fig. 8A, D) could represent the valley's initial connection points to the sea as it transitioned from a fresh water proglacial lake setting to an estuarine setting (Fig. 13C, D). A similar evolution within a palaeovalley system SE of Dogger Bank was proposed by Prins & Andresen (2019), with channel systems initiated by subglacial erosion during the LGM evolving into fluvial and then marine systems after deglaciation. In contrast to the systems observed in the Danish sector, however, the SNII Palaeovalley does not appear to have had any dendritic tributary channels feeding into it. Instead, 3D seismic data indicate that several sinuous channels systems at some stage fed fresh water into the valley via its southern trunk (Fig. 8B). The lack of a well-developed dendritic system might be attributed to the stiffness and ruggedness of the surface of Unit 5 which represented the ground surface at the time, perhaps enhanced by permafrost during the earlier stages of the infilling of the valley.

Seismically, Unit 2 exhibits many similarities to incisional channel infills in other parts of the southern North Sea, including the lower part of Unit B of Andresen *et al.* (2022) in the Danish sector SE of Dogger Bank (Fig. 2). These comprise upwards coarsening, silty to clayey fine sand with layers of silty clay and organic matter, thought to correlate with the Channel Member of the Weichselian Limnic Fluvial Formation and possibly the Peat Member of the Buried River Valley Formation in the German sector (Hepp *et al.* 2017; Coughlan *et al.* 2018) and the Elbow Formation in the British sector (Cotterill *et al.* 2017b).

In the German sector, Holocene fluvial channel fills comprise clay, silt and fine sand, with varying organic content and peat layers with friction angles between 19 and 36°. The cohesive sediments in the channels are very soft with undrained shear strengths of less than 30 kPa. The 3/6-1 geotechnical boring did not penetrate any Unit 2 channel fills, but our vibrocore data set indicates densities similar to the overlying Holocene sands, while the upper SNII Palaeovalley fill largely comprises low shear strength clay and fine sand. Unit 2, like the underlying Subunit 4a sand, is therefore assigned a low risk of foundation installation challenges, except where potential shallow gas may have accumulated, i.e. where seismic anomalies are present in the conventional seismic data (Fig. 15).

Unit 1, shallow marine sands. – The progradational parts of Subunit 1b which build out from highs at top Unit 2/top Subunit 3a in southern parts of the Western Province are interpreted as shoreface deposits related to the early phase of

marine inundation at SNII (Fig. 13D). Similar facies observed at Dogger Bank are interpreted as beach barriers that show progradation owing to longshore drift but were eventually drowned by rapid sea-level rise (Emery *et al.* 2019a). The internal erosion surfaces within Subunit 1b were difficult to map out in detail between the widely spaced sub-bottom profiles but indicate that the relative sea-level changes were pulsed. Similar variability within the Holocene marine unit is documented at Dogger Bank where three Holocene marine ravinement surfaces are observed (Cotterill *et al.* 2017b).

Despite its more heterogeneous appearance on sub-bottom profiler data, the density and grain size of Subunit 1b within our vibrocore data set is almost identical to that of Subunit 1a in the Western Province, both representing loose, fine-grained shelly sand. In the Western Province, Subunit 1b is therefore not considered a risk to foundation installation, although Unit 1 as a whole should be assessed for scour potential. The coarser occurrences of Subunit 1b, located in the Eastern Province, derived from marine reworking of tills, are considered at moderate risk of causing foundation installation issues. However, this risk can be combined with that of encountering coarse, stiff tills in the Eastern Province (Fig. 15). More closely spaced sub-bottom profiles and *in-situ* soil tests will allow more detailed mapping of the distribution of the Subunit 1b pebble beds and Unit 5 till(s).

Unit 1 as a whole comprises Holocene sea floor sediments termed S1 (Knudsen 1985) or Unit 1 (Prins & Andresen 2021) in the Danish sector, the Upper Marine Formation and Mobile Sands Member (Coughlan *et al.* 2018) in the German sector, and the Nieuw Zeeland Gronden Formation in the UK sector of the North Sea (Cotterill *et al.* 2017b) (Fig. 2). There is a large difference in friction angle measurements between the Holocene sands sampled in the 3/6-1 core in southwestern SNII, with a friction angle of 15°, and the average friction angle of the Unit 1 sediments sampled in the Danish North Sea, with a range of average friction angles between ~38° and 44° (Prins & Andresen 2021). These values indicate that the Holocene sand unit in the SNII area is very loose, and Fugro (2000) summarized that there is a possibility of scouring around installed structures within these sediments.

Prins & Andresen (2021) found that in the Danish sector, the lowest friction angles of the Holocene sands occurred where they were underlain by Holocene channel fills, which contained higher amounts of cohesive soil. The cone resistances and friction ratios were also lower in the vicinity of buried Holocene channel systems. The low-friction angle sands cored in 3/6-1 are occasionally clayey or silty and are located above hard to stiff Late Weichselian clays, which could perhaps account for lower friction angles, although 15° is an extremely low value and should be taken with a degree of caution given that it is a single datapoint within the SNII site, acquired many years ago.

In parts of Dogger Bank, the Holocene cover comprises a loose silty layer at the seabed, overlying a thicker sequence of dense to very dense sand. We did not encounter any very dense Holocene sands in our data set, but variations in the geotechnical properties of Unit 1 at SNII should not be ruled out, despite appearing relatively homogenous in sub-bottom profiler data. A detailed overview of geotechnical design parameters derived from offshore *in-situ* testing and onshore laboratory tests for the Holocene marine sand cover in the German sector is given in Fleischer *et al.* (2023). Here, the Holocene sand cover is thinner than in the SNII/Dogger Bank areas (>1–2 m), and the underlying stratigraphy from which they are derived is dominated by sandy deposits from the Doggerland tundra plain, as the Late Weichselian ice sheet did not extend into the German sector. Thus, the Holocene sands in the Dogger Bank/SNII region are probably derived from a wider range of sediment types including overconsolidated clays, tills and dense Eemian to Weichselian sands and silts. The friction angle range measured in the Fleischer *et al.* (2023) study area is 34–38°. This is somewhat lower than the 38–44° range measured in the Prins & Andresen (2021) study area SE of Dogger Bank.

Shallow gas and diapirism

Figure 15 highlights features within the upper ~40 m of the shallow subsurface considered at high risk of containing shallow gas (most likely in solution rather than free gas at such shallow depths) based on the seismic anomalies observed on the 3D seismic data set and where gas blanking is observed on sub-bottom profiles (in the SNII Palaeovalley, in the CLS 1 system, and above Salt Diapirs 1 and 2). The locations of possible pockmarks indicative of potential gas seepage at seabed observed on both conventional seismic data and sub-bottom profiles are also highlighted as white crosses.

Shallow gas seepage and minor gas in solution constitute potential hazards to safe subsurface operations relating to site surveying (e.g. blow out during boring), installation and stability of foundation structures and should be tested or mitigated for during site survey investigations. The shallow subsurface above Salt Diapirs 1 and 2 should also be considered at risk of instability, given the possibility of continuing movement of the salt after the retreat of the Late Weichselian ice sheet and of potential structural deformation of the sediments.

Pre-Saalian stratigraphy

At SNII, the upper ~300–400 m of subsurface stratigraphy is dominated by multigenerational tunnel valley infills, although small remnants of gently dipping Early Quaternary sediments may be present locally below ~50 m. In the German North Sea, the Early to Middle

Table 2. Preliminary foundation recommendations and remaining uncertainties regarding soil conditions and geohazards present within each of the defined risk zones shown in Fig. 15.

Risk zone	Description of soil conditions in upper ~40 m	Preliminary foundation recommendation	Uncertainties
Low	Predominantly medium density sand (Subunit 4a) with layered, low shear strength channel infills in upper ~10 m (Unit 2) and loose, surficial sand cover (Unit 1)	Probably suitable for all foundation types	Degree of lateral grain size and density heterogeneity within Subunit 4a
Medium 1	Predominantly heterogeneous glacitectonized deposits (Subunit 4b/Unit 5) with overconsolidated glacial diamictons (Unit 5) and very coarse beach type deposits in upper ~5 m (Subunit 1b)	Probably suitable for all pile-based foundation types. Possibly unsuitable for suction caissons	Frequency and size range of pebbles, cobbles and boulders. Stiffness of Unit 5 below ~5 m
Medium 2	5–10 m stiff to hard clay (Subunit 3a) between loose, surficial sand cover (Unit 1) and underlying layered, folded Subunit 4b (properties unknown)	Probably suitable for all pile-based foundation types. Possibly unsuitable for suction caissons	Pile driveability in Subunit 3a stiff to hard clays and folded Subunit 4b layers
High 1	10–20 m low shear strength, layered sediments (valley infills, Unit 2/Subunit 3b) representing seismic anomalies (possible gas)	Though probably suitable for all foundation types, recommend avoiding foundation placement in this zone to avoid unnecessary foundation design alterations	Presence of gas, presence of minor peat mats or coarse deposits
High 2	~100 m disturbed zone above top of salt diapirs (potential fluid flow, gas, instability, structural heterogeneity)	Further investigation required	Presence of gas, fluid flow, structural heterogeneity or instability, thermal anomalies and diagenesis

Pleistocene sediments are termed the Lower Sands Formation (Fig. 2) and comprise fine to coarse, sometimes gravelly, very dense sands, with tip resistances higher than 60 MPa. In the southern Norwegian North Sea, however, the Early to Middle Pleistocene section comprises finer pro-deltaic sediments known variously as the Zulu Group or Southern North Sea Deltaic Group (Stoker *et al.* 2011). It is uncertain what degree of consolidation these have undergone within the SNII area and therefore what their geotechnical properties may be. Lamb *et al.* (2018) highlight that although sediments which have experienced glacial loading are commonly overconsolidated, excess pore pressures and under-consolidation of sediment can also occur, and that there are limited data on the effects of ice loading prior to the LGM in the North Sea.

The properties and ages of the deepest tunnel valley infills at SNII are also uncertain, although they are assumed to comprise Elsterian to Holsteinian deposits. The oldest tunnel valleys in the North Sea are often assumed to be of Elsterian age, but often with low confidence owing to the sparsity of stratigraphic age data collected from them (Huuse & Lykke-Andersen 2000; Lutz *et al.* 2009; Müther *et al.* 2012). The infill of the deepest valleys at SNII appears highly heterogeneous, with multiple internal erosion surfaces, and variable seismic facies. These are probably Elsterian to Early Saalian in age, as documented in other parts of the southern North Sea. At Dogger Bank, the deepest and oldest tunnel valleys are interpreted to be Elsterian, infilled by sediments called the Swarte Bank Formation (Cotterill *et al.* 2017b). The lower parts of the valleys there contain a coarse diamicton with lenses of glacio-fluvial sand, possibly representing ice-marginal deposits. These are overlain by laminated glacilacustrine muds passing upwards into shallow marine clays interpreted to represent the retreat of the Elsterian ice front and incursion of the Holsteinian Sea. In the Danish sector immediately to the south of SNII, however, the Elsterian and Holsteinian sediments have been entirely removed in places, e.g. hydrocarbon well TWB-12 (Pedersen 1995), with early Mid-Pleistocene sediments directly overlain by Saalian sediments.

Implications of mapped risk zones for offshore wind foundations

Preliminary foundation recommendations and remaining uncertainties for each of the identified 'risk zones' at SNII are outlined in Table 2. Overall, the predominantly sandy shallow stratigraphy within the Western Province of SNII is likely to be a generally good substrate for any foundation type (broadly analogous to conditions in the Danish and German sectors of the North Sea, e.g. Jensen *et al.* (2008), Fleischer *et al.* (2023)). However, the predominant soil type(s) within the deeper parts of the Eastern Province (i.e. below vibrocoring depth) are highly uncertain and borehole data will be required to confirm if the shallow stratigraphy is also predominantly sandy within the Eastern Province. In the German sector of the southern North Sea, sand-rich soil units of the same age (Saalian to Late Weichselian), have proved to be a competent substate for monopile foundations in water depths down to ~40 m (e.g. Deutsche Bucht, Hohe See, OWP Albatros (Díaz & Guedes Soares 2020)). It should be noted however that the German sector did not

experience the impacts of ice-sheet coverage during the Late Weichselian, and so the equivalent Saalian to Weichselian sand units at SNII are likely to be denser, with more heterogeneities in the Late Weichselian sediments.

There are a number of zones, as highlighted in Fig. 15, which represent potential risks to foundation stability and successful installation of different foundation types. As summarized in Table 2, the low-risk (green) zone is probably suitable for all foundation types. This is the least heterogeneous zone, comprising predominantly medium density sand (Subunit 4a), with layered, low-shear-strength channel infills (Unit 2) and loose surficial marine sand cover (Unit 1) in the upper ~10 m of the subsurface. The degree of lateral variability in grain size and density of Subunit 4a should be a focus of further investigations to determine both pile and bucket specification variation requirements in the zone.

In the medium (yellow and orange) zones, the soil conditions are likely to be generally suitable for monopiles and pile-based, multilegged foundation structures, but may not be suitable for suction-caisson-based, multilegged foundation structures. In the Western Province, this is due to the presence of Subunit 4b, which probably represents stiffer/denser sediments than Subunit 4a, and the presence of small-localized occurrences of Subunit 3a, which comprise stiff to hard clays. For suction caissons, clay layers overlying sand can be problematic, as the tip resistance in the sand during installation is not reduced by the water gradient as it would be in a homogeneous sandy substrate (Tjelta 2015; Sturm 2017). The driveability in Subunit 3a for pile-based solutions will also need to be investigated further to evaluate foundation design suitability.

In the Eastern Province, the presence of stiff, coarse till, beach-like pebble deposits and boulders close to and at the seabed, in addition to heterogeneities within the deeper parts of Unit 5, could possibly represent a challenge to successful suction caissons (frequent boulders >50 cm diameter are problematic) and possibly also to pile driving (see challenges to monopile placement in glacitectonized Late Weichselian deposits at Dogger Bank, e.g. Cotterill *et al*. 2017a, b). The frequency and size range of pebbles, cobbles and boulders in the Eastern Province is uncertain, however, and should be investigated further with regard to foundation suitability, e.g. through 3D seismic diffraction imaging (Grasmueck *et al*. 2012; Wenau *et al*. 2018).

The red high-risk zones identified in narrow, localized parts of the site represent areas where accumulations of low-shear-strength Unit 2 deposits are particularly thick (~10–20 m) and represent shallow seismic anomalies on 3D seismic data that indicate the possible presence of shallow gas. Although significant free gas accumulations are unlikely at such shallow depths, the presence of gas will have to be tested or mitigated for if these zones are to be developed. In addition, the upper 10–20 m of the shallow subsurface in these zones have significantly lower shear strengths than their surroundings and will require foundation specification variations if developed. Although probably suitable for all foundation types, the softness of the predominant sediment type within the red zones will require different design specifications of any foundations placed either fully or partly within these zones. The implications of the seismic anomalies present above the shallow salt diapirs (dark red high-risk zones) for foundation design specifications are uncertain, and these zones should be investigated to evaluate the presence of shallow gas, fluid migration, diagenesis, structural heterogeneities and thermal anomalies.

Conclusions

In this study, we have demonstrated how the integration of legacy 3D seismic data with high-resolution 2D sub-bottom profiles and shallow sediment cores can be a powerful preliminary method for mapping out geotechnical risks and uncertainties at offshore wind sites in previously glaciated marine areas. The preliminary ground model presented defines five main seismic-based geological units and associated subunits: Subunit 1a – loose, fine- to medium-grained marine sands covering most of the site, with patchier distribution in the east; Subunit 1b – loose, fine-grained, prograding shallow marine sands associated with palaeohighs in the west, and coarse, pebbly deposits associated with reworked ground moraines in the east; Unit 2 – soft, layered channel deposits containing organic material and possible peat layers with associated shallow gas occurring in the west and soft, organic rich clays with possible shallow gas occurring in the SNII Palaeovalley in the east; Unit 3 – localized stiff glacilacustrine clays in the SW and soft glacilacustrine clays in the lower part of the SNII Palaeovalley; Unit 4 – a buried, probably stiff, glacitectonized, layered unit found locally in the SW, incised by tunnel valleys infilled with glacimarine to marine sediments of medium density; and Unit 5 – tills and glacitectonized deposits, found at and close to the seabed in the east. A risk mapping technique was used to summarize the key potential geotechnical risks associated with the mapped seismic facies within the upper ~40 m of the subsurface which includes a broad central low-risk zone characterized by: (1) medium density Saalian to Weichselian sand, overlain by low-density Late Weichselian channel deposits and Holocene marine sands; (2) medium-risk zones in the eastern and southwestern parts of the site characterized by potentially stiff glacitectonized deposits below Holocene marine deposits; and (3) several localized high-risk zones representing overconsolidated glacilacustrine lake infills, potential shallow gas accumulations and sediments affected by salt diapirism.

To inform effective foundation design, installation planning and risk mitigation, we recommend that

geophysical and geotechnical site surveys focus on reducing uncertainties around the degree of density and grain size heterogeneity within the seismically homogeneous Subunit 4a and seismically transparent to chaotic Unit 5. In addition, more detailed mapping of the upper Unit 5 ground moraine and its boulder content and the distribution of the lower Unit 1b pebble interval is recommended to assess potential foundation and cable installation issues in the eastern part of the site. Further work is also required to determine with certainty whether shallow gas is present within the Unit 2 layered incision infills and within the sediments located above Salt Diapirs 1 and 2.

In addition to providing a more detailed understanding of the subsurface of the southern Norwegian North Sea for preliminary ground modelling for offshore wind turbine foundations, this study also highlights the importance of the SNII site and surrounding area as an understudied but key area for understanding the break-up and retreat of the Late Weichselian ice sheets. Large uncertainties remain around the exact mechanisms and timing of the creation of the breach between the Dogger and Jutland banks and how these initiated changes in the depositional environment in the southern North Sea, and around the dynamics of retreat of the British–Irish and Fennoscandian ice sheets and the timing of marine inundation in the southern Norwegian North Sea. With plans for many more large offshore site developments in the region, a better understanding of the Late Weichselian and Early Holocene palaeoenvironment will be of great benefit to both Quaternary research and the advancement of offshore wind foundation technology.

Acknowledgements. – This study is part of a PhD project at the University of Bergen funded by the Akademia Agreement. We would like to thank all of the crew members and students who worked on the GS22-241 cruise on RV 'G.O. Sars' to collect the data for this project, particularly the Vibrocoring engineers Daniel Otto and Saskia Stanjura of Geo-Engineering, Bremen and University of Bergen engineers Dag Inge Blindheim and Stig Monsen. We also thank Victoria Adestål and the other geologists, geophysicists and geotechnical engineers within Equinor Energy AS who have contributed to useful discussions about our geological interpretations, and their implications for offshore wind foundation placement and design. Katrine Juul Andresen and Jonathan Lee are acknowledged for their constructive reviews of the paper. Thanks to PGS for providing the 3D seismic surveys MC3D-NDB2008 and MC3D-NDB2013, and for giving us permission to use the data in the figures in this paper. Thanks also to ENI for providing a copy of the 3/6-1 geotechnical boring report and to Olex AS, Trondheim for giving us permission to show their bathymetric data. Schlumberger are acknowledged for an academic licence of Petrel which was used for seismic interpretation and visualization.

Author contributions. – The project was conceived by HH and CHE. HH, JB and HEP were involved in data analysis. HEP wrote the full manuscript. CHE, HH, JB and TW gave comments and suggested corrections to the manuscript.

Data availability statement. – The data that support the findings of this study are available on request from the corresponding author. The data are not publicly available owing to privacy restrictions.

References

Andresen, K. J., Hepp, D. A., Keil, H. & Speiss, V. 2022: Seismic morphologies of submerged late glacial to Early Holocene landscapes at the eastern Dogger Bank, central North Sea Basin – implications for geo-archaeological potential. *Geological Society, London, Special Publications 525*, https://doi.org/10.1144/SP525-2021-155.

Andresen, K. J., Huuse, M. & Clausen, O. R. 2008: Morphology and distribution of Oligocene and Miocene pockmarks in the Danish North Sea–implications for bottom current activity and fluid migration. *Basin Research 20*, 445–466.

Anell, I., Thybo, H. & Rasmussen, E. 2012: A synthesis of Cenozoic sedimentation in the North Sea. *Basin Research 24*, 154–179.

Ballantyne, C. K. 2010: Extent and deglacial chronology of the last British-Irish Ice Sheet: implications of exposure dating using cosmogenic isotopes. *Journal of Quaternary Science 25*, 515–534.

Becker, L. W. M., Sejrup, H. P., Hjelstuen, B. O., Haflidason, H. & Dokken, T. M. 2018: Ocean-ice sheet interaction along the SE Nordic Seas margin from 35 to 15 ka BP. *Marine Geology 402*, 99–117.

Bellwald, B., Planke, S., Polteau, S., Lebedeva-Ivanova, N., Faleide, J. I., Morris, S. M., Morse, S. & Castelltort, S. 2021: Characterization of a glacial paleo-outburst flood using high resolution 3-D seismic data: Bjørnelva River Valley, SW Barents Sea. *Journal of Glaciology 67*, 404–420.

Benn, D. I. & Evans, D. J. A. 2010: *Glaciers and Glaciation*. 801 pp. Hodder Education, London.

Benvenuti, A., Šegvić, B. & Moscariello, A. 2018: Tunnel valley deposits from the southern North Sea–material provenance and depositional processes. *Boreas 47*, 625–642.

Bhattacharya, S. 2014: Challenges in design of foundations for offshore wind turbines. *Engineering and Technology Reference 1*, 922.

Bjerck, H. B. 2021: What could the 'sea ice machine' do to its people? On Lateglacial Doggerland, marine foraging, and the colonisation of Scandinavian seascapes. *Environmental Archaeology 26*, 51–63.

Böse, M., Lüthgens, C., Lee, J. R. & Rose, J. 2012: Quaternary glaciations of northern Europe. *Quaternary Science Reviews 44*, 1–25.

Bradley, S. L., Milne, G. A., Shennan, I. & Edwards, R. 2011: An improved glacial isostatic adjustment model for the British Isles. *Journal of Quaternary Science 26*, 541–552.

Bradwell, T., Stoker, M. S., Golledge, N. R., Wilson, C. K., Merritt, J. W. & Long, D. 2008: The northern sector of the last British Ice Sheet: maximum extent and demise. *Earth Science Reviews 88*, 207–226.

Brendryen, J., Haflidason, H. & Yokoyama, Y. 2020: Eurasian Ice Sheet collapse was a major source of Meltwater Pulse 1A 14,600 years ago. *Nature Geoscience 13*, 363–368.

Bretz, J. H., Smith, H. T. U. & Neff, G. E. 1956: Channeled scabland of Washington: new data and interpretations. *Geological Society of America Bulletin 67*, 957–1049.

Bridge, J. S. & Lunt, I. A. 2006: Depositional models of braided Rivers. *In* Sambrook-Smith, G. H., Best, J. L., Bristow, C. S. & Petts, G. E. (eds.): *Braided Rivers: Process, Deposits, Ecology and Management*, 11–49. Blackwell Publishing, Oxford.

Cameron, T. D., Bulat, J. J. & Mesdag, C. S. 1993: High resolution seismic profile through a Late Cenozoic delta complex in the southern North Sea. *Marine and Petroleum Geology 10*, 591–599.

Campbell, K. J. 1984: Predicting offshore soil conditions. *Proceedings of the Annual Offshore Technology Conference*, 4692, https://doi.org/10.4043/4692-MS.

Carr, S. J., Holmes, R., van der Meer, J. J. M. & Rose, J. 2006: The Last Glacial Maximum in the North Sea Basin: micromorphological evidence of extensive glaciation. *Journal of Quaternary Science 21*, 131–153.

Cartelle, V., Barlow, N. L. M., Hodgson, D. M., Busschers, F. S., Cohen, K. M., Meijninger, B. L. M. & van Kesteren, W. P. 2021: Sedimentary architecture and landforms of the late Saalian (MIS 6) ice sheet margin offshore of The Netherlands. *Earth Surface Dynamics 9*, 1399–1421.

Clare, M. A., Rushton, D. & Balthes, R. 2012: A ground model-based approach to efficient assessment and management of risk for pile installation and behaviour. *Hans Lorenz Symposium on Soil Dynamics and Foundation Engineering*, 69–87.

Clark, C. D., Hughes, A. L. C., Greenwood, S. L., Jordan, C. & Sejrup, H. P. 2012: Pattern and timing of retreat of the last British-Irish Ice Sheet. *Quaternary Science Reviews 44*, 112–146.

Clayton, C. R. I. & Power, P. T. 2002: Managing geotechnical risk in deepwater. *Proceedings of the International Conference for Offshore Site Investigations, SUT-OSIG-02-425*, 425–439.

Cohen, K. M., Westley, K., Erkens, G., Hijma, M. P. & Weerts, H. J. T. 2017: Chapter 7 – The North Sea. *In* Flemming, N. C., Harff, J., Moura, D., Burgess, A. & Bailey, G. N. (eds.): *Submerged Landscapes of the European Continental Shelf: Quaternary Paleoenvironments*, 147–186. Wiley, Chichester.

Coles, B. J. 1998: Doggerland: a speculative survey. *Proceedings of the Prehistoric Society 64*, 45–81.

Cotterill, C. J., Phillips, E., James, L., Forsberg, C. F. & Tjelta, T. I. 2017a: How understanding past landscapes might inform present-day site investigations: a case study from Dogger Bank, southern central North Sea. *Near Surface Geophysics 15*, 403–413.

Cotterill, C. J., Phillips, E., James, L., Forsberg, C. F., Tjelta, T. I., Carter, G. & Dove, D. 2017b: The evolution of the Dogger Bank, North Sea: a complex history of terrestrial, glacial and marine environmental change. *Quaternary Science Reviews 171*, 136–153.

Coughlan, M., Fleischer, M., Wheeler, A. J., Hepp, D. A., Hebbeln, D. & Mörz, T. 2018: A revised stratigraphical framework for the quaternary deposits of the German North Sea sector: a geological-geotechnical approach. *Boreas 47*, 80–105.

Díaz, H. & Guedes Soares, C. 2020: Review of the current status, technology and future trends of offshore wind farms. *Ocean Engineering 209*, 107381, https://doi.org/10.1016/j.oceaneng.2020.107381.

DNV 2014: *DNV-OS-J101 Design of Offshore Wind Turbine Structures*. Det Norsk Veritas, Høvik.

Doré, A. G. 1992: The base tertiary surface of southern Norway and the northern North Sea. *In* Jensen, L. N. & Riis, F. (eds.): *Post-Cretaceous Uplift and Sedimentation along the Western Fennoscandian Shield*, 259–266. *Norsk Geologisk Tidsskrift 72*.

Dowdeswell, J. A. & Ottesen, D. 2013: Buried iceberg ploughmarks in the early Quaternary sediments of the central North Sea: a two-million year record of glacial influence from 3D seismic data. *Marine Geology 344*, 1–9.

Dykes, R. C., Brook, M. S. & Winkler, S. 2010: The contemporary retreat of Tasman Glacier, Southern Alps, New Zealand, and the evolution of Tasman proglacial lake since AD 2000. *Erdkunde 64*, 141–154.

Ehlers, J. 1990: Reconstructing the dynamics of the north-west European Pleistocene ice sheets. *Quaternary Science Reviews 9*, 71–83.

Ehlers, J. & Gibbard, P. L. (eds.)2004: Quaternary glaciations-extent and chronology, part I: Europe. *In Developments in Quaternary Science 2*, 488 pp. Elsevier, Amsterdam.

Ehlers, J., Meyer, K. D. & Stephan, H. J. 1984: The pre-Weichselian glaciations of North-West Europe. *Quaternary Science Reviews 3*, 1–40.

Emery, A. R., Hodgson, D. M., Barlow, N. L. M., Carrivick, J. L., Cotterill, C. J., Mellett, C. L. & Booth, A. D. 2019a: Topographic and hydrodynamic controls on barrier retreat and preservation: an example from Dogger Bank, North Sea. *Marine Geology 416*, 105981, https://doi.org/10.1016/j.margeo.2019.105981.

Emery, A. R., Hodgson, D. M., Barlow, N. L. M., Carrivick, J. L., Cotterill, C. J. & Phillips, E. 2019b: Left high and dry: deglaciation of Dogger Bank, North Sea, recorded in proglacial Lake evolution. *Frontiers in Earth Science 7*, 234, https://doi.org/10.3389/feart.2019.00234.

Emery, A. R., Hodgson, D. M., Barlow, N. L. M., Carrivick, J. L., Cotterill, C. J., Richardson, J. C., Ivanovic, R. F. & Mellett, C. L. 2020: Ice sheet and palaeoclimate controls on drainage network evolution: an example from Dogger Bank, North Sea. *Earth Surface Dynamics 8*, 869–891.

Evans, D. J. A. & Thomson, S. A. 2010: Glacial sediments and landforms of Holderness, eastern England: a glacial depositional model for the North Sea Lobe of the British-Irish Ice Sheet. *Earth Science Reviews 101*, 147–189.

Evans, D. J. A., Roberts, D. H., Bateman, M. D., Clark, C. D., Medialdea, A., Callard, L., Grimoldi, E., Chiverrell, R. C., Ely, J., Dove, D., Ó Cofaigh, C., Saher, M., Bradwell, T., Moreton, S. G., Fabel, D. & Bradley, S. L. 2021: Retreat dynamics of the eastern sector of the British-Irish Ice Sheet during the last glaciation. *Journal of Quaternary Science 36*, 723–751.

Evans, T. G., Gourvenec, S. & White, D. 2010: A systematic approach to offshore engineering for multiple-project developments in geohazardous areas. *In Frontiers in Offshore Geotechnics II*, 3–32. CRC Press, London.

Evenson, E. B., Dreimanis, A. & Newsome, J. W. 1977: Subaquatic flow tills: a new interpretation for the genesis of some laminated till deposits. *Boreas 6*, 15–133.

Faleide, J. I., Bjørlykke, K. & Gabrielsen, R. H. 2015: Chapter 25 – Geology of the Norwegian continental shelf. *In* Bjørlykke, K. (ed.): *Petroleum Geoscience: From Sedimentary Environments to Rock Physics*, 603–637. Springer-Verlag, Berlin.

Fitch, S., Thomson, K. & Gaffney, V. 2005: Late Pleistocene and Holocene depositional systems and the palaeogeography of the Dogger Bank, North Sea. *Quaternary Research 64*, 185–196.

Fitzsimons, S. & Howarth, J. 2017: Chapter 9 – Glaciolacustrine processes. *In* Menzies, J. & van der Meer, J. J. M. (eds.): *Past Glacial Environments*, 309–334. Elsevier, Amsterdam.

Fleischer, M., Abegunrin, A., Hepp, D. A., Kreiter, S., Coughlan, M. & Mörz, T. 2023: Stratigraphic and geotechnical characterization of regionally extensive and highly competent shallow sand units in the southern North Sea. *Boreas 52*, 78–98.

Fugro 2000: Soil investigation spud can analysis. Transocean Nordic Jack-Up Rig, Block3/6, Norwegian Sector, North Sea. *Report No. 03319-2*. Client: Norsk Agip AS.

Gaffney, V., Allaby, R., Bates, R., Bates, M., Ch'ng, E., Fitch, S., Garwood, P., Momber, G., Murgatroyd, P., Pallen, M., Ramsey, E., Smith, D. & Smith, O. 2017: Doggerland and the Lost Frontiers Project (2015–2020). *In* Bailey, G., Harff, J. & Sakellariou, D. (eds.): *Under the Sea: Archaeology and Palaeolandscapes of the Continental Shelf. Coastal Research Library 20*. Springer, Cham.

Gaffney, V., Finch, S. & Thomson, K. 2007: *Mapping Doggerland: The Mesolithic Landscapes of the Southern North Sea*. 143 pp. Archaeopress, Oxford.

Gaffney, V., Fitch, S., Bates, M., Ware, R. L., Kinnaird, T., Gearey, B., Hill, T., Telford, R., Batt, C., Stern, B., Whittaker, J., Davies, S., Sharada, M. B., Everett, R., Cribdon, R., Kistler, L., Harris, S., Kearney, K., Walker, J., Muru, M., Hamilton, D., Law, M., Finlay, A., Bates, R. & Allaby, R. G. 2020: Multi-proxy characterisation of the Storegga tsunami and its impact on the early Holocene landscapes of the southern North Sea. *Geosciences 10*, 270, https://doi.org/10.3390/geosciences10070270.

Gandy, N., Gregoire, L. J., Ely, J. C., Cornford, S. L., Clark, C. D. & Hodgson, D. M. 2021: Collapse of the last Eurasian Ice Sheet in the North Sea modulated by combined processes of ice flow, surface melt, and marine ice sheet instabilities. *Journal of Geophysical Research: Earth Surface 126*, e2020JF005755, https://doi.org/10.1029/2020JF005755.

General Bathymetric Chart of the Oceans 2020: GEBCO_2020 Grid. Available at: https://www.gebco.net/data_and_products/gridded_bathymetry_data/gebco_2020/.

Gibbard, P. L. & Clark, C. D. 2011: Pleistocene glaciation limits in Great Britain. *In* Ehlers, J., Gibbard, P. L. & Hughes, P. D. (eds.): *Quaternary Glaciations – Extent and Chronology, Part IV – A Closer Look*, 75–94. Elsevier, Amsterdam.

Graham, A. G. C., Lonergan, L. & Stoker, M. S. 2010: Depositional environments and chronology of Late Weichselian glaciation and deglaciation in the central North Sea. *Boreas 39*, 471–491.

Graham, A. G. C., Stoker, M. S., Lonergan, L., Bradwell, T. & Stewart, M. A. 2011: Chapter 21 – The Pleistocene glaciations of the North Sea Basin. *In* Ehlers, J., Gibbard, P. L. & Hughes, P. D. (eds.): *Developments in Quaternary Sciences*, 261–278. Elsevier, Amsterdam.

Grasmueck, M., Moser, T. J. & Pelissier, M. A. 2012: Stop treating diffractions as noise – use them for imaging of fractures and karst. Adapted from extended abstract prepared in conjunction with poster

presentation at AAPG Hedberg Conference, Fundamental Controls on Flow in Carbonates, July 8–13, 2012, Saint-Cyr Sur Mer, Provence, France, AAPG.
Gunn, D. E. & Best, A. I. 1998: A new automated nondestructive system for high resolution multi-sensor core logging of open sediment cores. *Geo-Marine Letters 18*, 70–77.
Hamman, E. C. F. 2009: Qualitative geotechnical hazard and risk assessment. *Proceedings of the International Symposium on Rock Slope Stability in Open Pit Mining and Civil Engineering*, 9–11.
Hammer, Ø., Planke, S., Hafeez, A., Hjelstuen, B. O., Faleide, J. I. & Kvalø, F. 2016: Agderia – a postglacial lost land in the southern Norwegian North Sea. *Norwegian Journal of Geology 96*, 43–60.
Hansbo, S. 1957: A new approach to the determination of shear strength of clay by the fall-cone test. *Royal Swedish Geotechnical Institute Proceedings 14*, 1–46.
Hepp, D. A., Warnke, U., Hebbeln, D. & Mörz, T. 2017: Chapter 14 – Tributaries of the Elbe Palaeovalley: features of a hidden Palaeolandscape in the German Bight, North Sea. *In* Bailey, G., Harff, J. & Sakellariou, D. (eds.): *Under the Sea: Archaeology and Palaeolandscapes of the Continental Shelf. Coastal Research Library 20*. Springer, Cambridge.
Hjelstuen, B. O., Sejrup, H. P., Valvik, E. & Becker, L. W. M. 2018: Evidence of an ice-dammed lake outburst in the North Sea during the last deglaciation. *Marine Geology 402*, 118–130.
Howell, J. A., Martinius, A. W. & Good, T. R. 2014: The application of outcrop analogues in geological modelling: a review, present status and future outlook. *Geological Society, London, Special Publications 387*, 1–25.
Hughes, A. L. C., Gyllencreutz, R., Lohne, Ø. S., Mangerud, J. & Svendsen, J. I. 2016: The last Eurasian ice sheets – a chronological database and time-slice reconstruction, DATED-1. *Boreas 45*, 1–45.
Hughes, P. D., Gibbard, P. L. & Ehlers, J. 2020: The "missing glaciations" of the Middle Pleistocene. *Quaternary Research 96*, 161–183.
Huuse, M. & Lykke-Andersen, H. 2000: Overdeepened Quaternary valleys in the eastern Danish North Sea: morphology and origin. *Quaternary Science Reviews 19*, 1233–1253.
Huuse, M., Lykke-Andersen, H. & Michelsen, O. 2001: Cenozoic evolution of the eastern Danish North Sea. *Marine Geology 177*, 243–269.
IEA 2019: *Offshore Wind Outlook 2019*. IEA, Paris. Available at: https://www.iea.org/reports/offshore-wind-outlook-2019.
Jeanjean, P., Liedtke, E., Clukey, E. C., Hampson, K. & Evans, T. 2005: An operator's perspective on offshore risk assessment and geotechnical design in geohazards-prone areas. *First International Symposium on Frontiers in Offshore Geotechnics: ISFOG*, https://doi.org/10.1201/NOE0415390637.ch6.
Jensen, J. B., Gravesen, P. & Lomholt, S. 2008: Geology of outer Horns Rev, Danish North Sea. *GEUS Bulletin 15*, 41–44.
Jørgensen, F. & Sandersen, P. B. 2006: Buried and open tunnel valleys in Denmark – erosion beneath multiple ice sheets. *Quaternary Science Reviews 25*, 1339–1363.
Kehew, A. E., Piotrowski, J. A. & Jørgensen, F. 2012: Tunnel valleys: concepts and controversies – a review. *Earth-Science Reviews 113*, 33–58.
Kirkham, J. D., Hogan, K. A., Larter, R. D., Self, E., Games, K., Huuse, M., Stewart, M. A., Ottesen, D., Arnold, N. S. & Dowdeswell, J. A. 2021: Tunnel valley infill and genesis revealed by high-resolution 3-D seismic data. *Geology 49*, 1516–1520.
Knudsen, K. L. 1985: Foraminiferal stratigraphy of Quaternary deposits in the Roar, Skjold and Dan fields, central North Sea. *Boreas 14*, 311–324.
Knudsen, K. L. 2000: Internal report on foraminiferal analysis. *Norsk Agip, Norwegian well 3/6-1*.
Kongsberg 2019: TOPAS PS18. Available at: https://www.kongsberg.com/globalassets/maritime/km-products/product-documents/topas-ps-18-parametric-sub-bottom-profiler.pdf.
Konradi, P. D. 2000: Biostratigraphy and environment of the Holocene marine transgression in the Heligoland Channel, North Sea. *Bulletin of the Geological Society of Denmark 47*, 71–79.
Kristensen, T. B., Huuse, M., Piotrowski, J. A. & Clausen, O. R. 2007: A morphometric analysis of tunnel valleys in the eastern North Sea based on 3D seismic data. *Journal of Quaternary Science 22*, 801–815.
Lamb, R. M., Harding, R., Huuse, M., Stewart, M. & Brocklehurst, S. H. 2018: The early Quaternary North Sea Basin. *Journal of the Geological Society 175*, 275–290.
Lambeck, K., Rouby, H., Purcell, A., Sun, Y. & Sambridge, M. 2014: Sea level and global ice volumes from the Last Glacial Maximum to the Holocene. *Earth, Atmospheric, and Planetary Sciences 111*, 15296–15303.
Lauer, T. & Weiss, M. 2018: Timing of the Saalian- and Elsterian glacial cycles and the implications for Middle–Pleistocene hominin presence in central Europe. *Scientific Reports 8*, 5111, https://doi.org/10.1038/s41598-018-23541-w.
Le, T. M. H., Eiksund, G. R., Strøm, P. J. & Saue, M. 2014: Geological and geotechnical characterisation for offshore wind turbine foundations: a case study of the Sheringham Shoal wind farm. *Engineering Geology 177*, 40–53.
Lee, J. R., Busschers, F. S. & Sejrup, H. P. 2012: Pre-Weichselian Quaternary glaciations of the British Isles, The Netherlands, Norway and adjacent marine areas south of 68°N: implications for long-term ice sheet development in northern Europe. *Quaternary Science Reviews 44*, 213–228.
Lutz, R., Kalka, S., Gaedicke, C., Reinhardt, L. & Winsemann, J. 2009: Pleistocene tunnel valleys in the German North Sea: spatial distribution and morphology. *Zeitschrift der Deutschen Gesellschaft für Gewissenschaften 160*, 225–235.
Mangerud, J. 1991: The last interglacial/glacial cycle in Northern Europe. *In* Shane, L. C. K. & Cushing, E. J. (eds.): *Quaternary Landscapes*, 38–75. University of Minnesota Press, Minneapolis.
Mangerud, J., Sonstegaard, E. & Sejrup, H. P. 1979: Correlation of the Eemian (interglacial) Stage and the deep-sea oxygen-isotope stratigraphy. *Nature 277*, 189–192.
MAREANO/NGU 2021: *Seabed sediments (grain size)*. Available at: https://www.ngu.no/Mareano/Grainsize.html.
Martin, C. J., Morley, A. L. & Griffiths, J. S. 2017: Chapter 1 – Introduction to engineering geology and geomorphology of glaciated and periglaciated terrains. *In* Griffiths, J. S. & Martin, C. J. (eds.): *Engineering Geology and Geomorphology of Glaciated and Periglaciated Terrains – Engineering Group Working Party Report*, 1–30. *Geological Society, London, Engineering Geology Special Publications 28*.
Mesri, G. & Ali, S. 1999: Undrained shear strength of a glacial clay overconsolidated by desiccation. *Geotechnique 49*, 181–198.
Moreau, J. & Huuse, M. 2014: Infill of tunnel valleys associated with landward-flowing ice sheets: the missing Middle Pleistocene record of the NW European rivers? *Geochemistry, Geophysics, Geosystems 15*, 1–9.
Morén, B. M., Sejrup, H. P., Hjelstuen, B. O., Borge, M. V. & Schäuble, C. 2018: The last deglaciation of the Norwegian Channel-geomorphology, stratigraphy and radiocarbon dating. *Boreas 47*, 347–366.
Muir Wood, A. & Knight, P. 2013: Site investigation and geotechnical design strategy for offshore wind development. *Proceedings of the 18th International Conference on Soil Mechanics and Geotechnical Engineering*, 2375–2378.
Müther, D., Back, S., Reuning, L., Kukla, P. & Lehmkuhl, F. 2012: Middle Pleistocene landforms in the Danish Sector of the southern North Sea imaged on 3D seismic data. *In* Huuse, M., Redfern, J., Le Heron, D. P., Dixon, R. J., Moscariello, A. & Craig, J. (eds.): *Glaciogenic Reservoirs and Hydrocarbon Systems*, 111–127. *Geological Society, London, Special Publications 368*.
Norwegian Government 2022: Press Statement, 06.12.2022. Available at: https://www.regjeringen.no/no/aktuelt/regjeringen-gar-videre-i-sin-satsing-pa-havvind/id2949762/.
Ó Cofaigh, C. 1996: Tunnel valley genesis. *Progress in Physical Geography 20*, 1–19.
OSIG (Offshore Site Investigation and Geotechnics Committee) 2014: *Guidance Notes for the Planning and Execution of Geophysical and Geotechnical Ground Investigations for Offshore Renewable Energy Developments*. Society for Underwater Technology, London.

Available at: https://www.sut.org/wp-content/uploads/2014/07/OSIG-Guidance-Notes-2014_web.pdf.
Ottesen, D., Dowdeswell, J. A. & Bugge, T. 2014: Morphology, sedimentary infill and depositional environments of the Early Quaternary North Sea Basin (56°–62°N). *Marine and Petroleum Geology 56*, 123–146.
Ottesen, D., Stewart, M., Brönner, M. & Batchelor, C. L. 2020: Tunnel valleys of the central and northern North Sea (56°N to 62°N): distribution and characteristics. *Marine Geology 425*, 106199, https://doi.org/10.1016/j.margeo.2020.106199.
Özmaral, A. 2018: *Climatically controlled sedimentary processes on continental shelves*. Ph.D. thesis, Bremen University, 31 pp.
Özmaral, A., Abegunrin, A., Keil, H., Hepp, D. A., Schwenk, T., Lantzsch, H., Mörz, T. & Spiess, V. 2022: The Elbe Palaeovalley: evolution from an ice-marginal valley to a sedimentary trap (SE North Sea). *Quaternary Science Reviews 282*, 107453, https://doi.org/10.1016/j.quascirev.2022.107453.
Panin, A., Astakhov, V., Komatsu, G., Lotsari, E., Lang, J. & Winsemann, J. 2020: Middle and Late Quaternary glacial lake-outburst floods, drainage diversions and reorganization of fluvial systems in northwestern Eurasia. *Earth Science Reviews 201*, 103069, https://doi.org/10.1016/j.earscirev.2019.103069.
Papenmeier, S. & Hass, H. C. 2020: Revisiting the paleo Elbe Valley: Reconstruction of the Holocene, sedimentary development on basis of high-resolution grain size data and shallow seismics. *Geosciences 10*, 505.
Parry, S., Baynes, F. J., Culshaw, M. G., Eggers, M., Keaton, J. F., Lentfer, K., Novotny, J. & Paul, D. 2014: Engineering geological models: an introduction: IAEG commission 25. *Bulletin of Engineering Geology and the Environment 73*, 689–706.
Patruno, S., Kombrink, H. & Archer, S. G. 2021: Cross-border stratigraphy of the Northern, Central and Southern North Sea: a comparative tectono-stratigraphic megasequence synthesis. *Geological Society, London, Special Publications 494*, 13–83.
Pedersen, A. M. 1995: Pliocene-Middle Pleistocene biostratigraphy in the Central Danish North Sea wells E-1, P-1 and TWB-12. *Danmarks Geologiske Undersøgelse Serie C 13*, 1–28.
Phillips, E., Cotterill, C., Johnson, K., Crombie, K., James, L., Carr, S. & Ruiter, A. 2018: Large-scale glacitectonic deformation in response to active ice sheet retreat across Dogger Bank (southern central North Sea) during the Last Glacial Maximum. *Quaternary Science Reviews 179*, 24–47.
Phillips, E., Johnson, K., Ellen, R., Plenderleith, G., Dove, D., Carter, G., Dakin, N. & Cotterill, C. 2022: Glacitectonic evidence of ice sheet interaction and retreat across the western part of Dogger Bank (North Sea) during the Last Glaciation. *Proceedings of the Geologists' Association 133*, 87–111.
Phillips, E. R. 2018: Chapter 13 – Glacitectonics. *In* Menzies, J. & van der Meer, J. J. M. (eds.): *Past Glacial Environments*, 467–502. Elsevier, Amsterdam.
Piotrowski, J. A., Larsen, N. K. & Junge, F. W. 2004: Reflections on soft subglacial beds as a mosaic of deforming and stable spots. *Quaternary Science Reviews 23*, 993–1000.
Powell, R. D. & Molnia, B. F. 1989: Glacimarine sedimentary processes, facies and morphology of the south-southeast Alaska shelf and fjords. *Marine Geology 85*, 359–390.
Power, P. T., Clare, M., Rushton, D. & Rattley, M. 2011: Reducing geo-risks for offshore developments. *In* Vogt, N., Schuppener, B., Straub, D. & Bräu, G. (eds.): *Geotechnical Safety and Risk*, 217–224. Bundesanstalt für Wasserbau, Karlsruhe.
Praeg, D. 2003: Seismic imaging of Mid-Pleistocene tunnel-valleys in the North Sea Basin – high resolution from low frequencies. *Journal of Applied Geophysics 53*, 273–298.
Prins, L. T. & Andresen, K. J. 2019: Buried late Quaternary channel systems in the Danish North Sea – Genesis and geological evolution. *Quaternary Science Reviews 223*, 105943, https://doi.org/10.1016/j.quascirev.2019.105943.
Prins, L. T. & Andresen, K. J. 2021: A geotechnical stratigraphy for the shallow subsurface in the Southern Central Graben, North Sea. *Engineering Geology 286*, 106089, https://doi.org/10.1016/j.enggeo.2021.106089.
Prins, L. T., Andresen, K. J., Clausen, O. R. & Piotrowski, J. A. 2020: Formation and widening of a North Sea tunnel valley – the impact of slope processes on valley morphology. *Geomorphology 368*, 107347, https://doi.org/10.1016/j.geomorph.2020.107347.
Rea, B. R., Newton, A. M. W., Lamb, R. M., Harding, R., Bigg, G. R., Rose, P., Spagnolo, M., Huuse, M., Cater, J. M. L., Archer, S., Buckley, F., Halliyeva, M., Huuse, J., Cornwell, D. G., Brocklehurst, S. H. & Howell, J. A. 2018: Extensive marine-terminating ice sheets in Europe from 2.5 million years ago. *Science Advances 4*, eaar8327, https://doi.org/10.1126/sciadv.aar8327.
Roberts, D. H., Evans, D. J. A., Callard, S. L., Clark, C. D., Bateman, M. D., Medialdea, A., Dove, D., Cotterill, C. J., Saher, M., Ó Cofaigh, C., Chiverrell, R. C., Moreton, S. G., Fabel, D. & Bradwell, T. 2018: Ice marginal dynamics of the last British-Irish Ice Sheet in the southern North Sea: ice limits, timing and the influence of the Dogger Bank. *Quaternary Science Reviews 198*, 181–207.
Rohrig, K., Richts, C., Bofinger, S., Jansen, M., Siefert, M., Pfaffel, S. & Durstewitz, M. 2013: The importance of offshore wind energy in the energy sector and for the German Energiewende. *Fraunhofer Institute for Wind Energy and Energy System Technology Report*. Available at: https://www.offshorestiftung.de/sites/offshorelink.de/files/documents/SOW_Download_FraunhoferIWES_OffshoreStudy_ExecutiveSummary.pdf.
Rose, J. 1985: The Dimlington Stadial/Dimlington Chronozone: a proposal for naming the main glacial episode of the Late Devensian in Britain. *Boreas 14*, 225–230.
Salomonsen, I. 1995: Origin of a deep buried valley system in Pleistocene deposits of the eastern central North Sea. *Danmarks Geologiske Undersøgelse Serie C 12*, 7–19.
Seagreen Wind Energy. Available at: https://www.seagreenwindenergy.com/.
Sejrup, H. P., Aarseth, I., Haflidason, H., Løvlie, R., Bratten, Å., Tjøstheim, G., Forsberg, C. F. & Ellingsen, K. I. 1995: Quaternary of the Norwegian Channel: glaciation history and palaeoceanography. *Norwegian Journal of Geology 75*, 65–87.
Sejrup, H. P., Clark, C. D. & Hjelstuen, B. O. 2016: Rapid ice sheet retreat triggered by ice stream debuttressing: evidence from the North Sea. *Geology 44*, 355–358.
Sejrup, H. P., Hjelstuen, B. O., Dahlgren, K. I. T., Haflidason, H., Kuijpers, A., Nygård, A., Praeg, D., Stoker, M. S. & Vorren, T. O. 2005: Pleistocene glacial history of the NW European continental margin. *Marine and Petroleum Geology 22*, 1111–1129.
Sejrup, H. P., Nygård, A., Hall, A. M. & Haflidason, H. 2009: Middle and Late Weichselian (Devensian) glaciation history of South-Western Norway, North Sea and eastern UK. *Quaternary Science Reviews 28*, 370–380.
Shackleton, N. J. 1969: The last interglacial in the marine and terrestrial records. *Philosophical Transactions of the Royal Society of London, Series B 174*, 135–154.
Shennan, I., Lambeck, K., Horton, B., Innes, J., Lloyd, J., McArthur, J. & Rutherford, M. 2000: Holocene isostasy and relative sea-level changes on the east coast of England. *Geological Society, London, Special Publications 166*, 275–298.
Stackebrandt, W. 2009: Subglacial channels of Northern Germany–a brief review. *Zeitschrift der Deutschen Gesellschaft für Geowissenschaften 160*, 203–210, https://doi.org/10.1127/1860-1804/2009/0160-0203.
Stewart, M. A. 2016: Assemblage of buried and seabed tunnel valleys in the Central North Sea: from morphology to ice-sheet dynamics. *In* Dowdeswell, J. A., Canals, M., Jakobsson, M., Todd, B. J., Dowdeswell, E. K. & Hogan, K. A. (eds.): *Atlas of Submarine Glacial Landforms: Modern, Quaternary and Ancient*, 317–320. *Geological Society of London Memoirs 46*.
Stewart, M. A. & Lonergan, L. 2011: Seven glacial cycles in the middle-late Pleistocene of Northwest Europe; geomorphic evidence from buried tunnel valleys. *Geology 39*, 283–286.
Stewart, M. A., Lonergan, L. & Hampson, G. J. 2013: 3D seismic analysis of buried tunnel valleys in the central North Sea: morphology, cross-cutting generations and glacial history. *Quaternary Science Reviews 72*, 1–17.
Stoker, M. S., Balson, P. S., Long, D. & Tappin, D. R. 2011: An overview of the Lithostratigraphical framework for the quaternary deposits on the United Kingdom continental shelf. *British Geological Survey*, Report RR/11/03, 48 pp.

Sturm, H. 2017: Design aspects of suction caissons for offshore wind turbine foundations. *Proceedings of the 19th International Conference on Soil Mechanics and Geotechnical Engineering*.
Sturt, F., Garrow, D. & Bradley, S. 2013: New models of Northwest European Holocene palaeogeography and inundation. *Journal of Archaeological Science 40*, 3963–3976.
Svendsen, J. I., Alexanderson, H., Astakhov, V. I., Demidov, I., Dowdeswell, J. A., Funder, S., Gataullin, V., Henriksen, M., Hjort, C., Houmark-Nielsen, M. & Hubberten, H. W. 2004: Late Quaternary ice sheet history of northern Eurasia. *Quaternary Science Reviews 23*, 1229–1271.
Svensson, H. 1988: Ice-wedge casts and relict polygonal patterns in Scandinavia. *Journal of Quaternary Science 3*, 57–67.
TGS 2023: 4C offshore. *Global Offshore Renewable Map*. Available at: https://map.4coffshore.com/offshorewind/.
Thumann, V. M., Yetginer-Tjelta, T. & Van Foeken, R. J. 2017: Design and installation monitoring experience of large diameter monopiles for offshore wind farm in highly variable north sea soil conditions. *Offshore Technology Conference*.
Tjelta, T. I. 2015: The suction foundation technology. *In* Meyer, V. (ed.): *Frontiers in Offshore Geotechnics III*, 85 pp. CRC Press, Boca Raton.
Underhill, J. R. & Richardson, N. 2022: Geological controls on petroleum plays and future opportunities in the North Sea Rift Super Basin. *AAPG Bulletin 106*, 573–631.
van der Vegt, P., Janszen, A., Moscariallo, A. & Le Heron, D. P. 2012: Tunnel valleys: current knowledge and future perspectives. *In* Huuse, M., Redfern, J., Dixon, R. J., Moscariello, A. & Craig, J. (eds.): *Glaciogenic Reservoirs and Hydrocarbon Systems*, 75–97. *Geological Society, London, Special Publications 368*.
Velenturf, A. P. M., Emery, A. R., Hodgson, D. M., Barlow, N. L. M., Mohtaj Khorasani, A. M., Van Alstine, J., Peterson, E. L., Piazolo, S. & Thorp, M. 2021: Geoscience solutions for sustainable offshore wind development. *Earth Science, Systems and Society 1*, 10042, https://doi.org/10.3389/esss.2021.10042.
Vink, A., Steffen, H., Reinhardt, L. & Kaufmann, G. 2007: Holocene relative sea-level change, isostatic subsidence and the radial viscosity structure of the mantle of Northwest Europe (Belgium, The Netherlands, Germany, southern North Sea). *Quaternary Science Reviews 26*, 3249–3275.
Washburn, A. L. 1980: Permafrost features as evidence of climatic change. *Earth-Science Reviews 15*, 327–402.
Wenau, S., Stange, N., Keil, H., Ramos, C. & Spiess, V. 2018: A seismic beamforming approach for the detection of boulders in the shallow sub-seafloor. *Proceedings of the 3rd Applied Shallow Marine Geophysics Conference*, 1–5.
Westaway, R. 2017: Isostatic compensation of Quaternary vertical crustal motions: coupling between uplift of Britain and subsidence beneath the North Sea. *Journal of Quaternary Science 32*, 169–182.
Wingfield, R. T. R. 1989: Glacial incisions indicating middle and upper Pleistocene ice limits off Britain. *Terra Nova 1*, 538–548.
Zagwijn, W. H. 1989: The Netherlands during the tertiary and the quaternary: a case history of coastal lowland evolution. *In* van der Linden, W. J. M., Cloetingh, S. A. P. L., Kaasschieter, J. P. K., van de Graaff, W. J. E., Vandenberghe, J. & van der Gun, J. A. M. (eds.): *Coastal Lowlands: Geology and Geotechnology*, 107–120. Springer, Dordrecht.
Ziegler, P. A. 1990: Collision related intra-plate compression deformations in Western and Central Europe. *Journal of Geodynamics 11*, 357–388.

Supporting Information

Additional Supporting Information to this article is available at http://www.boreas.dk.

Fig. S1. Southwest to NE 2D seismic profile running from SNII in the southern Norwegian North Sea to the southwestern edge of the Norwegian Channel, without annotation. N. Channel = Norwegian Channel; TWT = two-way travel time.

Fig. S2. A. 2D seismic profile A–A′ from survey NSR04, without annotation. B. Close-up of a gas migration structure. C. −100 ms variance time slice from 3D seismic surveys DG15001 (DISKOS) and MC3D-NDB2013 (PGS) showing key seismic anomalies close to seabed and the location of seismic profiles A–A′ and D–D′. D. Annotated seismic profile D–D′ showing Salt Diapirs 1 and 2 in southern SNII. E. Close-up of Salt Diapir 1 in southwestern SNII. F. Salt Diapir 2 in southeastern SNII, showing high-amplitude, chaotic seismic reflections above the diapirs, within overlying Late Pleistocene sediments. TWT = two-way travel time.

Fig. S3. A. Seismic profile through central SNII from seismic survey DG15001 (DISKOS) without annotation. B. −90 ms frequency decomposition blend time slice. C. −150 ms frequency decomposition blend time slice. TWT = two-way travel time.

Fig. S4. A. Seismic profile through central SNII from seismic survey MC3D-NDB2013 (PGS), without annotation. B. −100 ms frequency decomposition blend time slice. C. −130 ms frequency decomposition time slice. D. −300 ms frequency decomposition time slice. TWT = two-way travel time.

Fig. S5. A. Seabed depth from MC3D-NDB2008 (PGS), MC3D-NDB2013 (PGS) and DG15001 (DISKOS) (background), without annotation. B. −80 ms seismic time slices with variance overlays from DG15001 (DISKOS), MC3D-NDB2013 (PGS) and MC3D-NDB2008 (PGS) (background), TOPAS profiles. C. An infilled proglacial lake system interpreted in western SNII. D. Northern branches of the SNII Palaeovalley. E. Main trunk of the SNII Palaeovalley. F. Ridges of surficial sand in northeastern SNII overlying moraines and glacitectonized deposits. G. Smaller infilled palaeovalley system SW of SNII Palaeovalley. H. Possibly structurally disturbed sediments above Salt Diapir 2. I. Infilled isolated incisional basins containing overconsolidated glacilacustrine clays, possibly pushed up in the eastern part of the profile by movement of Salt Diapir 1 after the LGM. TWT = two-way travel time.

Fig. S6. A. Southwest- to NE-trending sub-bottom profiles through SNII showing vibrocore locations and location of geotechnical boring. B. Seabed time map interpreted on sub-bottom profiler data set showing sub-bottom profile locations (yellow lines) presented in A and core locations (yellow circles). C. −100 ms time slice through frequency decomposition blends extracted from MC3D-NDB2013 (PGS) and

DG15001 (DISKOS) with time slice from MC3D-NDB2008 (PGS) in background for comparison between geomorphic features resolved on conventional 3D seismic time slices vs. those resolved on sub-bottom profiles. D. Annotated base Unit 1 (Holocene marine sand) time map interpreted on sub-bottom profile data set. E. Combined base Unit 2 and base Unit 3 (basal Late Weichselian subglacial/proglacial erosion surface) time map based on sub-bottom profile data set. F. annotated Unit 1 time thickness map (Holocene sediments). G. Unit 2/3 time thickness map (Late Weichselian to Holocene sediments). TWT = two-way travel time.

Fig. S7. A. Core scan photograph, sedimentary log and gamma density log for vibrocore 02VC. B. Northwest–SE sub-bottom profile correlated to 02VC without annotation. C. seabed depth map from surveys DG15001 (DISKOS) and MC3D-NDB2013 (PGS) showing the location of profile X–X′. D. Northwest–SE sub-bottom profiler cross-section through 02VC location, showing high-amplitude reflections present locally in upper Unit 5 and at base Unit 1 which are interpreted to correlate with the 02VC diamict and pebble layers respectively. Cl = clay; sc = silty clay; fs = fine sand; ms = medium sand; cs = coarse sand; g = gravel; p = pebbles; TWT = two-way travel time.

Fig. S8. A. Core scan photograph, sedimentary log, gamma density log and shear strength measurements for vibrocore 09VC. B. North–south sub-bottom profile correlated to 09VC, without annotation. C. Seabed depth map from surveys DG15001 (DISKOS) and MC3D-NDB2013 (PGS) showing the location of profile X–X′. D. North–south TOPAS profile through 09VC showing the multigenerational infill of the northwestern and northeastern branches of the SNII Palaeovalley. E. Zoomed in section of high-amplitude, discontinuous seismic facies in upper part of Subunit 3b and lower part of Unit 2 in SNII Palaeovalley. Cl = clay; sc = silty clay; fs = fine sand; ms = medium sand; cs = coarse sand; g = gravel; p = pebbles; TWT = two-way travel time.

Fig. S9. A. Core scan photograph, sedimentary log, gamma density log and shear strength measurements for vibrocore 11VC. B. Southwest–NE sub-bottom profile correlated to 11VC, without annotation. C. Seabed depth map from surveys MC3D-NDB2013 (PGS) and DG15001 (DISKOS) showing the location of profile X–X′. D. Southwest–NE sub-bottom profile through 11VC showing the zone of shallow stratigraphy located above Salt Diapir 1 (the diapir is located below the penetration depths of the sub-bottom profiler). Cl = clay; sc = silty clay; fs = fine sand; ms = medium sand; cs = coarse sand; g = gravel; p = pebbles; TWT = two-way travel time.